NTNU
Norwegian University of
Science and Technology

The Effect of Potassium on Cobalt-based Fischer-Tropsch Catalysts of Small and Medium Cobalt Particle Sizes

Jonas Save

Chemical Engineering and Biotechnology
Submission date: June 2018
Supervisor: Edd Anders Blekkan, IKP
Co-supervisor: Ljubisa Gavrilovic, IKP

Norwegian University of Science and Technology
Department of Chemical Engineering

Preface

This thesis was a continuation of the course TKP4580 and part of the course TKP4900 in the spring of 2018 for a duration of 21 weeks. Therefore, a lot of the contents in the first three chapters as well as some of the contents in the appendix originates from the report delivered from the course TKP4580. The work was carried out at the Department of Chemical Engineering, at the Norwegian University of Science and Technology (NTNU).

I would like to extent my sincere thanks to my supervisor Professor Edd A. Blekkan and my co-supervisor Ph.D Ljubiša Gavrilovič for their guidance and mentoring during this project. Their open door policy allowed me to ask questions whenever they popped up. I would also like to express my appreciation for the help I got with the Fischer-Tropsch rig from Ph.D candidate Joakim Tafjord. I would like to thank Senior Engineer Syverin Lierhagen for performing ICP-MS experiments for me. I would especially like to thank my two very good friends Henrik Jenssen and Hans Sigurd Amundsen for all the great talks we had during coffee breaks, this was fuel for the soul in challenging days. Finally, I would like to thank my parents for their unconditional support throughout the course of my education.

Trondheim, June 2018

Jonas Save

Sammendrag

I dag står verdenssamfunnet overfor kompliserte og viktige problemstillinger i forbindelse med overpopulasjon og økt industrialisering av u-land og derav et økende energibehov. En annen problemstilling som er nært knyttet til disse temaene er økte klimautslipp. Et tiltak som kan bidra som del av løsningen på overnevnte problemer er økt satsning på utvikling av drivstoff basert på biomasse. Biodrivstoff kan produseres via utallige fremstillingsmetoder. En av disse metodene baseres på produksjon av Fischer-Tropsch (FT) produkter ved bruk av syntesegass (H_2 og CO), hvor produktene blant annet er diesel og bensin, og syntesegassen kommer fra gasifisert biomasse. FT syntesen har vært tilstede i rundt hundre år og det finnes fortsatt fabrikker med produksjon, men her brukes hovedsaklig kull eller naturgass som kilde til syntesegass. Det finnes et stort potensiale i det å tilpasse slike fabrikker til samme prosess, men istedet ved bruk av syntesegass fra biomasse. Hovedproblemet ved industrialisering av denne prosessen er rengjøring av urenhetene som oppstår fra gasifiseringen.

I denne oppgaven ble effekten av alkalimaterialet kalium på ytelsen til en kobolt-basert FT katalysator studert. Mer spesifikt var hovedmålet å endre størrelsen på koboltpartiklene for deretter å se om kalium deaktiverte medium størrelse partikler annerledes enn små. Forfatteren var av den oppfatning at FT reaksjonen hovedsaklig skjer på trinn, kanter og lignende punkter på kobolt i motsetning til på for eksempel terrassepunkter. Det er også påvist at kalium har høyest adsorpsjonsenergi på de førstnevnte punktene, i tilleg til at små partikler er kjent for å ha høyere tetthet av disse punktene. Hypotesen ble derfor at små partikler ville deaktiveres kraftigere enn store, da det var antatt at disse utsagnene stemte. Katalysatorene ble testet ved relevante FT betingelser (H_2/CO=2.1, 210°C og 20 bar) og bestod av 20 vekt% Co, 0,5 vekt% Re, på en γ-Al_2O_3 bærer. Disse ble laget via en metode kalt ”incipient wetness impregnation” (IWI), der IWI løsningen bestod av metallforløperene og en vektprosent-blanding av 80 % vann over etylen glykol (EG) og 100 % vann. Katalysatorene ble kalt CoRe80(15ppm) og CoRe100(6ppm), henholdsvis. ”Inductively coupled plasma - mass spectrometry” (ICP-MS) eksperimenter bekreftet metall- og kaliumandelen i katalysatorene, hvor sistnevnte ble inkludert i katalysatornavnene.

Katalysatorene ble post-impregnert med kaliumnivåer på rundt 500 og 1000 ppm, noe som ikke endret overflaten eller porene til bæreren, metall dispersjonen eller reduksjonstemperaturen. Dette ble funnet ved bruk av N_2-fysisorpsjon, H_2-kjemisorpsjon og temperatur programmert reduksjon. XRD og H_2-kjemisorpsjon sørget for estimater på partikkelstørrelsene og disse var 11,1-12,5 og 3,7-6,2 nm, for CoRe100(6ppm) og CoRe80(15ppm), henholdsvis.

Avtagende størrelse av koboltpartikler viste seg å kraftig senke aktiviteten, C_{5+}-selektiviten,

og en økning i CH_4- og CO_2-selektiviteten. Disse effektene ble tilskrevet den lavere reduserbarheten til mindre koboltpartikler, indusert av metall-bærer interaksjoner. Kalium tilsats førte til en tydelig nedgang i aktivitet, mulig økning i C_{5+}-selektivitet og en tydelig avtakning i CH_4- og CO_2-selektivitet. Disse effektene er vanskeligere å vite bakgrunnen til, men kan tenkes å være på grunn av en mer spesifik posisjonering av mobile kaliumspesier på aktive FT punkter eller på grunn av kalium-induserte elektroniske effekter. Hovedkonklusjonen var at det ikke ble funnet noen forskjell i deaktiveringsraten til kalium på små partikler i forhold til på store. Dette betød at hypotesen ble avkreftet og kan bety at viktigheten av punkter som trinn, kanter og lignende på kobolt i forbindelse med FT reaksjonen ikke er like betydelig som for eksempel terrassepunkter.

Abstract

As the population of the world increase and the developing countries become more industrialized, the need for alternative energy sources increases along with it. In addition, the harmful climate emissions have to be reduced. In an attempt to solve these problems, the investigation of various routes for the production of biofuels should be performed. Biofuels can be produced via multiple routes, among them are the production of synthesis gas (H_2 and CO) from biomass, which subsequently can be used in the production of diesel and gasoline through the Fischer-Tropsch (FT) synthesis. This process has been around for about a century, using coal and natural gas as the synthesis gas source. Therefore, there are a lot of FT production plants already in operation, which present a great opportunity as they can be altered for biomass-based fuel production. However, the most expensive and limiting step upon industrializing this process is the removal of the impurities present after gasification of biomass to syngas.

In this thesis the way in which the alkali impurity potassium deactivate the cobalt-based FT catalyst was investigated. More specifically, the goal was to alter the size of the cobalt particles, before looking at whether or not potassium has a different deactivation rate on small versus medium particles. The hypothesis was that small particles would have a higher deactivation rate than medium particles. This was based on the authors believe that the larger fraction of possibly more active FT sites such as step, edge, and kink sites on small particles, that also have proven to have a higher potassium adsorption energy, would be more severely deactivated as potassium potentially could block more active sites.

The catalysts were tested in relevant FT conditions (H_2/CO=2.1, 210°C, and 20 bars) and consisted of 20 wt.% Co, 0.5 wt.% Re, on a γ-Al_2O_3 support. They were prepared via incipient wetness impregnation (IWI), where the IWI solution consisted of 80 % water over ethylene glycol and 100 % water. The catalysts were then denoted CoRe80(15ppm) and CoRe100(6ppm), respectively. Inductively coupled plasma - mass spectrometry (ICP-MS) experiments confirmed the metal and potassium loadings, where the latter was included in the catalyst names.

The catalysts were post-impregnated with potassium levels around 500 and 1000 ppm, showing no significant change in support properties, dispersion, or reduction temperatures, found through N_2-physisorption, H_2-chemisorption, and temperature programmed reduction measurements. XRD and H_2-chemisorption measurements provided particle size estimates of 11.1-12.5 and 3.7-6.2 nm, for CoRe100(6ppm) and CoRe80(15ppm), respectively.

Decreased cobalt particle sizes lead to a clear decrease in catalytic activity, C_{5+}-selectivity, and an increase in CH_4- and CO_2-selectivity. These effects are ascribed to the lower re-

ducibility of smaller cobalt particles, induced by metal-support interactions. Potassium contaminations lead to severely decreased activities, possibly increased C_{5+}-selectivities, and clear decrease in CH_4- and CO_2-selectivities. These effects are harder to explain but could be because of the more specific positioning of mobile potassium species on active FT sites, or of electronic effects induced by potassium. The main conclusion was that no difference in the deactivation rate was seen upon potassium addition on small cobalt particles compared to medium cobalt particles. Therefore, the hypothesis was disproved, which could indicate that the important sites for FT activity are not step, kink, or edge sites, but perhaps terrace sites.

Table of Contents

List of Tables

List of Figures

List of symbols

Latin letters

$A_{CH_4,xh}$	Area of the CH_4 GC signal at hour x
A_{CO}	Area of the CO GC signal
$A_{CO_2,xh}$	Area of the CO_2 signal registered by the GC at hour x
A_{N_2}	Area of the N_2 GC signal
$A_{N_2,xh}$	Area of the CH_4 GC signal at hour x
A_{sp}	Specific surface area in the BET model
C_{KNO_3}	Concentration of KNO_3
D	Dispersion in the H_2-chemisorption
d	Distance between two lattice planes in the Bragg relation
$d(Co^0)$	Particle size of metallic cobalt
$d(Co_3O_4)$	Particle size of cobalt oxide in the Scherrer equation
F	Number of surface atoms covered by one adsorbed molecule in the H_2-chemisorption
F	Flow rate of syngas
$F_{CH4,xh}$	Flow of CH_4 at hour x
$F^{CO}_{feed,av}$	Average flow of CO in the feed
$F_{CO,xh}$	Flow of CO at hour x
$F_{CO2,xh}$	Flow of CO_2 at hour x
F^{CO}_{xh}	Flow of CO at hour x
$F_{N2,xh}$	Flow of N_2 at hour x
K	Particle shape constant in the Scherrer equation
$< L >$	Measure of particle dimensions in the direction perpendicular to the reflecting plane in the Scherrer equation
m_{Co}	Mass of Co
$m_{Co(NH_22*6H2O}$	Mass of $Co(NH_2)_2 \cdot 6\,H_2O$
m_{EG}	Mass of EG
m_{H_2O}	Mass of de-ionized water
$m_{\gamma-Al_2O_3}$	Mass of γ-Al_2O_4
m_{HReO_4}	Mass of $HReO_4$
m_{KNO_3}	Mass of KNO_3
M_m	Molar mass

m_{Re}	Mass of Re
n	Order of reflection in the Bragg relation
p	Pressure in N_2-physisorption
p_0	Saturation pressure in N_2-physisorption
q_L	Heat of condensation of the adsorbate N_2 in the BET model
q_1	Heat of adsorption of the first monolayer in the BET model
R	Gas constant
r	Reaction rate per catalyst weight
r_k	Radius of capillary in the BJH model
RRF_{CH_4}	Relative response factor
$S_{CH_4,xh}$	CH_4-selectivity
$S_{CO_2,xh}$	CO_2-selectivity
$S_{CO_2,xh}$	CO_2-selectivity
$S_{C2,xh}$	selectivities towards C2 products
$S_{C3,xh}$	Selectivities towards C3 products
$S_{C4,xh}$	Selectivities towards C4 products
$S_{C_{5+},xh}$	C_{5+}-selectivity at hour x
T	Temperature of the liquid N_2 bath in N_2-physisorption
V	Liquid molar volume of N_2 in the N_2-physisorption
V	Total volume adsorbed in the BET model
V	Volume adsorbed in the H_2-chemisorption
v_{ads}	Volume of H_2 adsorbed in the H_2-chemisorption
V_m	Volume adsorbed at monolayer coverage in the BET model
V_m	Volume of one mole of ideal gas in the H_2-chemisorption
V_m	Volumetric flow per mole of syngas
W	Weight of the cobalt catalyst
w(corr)	Correlated weight actually used in the H_2-chemisorption software
W(fin)	Weight of catalyst, quartz wool and reactor before H_2-chemisorption analysis
W(in)	Weight of the catalyst, quartz wool and reactor after H_2-chemisorption analysis
w(in)	Initial weigth of the catalyst before H_2-chemisorption analysis
X	CO conversion
$X_{CO,xh}$	CO conversion at hour x
x_m	Weight fraction of metal in the catalyst in the H_2-chemisorption
Y	CO-content of the syngas

Greek letters

α	Probability of chain growth in the ASF model
β	Full width at half the maximum of the relevant peak in the Scherrer equation
θ	Angle between the incoming X-rays and the normal to the reflecting lattice plane in the Bragg relation
θ_i	Coverage fraction of monolayer i in the BET model
λ	Wavelength of X-rays in the Bragg relation
σ	Surface tension of liquid N_2 in N_2-physisorption

List of abbreviations

ASF	Anderson-Schulz-Flory
BET	Brunauer-Emmet-Teller
BJH	Barret-Joyner-Halenda
CNF	Carbon Nanofibers
DEG	Diethylene Glycol
EG	Ethylene Glycol
FT	Fischer-Tropsch
FTS	Fischer-Tropsch Synthesis
FT-BTL	Fischer-Tropsch Biomass-to-liquids
FT-CTL	Fischer-Tropsch Coal-to-liquids
FT-GTL	Fischer-Tropsch Gas-to-liquids
GC	Gas Chromatograph
HTFT	High-temperature Fischer-Tropsch
ICP-MS	Inductively Coupled Plasma - Mass Spectrometry
IWI	Incipient Wetness Impregnation
LFC	Liquid Flow Controller
LTFT	Low-temperature Fischer-Tropsch
MFC	Mass Flow Controller
MTFT	Medium-temperature Fischer-Tropsch
PC	Pressure Controller
ppm	Parts Per Million
PR	Pressure Regulator
STY	Site Time Yield
TCD	Thermal Conductivity Detector
TEM	Transmission Electron Microscopy
TOF	Turnover Frequency
TPR	Temperature Programmed Reduction
WGS	Water-gas-shift
XRD	X-ray Diffraction

Chapter 1

Introduction

1.1 Global Challenges

The population of the world is steadily increasing along with the demand for energy, while the fossil reserves are being depleted (Shahsavari and Akbari, 2018). At the same time, the climate is changing, which means that the task of reducing harmful emissions is one of great importance. Therefore, in order to uphold measures that aim to solve these problems, such as the Paris agreement, renewable and more climate-friendly fuels should be considered (Rogelj et al., 2016).

There are many technologies that can be part of solving these complex issues, among them are biofuel technologies. Biofuels can be produced via multiple routes, as shown in figure 1.2. These routes are either based on first-, second- or third-generation biofuels (Ullah et al., 2017), illustrated in figure 1.1. First-generation biofuels are based on crops that would otherwise be used as food sources, e.g., sugar cane and starch. Second-generation biofuels are based on lignocellulosic crops that are non-edible while third-generation biofuels are based on lipids such as algae crops.

Countries such as Brazil and USA are currently producing first-generation biofuels on an industrial scale, but as the crops being grown otherwise could be used as a food source, ethical questions are frequently raised (Alam et al., 2015). The introduction of third-generation biofuels presents a very promising biofuel route due to microalgae of high growth rates, zero net emissions of greenhouse gases, high production capacity of lipids and the ability of crop growth in non-arable land and saline water. Unfortunately, the technology needed to make this an industrially feasible process is out of reach. The second-generation biofuels do not replace food crops on the scale that first-generation biofuels do. In addition, this route is closer to being able to compete with fossil fuels than to third-generation biofuels, making it an important field of study (Kasthuraiah and Kishore, 2017). One of the possible production routes for second-generation biofuels is via the Fischer-Tropsch synthesis.

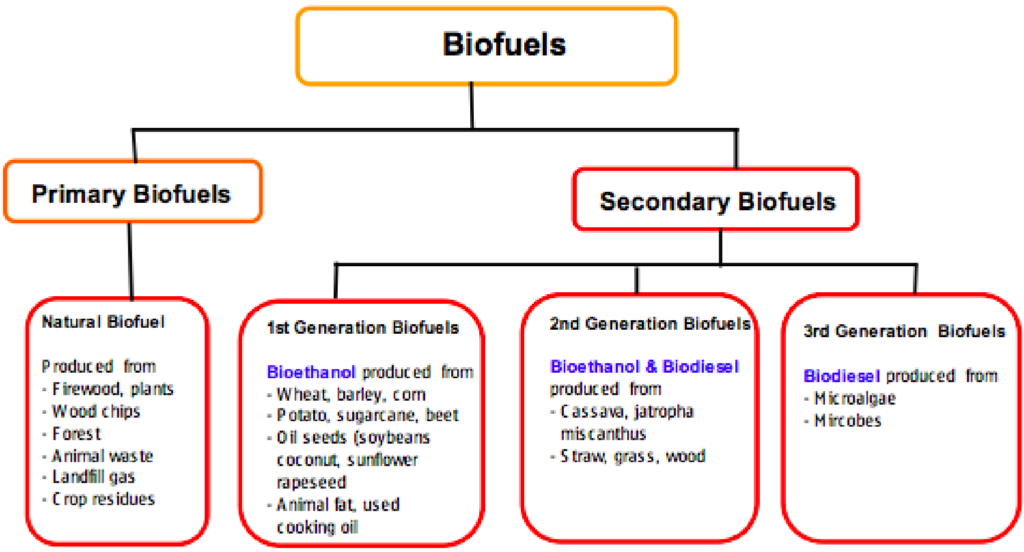

Figure 1.1: Different sources of first-, second- and third generation biofuels (Alam et al., 2015).

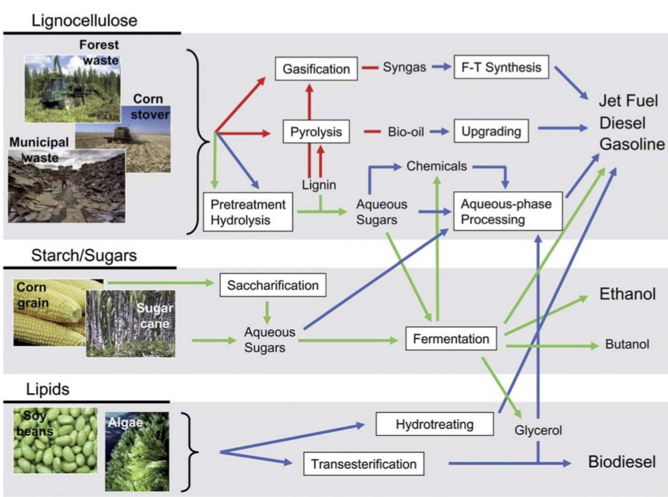

Figure 1.2: Possible routes for production of biofuels (Serrano-Ruiz and Dumesic, 2011).

1.2 The Fischer-Tropsch Synthesis

The Fischer-Tropsch (FT) synthesis is a process that converts synthesis gas (H_2 and CO), or syngas, into hydrocarbons such as gasoline, diesel fuel, and other chemicals (Chorkendorff and Niemantsverdriet, 2005b). The syngas is derived from carbon-based sources such as natural gas, coal or biomass and the terms gas-to-liquids (GTL), coal-to-liquids (CTL) or biomass-to-liquids (BTL) are commonly used for their overall process from raw material to liquid fuel. The feedstock of choice will affect only the ratio between hydrogen and carbon monoxide as well as the impurity content in the syngas. This implies that the same products can be achieved whether the feedstock originates from fossil reserves, biomass or coal. Therefore, if the FT-BTL process becomes economically viable, countries without fossil reserves will have the opportunity to be self-sufficient in terms of fuel. It also means that global warming can be countered, as the biomass-based FT fuels are considered carbon neutral (Ail and Dasappa, 2016). The diesel produced from FT contains no sulfur, no aromatic compounds and has a high cetane number of around 70, which means it provides a cleaner fuel burning (Eilers et al., 1990).

1.2.1 Process conditions, thermodynamics and reactors

The FT synthesis is industrially operated at pressures of 25-45 bar and three different temperature intervals: low, medium and high temperature, denoted LTFT, MTFT, and HTFT, respectively (Chorkendorff and Niemantsverdriet, 2005b). The ranges are around 220-240, 270-280 and 350°C, respectively. High temperatures provide high CO conversions and reaction rates but tend to favor the formation of methane. High pressures provide high CO conversions and C_{5+}-selectivities, meaning increased selectivity towards chains of five or more carbon atoms, which is where the product becomes liquid (Moulijn et al., 2013).

LTFT and MTFT have a higher selectivity towards linear high molecular mass wax, often defined as C_{5+}-selectivity. Both iron and cobalt catalysts are used in LTFT and only iron in MTFT (Dry, 2002). The products (wax, diesel, and naphtha) are liquid during reaction conditions, which means that the reaction takes place in a three-phase domain (Chorkendorff and Niemantsverdriet, 2005b). In general, the FT reaction requires reactors with great cooling abilities as the formation of one mole $-CH_2-$ releases 145 kJ of heat, meaning it is highly exothermic (Moulijn et al., 2013). The most commonly used reactors are slurry-phase or fixed-bed multitubular reactors, illustrated in figure 1.3. The former has great isothermal and gradientless properties with the possibility of continuous removal and refilling of catalyst. The latter is often placed in parallel so that the catalyst can be replaced in one reactor while the rest of the reactors still operate. However, the fixed-bed multitubular reactor comes short in cooling abilities and production capacity compared to the slurry-phase reactor.

HTFT have a lower C_{5+}-selectivity and mostly produce shorter carbon-chains which better suit the production of gasoline and chemicals such as olefins and naphtha. At these conditions, the iron catalyst is used. As the products are mostly gaseous at reaction conditions a gas-solid domain dominate and the reactors best suited for this domain are the circulating fluidized bed and fixed fluidized bed, illustrated in figure 1.3.

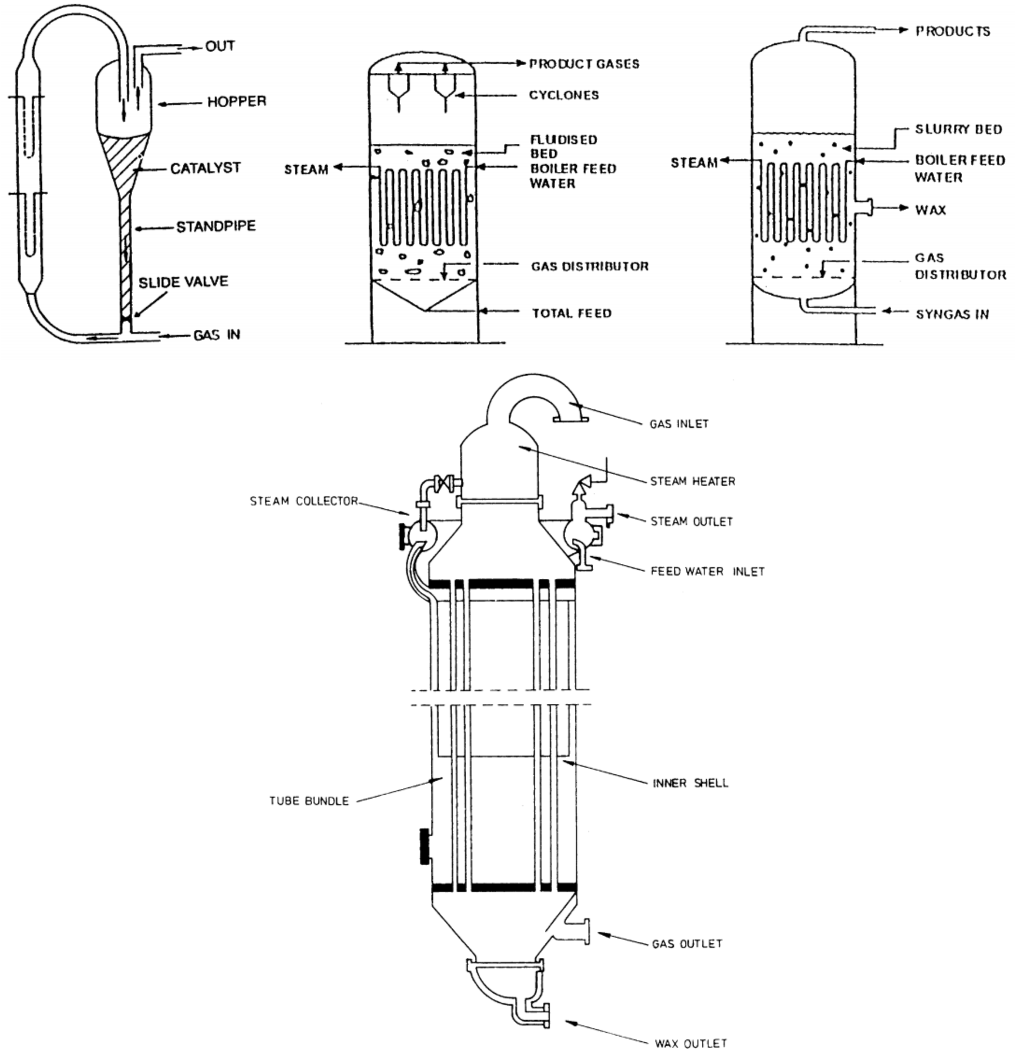

Figure 1.3: The top left illustrate the circulating fluidized bed reactor, the top middle the fixed fluidized bed reactor, the top right the slurry-phase reactor and the bottom the multitubular fixed bed reactor (Dry, 2002).

The reactors illustrated above have different cooling features. The multitubular fixed bed reactor operates with a circulation of boiler feed water around the reactor tubes, while the cooling in the slurry-phase and fluidized bed reactors use internal coils filled with a cooling medium (Moulijn et al., 2013). The reactors using iron as catalyst normally operate at H_2/CO-ratios around 1 and the reactors using cobalt catalysts normally operate at H_2/CO-ratios around 2.05.

1.2.2 Catalyst material

As mentioned previously, the catalysts used in the FT industry are either iron- or cobalt-based. Ruthenium and nickel have proven active catalysts for the FT synthesis, but the former is too expensive and the latter is too selective towards methane products (Vannice, 1975). A cobalt-based FT synthesis catalyst is preferred for the GTL process as it has a better catalytic performance, better resistance towards deactivation than the iron-based catalyst and because the GTL syngas provides high H_2/CO-ratios, i.e., water-gas-shift (WGS) activity is not desired. The cobalt catalyst is the best catalyst for LTFT synthesis as it has a higher per single pass conversion at around 60-70 %, higher stability, and high selectivity towards heavier hydrocarbons (Khodakov, 2009). Cobalt-based catalysts are the most cost-and performance-efficient in FT synthesis aimed at making long-chained hydrocarbons (Iglesia, 1997), or wax, which is the desired product in modern days (Borg et al., 2008). The iron catalyst is less sensitive to impurities to the extent that some impurities even promote the catalytic performance. The iron catalyst also has a high WGS activity, which is important in CTL applications as the H_2/CO-ratios are low. Both the cobalt and iron catalyst have been tried and tested for BTL applications as the BTL process provides somewhat higher H_2/CO-ratios than the CTL process. Using a cobalt catalyst at these lower syngas ratios does require a WGS unit before the FT reactor, but can still be a better fit for the process due to its selectivity towards wax and its lifetime, as replacing catalysts is an expensive task. However, the impurities in the BTL syngas introduce a lot more alkali material than the CTL syngas and their effect on the cobalt-based FT catalyst have to be investigated at great lengths in order for optimal syngas cleaning requirements to be found.

1.3 Particle size effects on cobalt-based FT catalysts

The effects of Co particle size on cobalt-based FT catalysts have been studied extensively ever since what the author considers to be its first discovery (Bezemer et al., 2004). The initial discovery was that as the particle size of cobalt resided below a certain value, the catalytic activity decreased dramatically. The discovery catalyzed a number of investigations, and a few years later the same author confirmed the particle size effect with a more extensive investigation (Bezemer et al., 2006). The investigation of cobalt-based catalysts supported on inert carbon nanofibers (CNF) yielded results indicating a decrease in activity as cobalt particle sizes went below 6 nm at reaction conditions of 1 bar and 220°C, and below 8 nm at 35 bar and 220°C. It was also reported that the C_{5+}-selectivity decreased significantly upon the same changes in particle size. The effects were ascribed to a combination of CO-induced surface reconstruction and nonclassical structure sensitivity. SSITKA studies also reported that smaller particles in FTS have a higher coverage of irreversible CO, which blocks the surface, as well as a higher coverage of H, which leads to more CH_4-formation (Den Breejen et al., 2009). It should be mentioned that contradictory studies have reported a positive effect of increasing cobalt dispersion, which directly relates to particle size, on catalytic performance in the FT synthesis (Iglesia, 1997; Lok, 2004). These studies looked at a range of particle sizes above 8 nm and around 3-5 nm, respectively.

The catalytic activity of the FT synthesis depends on the number of active sites on the surface of the support, dispersion (Park et al., 2012). The dispersion depends on Co loading, crystal size, the degree of reduction and metal-support interaction. In order to get a highly dispersed catalyst, the cobalt oxide particles (Co_3O_4 and CoO) initially formed have to be small. However, the smaller the particles are, the stronger the interaction between them and the support are, which in turn leads to a decreased degree of reduction (Khodakov et al., 1997, 2002; Yang et al., 2010). Studies have reported that the lowered reducibility of small cobalt oxides could be an explanation for decreased activity and increased CH_4-selectivity in FT reactions (Khodakov et al., 1997, 2002). Another report confirmed the particle size effects once more. The site-time yield (STY) increased with a factor of 2 found that when the particle size of cobalt increased from 4 to 11 nm, respectively (Martínez and Prieto, 2007). In this paper, there were no suggestions as to why the activity decreased upon decreased particle size.

A study reported no effect of particle size on intrinsic activity (STY), but Borg *et al.* found a significant increase in C_{5+}-selectivity and decrease in CH_4-selectivity was seen as the particle size increased up to 8 nm (Borg et al., 2008). Yet another study using a batch reactor, atmospheric pressures and 240°C reported a decreased TOF and increased CH_4-selectivity at metallic cobalt particle sizes in the range 1.4-2.5 nm and relatively constant catalytic performance in the range 3.5-10 nm (Wang et al., 2012). The effects on TOF was here ascribed to the re-oxidation of cobalt particles by the water vapor present at relevant FT reaction conditions as the particles reached a certain size. This explanation has been confirmed in other studies as well, where an increased selectivity towards CH_4 and CO_2 was also seen, while the C_{5+}-selectivity decreased (Azzam et al., 2014; Fischer et al., 2014).

More recent studies claim to provide evidence of a structure sensitivity at small cobalt particle sizes. One study using a chemical transient kinetic reactor measuring cobalt-based FT catalysts of 9.5 to 4.3 nm cobalt particle size at atmospheric pressures claimed that the decrease in activity was due to structure sensitivity induced by a loss of specific sites, such as the B_5-B site, important for the CO-dissociation, at small particle sizes (Ralston et al., 2017). Another study found that upon increased particle size, an increase in the site fractions of edge, kink and step sites was seen (van Helden et al., 2016). However, this increase in site fractions was seen for the B_5-A site and B_6 site up to around 4 nm, while the B_5-B site increased all the way up to 8 nm and slightly above. It should be noted that these particle sizes are still fairly small. This means that at small particle sizes around 4-8 nm, there are more step, kink, and edge sites than in particle sizes above this value. These studies also indicate that these sites are of importance to the FT reaction.

To summarize, at particle sizes below a certain value around 6-10 nm, the catalytic activity decreases dramatically, while the selectivity towards CH_4 and CO_2 increase, and the selectivity towards C_{5+} decrease. However, the task of determining why these effects occur are more difficult to establish. The theories are many and include a combination of CO-induced surface reconstruction and non-classical structure sensitivity, decreased reducibility, re-oxidation of metallic cobalt at relevant FT conditions and loss of important sites.

In an attempt to alter the cobalt particle size in the use of different cobalt loadings and alumina supports, a study reported the use of ethylene glycol (EG) and diethylene glycol (DEG) in combination with de-ionized water in the impregnation solution during the incipient wetness impregnation of a cobalt-based FT catalyst (Borg et al., 2008). The particle sizes obtained were in the range 3-18 nm. The estimated BET surface areas for the γ-Al_2O_3 supported catalysts were all within the range of 103 to 162 m^2/g, while the pore volume and average pore diameter ranged from 0.38 to 0.60 cm^3/g and 10.3 to 12.4 nm, respectively. The EG was speculated to act as a surfactant on the cobalt salt solutions, increasing their wetting ability. The authors also found that when the mass fraction of water over EG in the impregnation solution was below 0.8, the Co_3O_4-crystallites were in the size range 4-6 nm and did not depend on the cobalt loading or alumina support, while at larger mass fractions, the crystallite sizes were in the range 6-18 nm and depended on cobalt loading and alumina support. It was discovered by TEM images that the Co_3O_4 particles were found uniformly distributed in a pure EG impregnation solution, whereas a pure water impregnation solution left aggregated particles of sizes above 100 nm. The authors also found through oxygen titration that the degree of reduction was lower for smaller particles. This was ascribed to a stronger interaction between smaller Co particles and support. The same author produced different particle sizes by varying the treatment of the alumina support (Borg et al., 2007). Here, the TPR profiles had broader peaks for the reduction of CoO to Co^0 for the larger particle sizes, which was explained by a broader distribution of particle sizes, as these would have varying degrees of interaction with the support.

The same procedure was followed by Yang *et al.*, where water over EG mass percentages was used in the impregnation solution in order to alter the Co particle sizes (Yang et al., 2010). 20 wt% Co catalysts on γ-Al_2O_3 supports were prepared using water over EG in the impregnation solution at 80, 93 and 96 wt%. The catalysts prepared gave rise to Co particle sizes of around 4, 8 and 11 nm through H_2-chemisorption and correcting for the degree of reduction (DOR), which was found to be 45, 59 and 73 %, respectively. The BET surface area of the catalysts with Co particle sizes 4, 8 and 11 nm was found to be 158, 136 and 140 m^2/g while the pore volume and pore diameter was 0.52, 0.48 and 0.51 cm^3/g and 10, 11.5 and 12.9 nm, respectively.

1.3.1 Reactions and mechanism

In the FT synthesis, the hydrocarbon chains formed are often described by a statistical model called the Anderson-Schulz-Flory (ASF) distribution (Chorkendorff and Niemantsverdriet, 2005b). The ASF model predicts the probability that the formation of n hydrocarbon-chains will form without regard to whether it is an alkane or alkene. According to the ASF model, the chain-growth occur through a stepwise addition of one carbon-segment at a time derived from CO at the end of an existing chain, as shown in figure 1.4. The factor α describe the probability that the chain will continue to react and is largely dependent on catalyst and process conditions. The distribution of FT products can be estimated pretty accurately by the ASF distribution, as shown in figure 1.5.

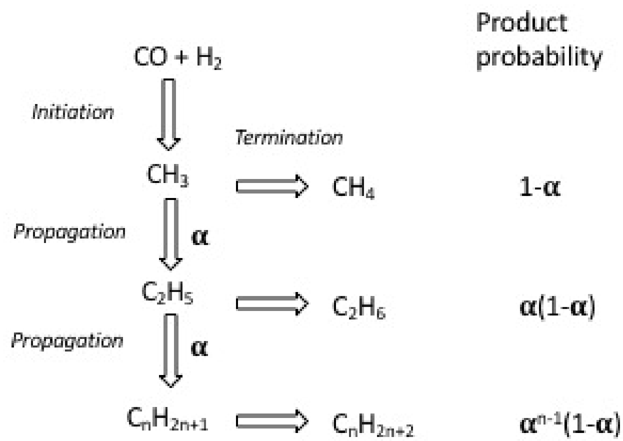

Figure 1.4: Chain growth in Fischer-Tropsch synthesis, according to the Anderson-Schulz-Flory model (Moulijn et al., 2013).

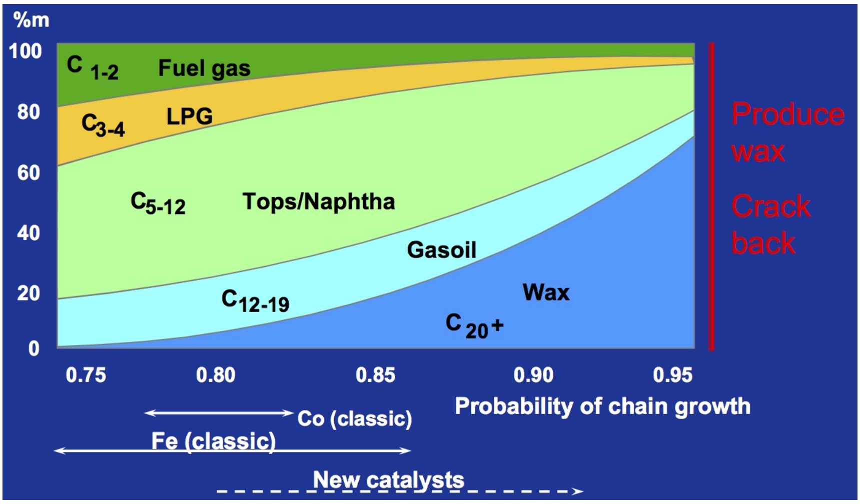

Figure 1.5: The product distribution of the Fischer-Tropsch process as a function of the Anderson-Schulz-Flory chain growth probability factor α (Hoek, 2005).

The probability of chain growth, α, decreases with increasing temperature and H_2/CO-ratio and is also dependent on reactor design and catalyst. As illustrated in figure 1.5, in order to produce the most desired product for fuel purposes, wax, the cobalt-based catalyst should be used.

At stoichiometric ratios of H_2/CO, as obtained from GTL syngas, the cobalt catalyst is preferred because of its low water-gas-shift (WGS) activity. The main reactions are shown in equation (1.1) and (1.2), where paraffins and olefins are produced, respectively.

$$\mathrm{nCO} + (2\mathrm{n}+1)\mathrm{H_2} \rightarrow \mathrm{C}_n\mathrm{H_{2n+2}} + \mathrm{nH_2O} \tag{1.1}$$
$$\mathrm{nCO} + 2\mathrm{nH_2} \rightarrow \mathrm{C_nH_{2n}} + \mathrm{nH_2O} \tag{1.2}$$

In addition, the thermodynamics allow not only for the formation of hydrocarbons, but alcohols and coke as well, following equation (1.3) and (1.4), respectively. However, the use of catalyst can ensure high selectivity towards paraffins and olefins instead of alcohols, while pressure regulation can provide a low coke formation.

$$\mathrm{nCO} + 2\mathrm{nH_2} \rightarrow \mathrm{H(CH_2)_nOH} + (\mathrm{n}-1)\mathrm{H_2O} \tag{1.3}$$
$$2\mathrm{CO} \rightleftharpoons \mathrm{CO_2} + \mathrm{C} \tag{1.4}$$

At low H_2/CO-ratios, as obtained in coal and biomass syngas, the iron-based catalyst has been used because of its high WGS activity. Therefore, it can be said that the Fischer-Tropsch process at low H_2/CO-ratios also has the WGS as an additional main reaction, shown in equation (1.5).

$$CO + H_2O \rightleftharpoons CO_2 + H_2 \tag{1.5}$$

1.3.2 Brief history and motivation for FT-BTL

The FT process has been around for almost a century (Bartholomew, 2003). A process for hydrogenation of CO was first patented by BASF in 1913, but as they chose to focus on other processes, it was discarded. Some years later, two scientists at the Kaiser-Wilhelm Institute in Mulheim, Franz Fischer and Hans Tropsch, picked up the pieces from BASF and ended up getting a patent for the Fischer-Tropsch process. In 1932, the first pilot plant was built and by 1939 there were nine FT plants in operation having an annual capacity of 5.4 million barrels. These plants were located in Germany, the main products at this time were transportation fuels and the catalyst material a mixture of cobalt and thorium (Stranges, 2000). After the war, from 1950 to 1974, a new era for the FT synthesis emerged, the "Iron Age". At this time, iron catalysts were utilized in the production of FT products using coal feedstocks, which mainly took place in South Africa. Later, the use of cobalt catalysts was rediscovered and during the years 1975-1990, cobalt was the favored catalyst for the FT-GTL process. Commercial FT-GTL and FT-CTL plants are still in operation today and it is clear that the largest obstacle for the FT-BTL to become a commercial possibility is the availability of clean and cheap enough syngas derived from biomass.

1.3.3 Main challenges in FT-BTL

The conversion of biomass to syngas is the first part of the BTL process, which involves complex pretreatment steps and thermochemical conversion of lignocellulosic biomass, normally through gasification (Nigam and Singh, 2011). The main challenge in syngas production from biomass is related to impurities and their effect on downstream catalysts (Ragauskas et al., 2006). The impurities can be alkalis, alkaline earth metals, sulfur gases, halides, and tars. The decomposition of biomass produces a lot of tars, which are slowly converted into CO and H_2 using water vapor or CO_2 and temperatures below 1100°C. Alternatively, the tars could be converted by catalysis at less severe conditions, but this requires a catalyst insensitive to multiple impurities. The most abundant contaminant in biomass is the chloride, which during gasification turns into HCl or attaches to potassium and sodium in an aerosol form. Most of the impurities mentioned above are removed from the syngas before FT synthesis, but these removal processes are expensive. Therefore, investigations of the effects of impurities on FT catalysts are of great economic importance. Impurities in the form of alkali and alkaline earth metals in the syngas can also come from the catalyst preparation stages, either via impure water, active material- or promoter precursor or through the process equipment (Borg et al., 2011).

Therefore, as the cobalt catalyst is showing promise in the FT-BTL, but have been limited by impurities in the syngas, many studies on their effects have been done in order for optimal syngas cleaning requirements to be found. The alkali impurities originate from the ash composition and these impurities are also found in the CTL syngas, but as can be seen from figure 1.6, a lot more alkali is introduced in the BTL syngas (Gavrilović et al., 2018; Dayton et al., 1999). The figure below illustrates that both sodium and potassium are found in greater quantities in biomass feedstock compared to coal feedstock. This implies that the effects of sodium and potassium on the cobalt-based FT catalyst is an important field of study.

	Pittsburgh No. 8 coal	Eastern Kentucky coal	red oak	Danish wheat straw	Imperial wheat straw
		proximate (wt % as received)			
Moisture	1,14	1,63	4,76	5,41	7,99
Ash	7,90	7,43	1,15	7,33	13,49
Volatile	36,80	35,44	82,88	73,39	65,14
fixed carbon	54,16	55,50	11,21	13,87	13,38
heating value (HHV as received - Btu/lb)	13691	13351	7800	7355	6318
		ultimate (wt % as received)			
Moisture	1,14	1,63	4,76	5,41	7,99
C	78,02	76,83	49,02	44,44	39,14
H	4,87	4,88	5,34	5,10	4,34
N	1,36	1,47	0,19	0,98	0,99
S	2,78	0,88	0,02	0,16	0,30
Ash	7,90	7,43	1,15	7,33	13,49
O	3,93	6,88	39,52	36,58	33,75
Cl	0,09	0,17	<0,01	0,60	2,00
		elemental ash analysis (wt % of fuel as received)			
SiO_2	3,411	3,897	0,464	2,909	5,016
Al_2O_3	1,786	2,453	0,097	0,062	0,097
TiO_2	0,073	0,107	0,065	0,003	0,005
Fe_2O_3	1,318	0,340	0,092	0,058	0,063
CaO	0,385	0,080	0,155	0,586	0,495
MgO	0,066	0,030	0,012	0,136	0,177
Na_2O	0,134	0,017	0,005	0,052	2,064
K_2O	0,108	0,098	0,104	2,507	3,049
P_2O_5	0,045	0,024	0,012	0,355	0,360
SO_3	0,885	0,096	0,022	0,302	0,762

Figure 1.6: The three first columns represent coal sources while the last two on the right represent biomass sources (Dayton et al., 1999).

1.4 Potassium effects on cobalt-based catalysts

The effects of potassium contaminations on cobalt-based FT catalysts are generally a severe decrease in activity, promotion of selectivity and no significant impact on adsorption characteristics (dispersion, surface area, pore size, pore volume). The reasons behind these effects have been speculated widely, but are still not completely understood.

Trpanier *et al.* studied the effects of K on carbon nanotubes (CNTs) supported 15 wt.% Co of FT catalysts by adding 16 ppm, 33 ppm, and 66 ppm K via impregnation (Trépanier et al., 2009). The authors found no significant changes in the surface area, pore volume or average pore diameter upon K addition. The particle size was 9.6 nm both with and without K, as found by XRD analysis using the Scherrer equation at the Co_3O_4-peak found at 36.8°. Upon addition of K, a slight increase in the reduction temperatures (about 5-15°C increase) of Co_3O_4 to CoO and CoO to Co were reported, while broadening the tailing of the second reduction peak slightly, indicating a more difficult reduction due to stronger interaction between cobalt particles and support upon K loadings. The catalytic activity was decreased with a magnitude of 7.5 upon 66 ppm K loading, while the C_{5+} selectivity was increased from 70 to 87 %, the CH_4-selectivity decreased from 23 to 4 %, and increased the CO_2-selectivity from 2 to 4 %. It was suggested that the severe decrease in activity and changes in selectivity was due to alkali-induced blockage of low-coordination edge and corner sites for dissociative adsorption of hydrogen, as reduced hydrogen mobility and hydrogen adsorption rates were observed.

Balonek *et al.* studied the effects of K on a 20 wt.% Co - 0.5 wt.% Re/γ-Al_2O_3 FT catalyst by adding 200, 500, and 1000 ppm K via impregnation (Balonek et al., 2010). No significant change in the dispersion was found through H_2-chemisorption, as the value always resided at around 8 % ± 0.5 %. However, a significant decrease in catalytic activity was found upon 200 ppm K loading. Also, a significant increase in C_{5+} and CO_2 selectivity was found at 200 ppm K, while a decrease was seen in selectivity towards CH_4. The reduction temperatures of both reduction peaks were increased with around 5-15°C upon all K loadings. The changes in catalytic performance being due to the blocking of active sites was assumed to be unlikely as the number of K atoms per cobalt surface atom was less than 2 %, while the drop in activity was around 22 %. Instead, the changes were assumed to be a result of the induced electronic effects by the K, decreasing the concentration of surface H and increasing the CO adsorption and dissociation.

Eliseev *et al.* (Eliseev et al., 2013) found that the addition of K of molar ratios K/Co 0.01, 0.02 and 0.05 had a promoting effect on the 20 wt.% Co catalyst selectivity and decreased the catalytic activity. The authors found no change in particle size upon alkali addition, using XRD estimates with the Scherrer equation. Here, the effects were ascribed to an increase in the amount of strongly bound CO on the catalyst surface.

Borg *et al.* (Borg et al., 2011) also studied the effects of different alkali impurities at 0-1000 ppm contamination via impregnation, here on various cobalt FT catalyst supported on various alumina supports. Here as well a trend where alkali generally decreased catalytic activity and increased C_{5+}- and CO_2-selectivity was reported. The authors of this study found no change in dispersion and speculated that the changes in catalytic activity were due to electronegative effects induced by the alkali material.

Lilleb *et al.* (Lillebø et al., 2013) studied the effects of alkali on a 20 wt.% Co - 0.5 wt.% Re/γ-Al_2O_3 FT catalyst by adding alkali of 0-20000 ppm via impregnation. No change in the dispersion was found by H_2-chemisorption for Li, Na, K or Ca or in heat of adsorption for Na loadings below or equal to 1000 ppm, but a decrease of 33-43 % in catalytic activity was found at 1000 ppm contamination of the alkali materials. The C_{5+}- and CO_2-selectivities increased, while the CH_4-selectivity decreased. The reduction temperatures were also increased slightly for both reduction peaks (about 5-10°C increase), indicating a slightly more difficult reduction upon alkali loading. The authors concluded that the alkali undetected by chemisorption experiments must sit on important sites for catalytic activity.

Gavrilovic *et al.* (Gavrilović et al., 2018) found through aerosol deposition of K on a 20 wt.% Co - 0.5 wt.% Re/γ-Al_2O_3 FT catalyst that the effect on the catalytic performance and characterization results were the same as for previous contaminations done by incipient wetness impregnation. The author found that the size of the K particles was much larger (>100 nm) than the pore diameters (around 13 nm), meaning the K initially deposits on the external surface of the catalyst. However, as the deactivation still was severe, the author believes that the K species have to be in close contact with the surface of the cobalt particles during FT synthesis, but the characterization results indicate no pore blockage. Therefore, the deactivating effects are speculated to be due to more mobile K species during FT reaction conditions, migrating towards active FT sites.

Density functional theory (DFT) studies found that the stepped facets on hcp cobalt had the highest adsorption energy towards potassium (Chen et al., 2017). It was also found that the mobility of K was high on the stepped facets during FTS conditions, but had a high diffusion barrier, whereas the terrace surface sites had negligible diffusion barriers. These findings indicate that the reason behind the severe deactivation from small amounts of potassium on cobalt catalysts is due to the fact that potassium places itself more easily onto important sites for FT activity, such as step sites and not terrace sites.

1.5 Scientific objective

The effect of K on the activity of cobalt-based FT catalysts have proven to be detrimental to catalytic activity and promoting on selectivities throughout years of investigations. The particle size of cobalt has also shown to affect the catalytic performance. However, as far as the author is aware, there is no previous literature reporting how potassium affects cobalt based FT catalysts of various cobalt particle sizes. Therefore, in an attempt to gain more insight on the nature of the dramatic effects seen on cobalt-based FT catalysts upon alkali addition, the effect of potassium on small and medium cobalt particle sizes in Co−Re/γ-Al_2O_3 catalysts will be investigated. Potassium has shown to have a higher adsorption energy potassium in step, kink, and edge sites. These sites are more present in smaller particles than large. Therefore, as it is the authors belief that these sites are also more important for the FT reaction, the hypothesis is that the catalysts with smaller particle will be more severely deactivated than the ones with medium particles.

Chapter 2

Theory

2.1 Preparation of supported catalysts

There are two main routes one can take when preparing supported catalysts (Chorkendorff and Niemantsverdriet, 2005a). The first route, co-precipitation of the catalytically active component and support with subsequent drying and calcination, can be followed if the materials are inexpensive and an optimum catalytic activity per unit volume of catalyst is the main objective. The second route, impregnation or precipitation from solution onto a pre-made support material, can be followed if the metals are expensive and are to be deposited onto the support as metal particles of sizes in the nanometer-scale. In the synthesis of cobalt-based FT catalysts, the common preparation method is the incipient wetness impregnation (IWI) technique.

2.1.1 Incipient wetness impregnation

Impregnation methods are very common in the preparation of catalysts but differ slightly in their methodology depending on the properties of the species involved (Schwarz et al., 1995). In general, impregnation is based on mixing a specific volume of solution with the amount of precursor that adds up to the desired loading. This solution is added to a solid support material. If the volume of the solution equals or is less than the volume of the pores in the support material, then the method is called IWI. If the case is such that a larger volume of solution than the pore volume of support is used, the method is called wet impregnation. Incipient wetness impregnation aims to deposit metal particles on the support surface by filling the pores with a metal salt solution, driven by capillary forces. The support material is usually dried before impregnation, in order to remove any moist residing within the pores, while the metal solution should be of such concentrations that both pores are filled and the outer surface is wetted.

2.1.2 Drying

Drying is done after impregnation to remove the solvent in the precursor solution and to crystallize the salt on the pore surface (Richardson, 1989). The rate of the drying will determine the distribution of salt on the surface. A drying rate that is too slow will result in a distribution where the salts crystallize at the bottom of the pores as evaporation occurs at the meniscus of the pore. On the other hand, if the rate is too rapid, most of the salts will deposit on the external surface as a temperature gradient is induced so that vaporization takes place deep down in the pore, resulting in forces pushing the solution to the external surface. The goal is to land somewhere in the middle of these two scenarios in order to get a homogeneous particle distribution.

2.1.3 Calcination

Calcination is a process in which the catalyst is heated and treated with a flow of air or nitrogen. This step is important as the metal salts are redissolved and chemically converted into a metal oxide or metal, depending on the conditions and gases flowed through the catalyst (Richardson, 1989).

2.1.4 Activation

The final step a catalyst has to go through before it can be tested for catalytic activity is reduction, or activation. If the catalyst is active in its oxide state, this step is neglected (Richardson, 1989). The reduction can either be done ex-situ or in-situ. The ex-situ reduction is a reduction performed in a separate setup than the one testing the catalyst for catalytic activity. The in-situ reduction is the reduction performed in the same setup as the activity testing. The reduction is a process that converts the metal oxide particles, obtained after calcination, into metal particles. The most common reducing agent is hydrogen, but others such as CO or hydrazine are also used in some cases. The temperature at which the catalyst is treated with a reducing agent is also of importance as high temperatures can form unwanted species and low temperatures can result in an incomplete reduction.

2.2 Characterization of catalyst

2.2.1 Nitrogen-physisorption

The Brunauer-Emmet-Teller (BET) model and the Barret-Joyner-Halenda (BJH) model can help find estimates of the surface area and pore diameter and volume, respectively, of catalyst supports. The Langmuir isotherm model is applied to several monolayers of adsorbate, giving the multilayer model (Chorkendorff and Niemantsverdriet, 2005a). The way the layers of adsorbate build up to a multilayer is illustrated in figure 2.1. The method starts with an inert gas, called the adsorbate (e.g. N_2), being flowed through the catalyst sample, the adsorbent, at very low temperatures. This step will allow the adsorbate molecules to physically adsorb onto the catalyst molecules. Physisorption interaction is mostly driven by van der Waals forces and a trait of this type of adsorption is that the electronic structure of the atoms or molecules involved is barely perturbed. The adsorbate molecules do not only adsorb onto the catalyst as monolayers but can form multilayers and condense in small pores, the latter as a result of capillary forces. A modified version of the Kelvin equation, describing capillary condensation, can be used to estimate the pore diameter and volume according to the Barret-Joyner-Halenda (BJH) model (Barrett et al., 1951). This is a practical version of the modified Kelvin equation and is shown in equation (2.1):

$$\log \frac{p}{p_0} = \frac{-2\sigma V}{8.314 \times 10^7 \times 2.303 T r_k} \tag{2.1}$$

where p/p_0 is the relative pressure, σ the surface tension of liquid nitrogen, V the liquid molar volume of nitrogen, r_k the radius of capillary in cm (usually converted to nm for practical purposes), T the temperature of the liquid nitrogen bath and 8.314×10^7 the gas constant in ergs per degree.

In order to account for the multilayer effect of physisorption, the BET adsorption isotherm was derived.

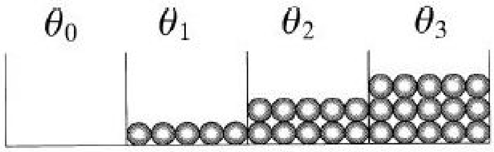

Figure 2.1: Derivation of the BET isotherm requires the surface of the adsorbent to be divided into regions with i monolayers of coverage, or θ_i (Chorkendorff and Niemantsverdriet, 2005a). Each region have a coverage fraction of θ_i.

In order to derive the BET isotherm, the underlying assumptions and equations should be known. First, its important to note that the BET surface areas are based on the following assumptions:

- Equal rate of adsorption and desorption in every layer - Dynamic equilibrium.
- Adsorption of adsorbate molecules on equivalent sites in the first monolayer.
- The adsorption sites in the first monolayer establishes the adsorption sites in all the following layers.
- No interaction between adsorbent and adsorbate.
- Equal adsorption-desorption conditions for all layers except for the first layer.
- Equal adsorption energy and condensation energy for molecules in all layers except the first.
- Infinite thickness of multilayer at saturation pressure.

Then, in short, the BET isotherm is derived by combining the assumptions above along with the equation for the number of atoms adsorbed on the adsorbent surface, the sum of surface coverage fractions from 0 to infinity monolayers and change in coverage fraction per time. The result after derivation is equation (2.2).

$$\frac{p}{V(p_0 - p)} = \left[\frac{(C-1)}{V_m C}\right]\frac{p}{p_0} + \frac{1}{V_m C} \tag{2.2}$$

Above, the saturation pressure is expressed as p_0, actual pressure as p, total volume adsorbed as V, volume adsorbed at monolayer coverage as V_m and the factor C as shown in equation (2.3):

$$C = exp\big(q_1 - q_L / RT\big) \tag{2.3}$$

where q_1 represents the heat of adsorption of the first monolayer, q_L the heat of condensation of the adsorbate N_2, R the gas constant and T the temperature.

A linear plot is produced when $\frac{p}{V(p_0-p)}$ is plotted as a function of $\frac{p}{p_0}$. The linearity allows for the extraction of the term $\frac{(C-1)}{V_m C}$ as the slope and $\frac{1}{V_m C}$ as the intercept. The assumption that C>>1 when N_2 is used as adsorbate can be applied so the slope $\approx \frac{1}{V_m}$ and a new equation emerges, providing the specific surface area:

$$A_{sp}\Big[\frac{m^2}{g}\Big] = V_m\Big[\frac{cm^3 STP}{g}\Big]\Big[\frac{6.023 \times 10^{23}\text{molecules}}{21400 cm^3 STP}\Big]\Big[\frac{\text{cross-section}, m^2}{\text{molecule}}\Big] \tag{2.4}$$

2.2.2 X-ray diffraction

X-ray diffraction (XRD) is a method that can be used to detect crystalline phases and give an approximation of particle size (Niemantsverdriet, 2010). The basic principle of XRD is based on X-ray photons providing an elastic scatter in a periodic lattice. The spacing in between the lattice can be found through the Bragg relation, equation (2.5):

$$n\lambda = 2d \sin\theta; n = 1, 2, ... \tag{2.5}$$

where λ represents the wavelength of the X-rays, d the distance between two lattice planes, θ the angle between the incoming rays and the normal to the reflecting lattice plane and n an integer better known as the order of reflection. The scattering in the lattice is shown in figure 2.2.

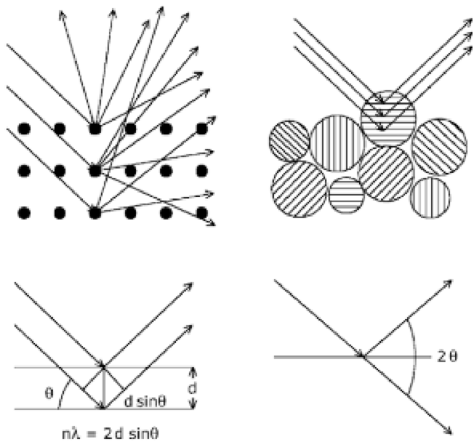

Figure 2.2: X-rays scattered by atoms in an ordered lattice and the directions it travels according to Braggs law (Niemantsverdriet, 2010).

The XRD pattern is measured with a stationary X-ray source and a movable detector, where the X-ray source normally consists of CuKα. The detector monitors the intensity of the diffracted radiation with respect to the angle 2θ between the incoming and diffracted beams. The peaks in the pattern are unique for every crystallographic phase making it easy to compare with old data and determine which phases a catalyst contains.

The particle size of the crystalline structure can be estimated using the Scherrer equation on a specific peak, as shown below:

$$< L >= \frac{K\lambda}{\beta \cos\theta} \tag{2.6}$$

where $< L >$ is a measure of the particles dimensions in the direction perpendicular to the reflecting plane, K the particle shape constant (often set to 1), λ the X-ray wavelength, β the full width at half the maximum of the relevant peak and θ the angle between the beam and the normal on the reflecting plane. However, it is important to note that the Scherrer equation particle size estimate only serves as an approximation and is not always precise. Therefore, the best use of the estimates is for comparing particle sizes of similar catalysts.

The diffraction peaks of perfect crystals are very sharp (large particles), while broader peaks generally indicate smaller particles, but can also be caused by instrumental effects or deformation of the atoms from ideal positions.

2.2.3 Hydrogen-chemisorption

Chemisorption is a method used for determining the dispersion of metal atoms on the catalyst surface. Dispersion is defined as the number of surface atoms in the metal divided by the total number of metal atoms in the catalyst (Holmen, 2002). The gases used in chemisorption are normally H_2, CO, N_2O or O_2. These gases are absorbed on the catalyst surface at increasing pressures and constant temperatures. The determination of the adsorbed species can be found by the Langmuir isotherm. An example of a Langmuir isotherm such as this is shown in figure 2.3.

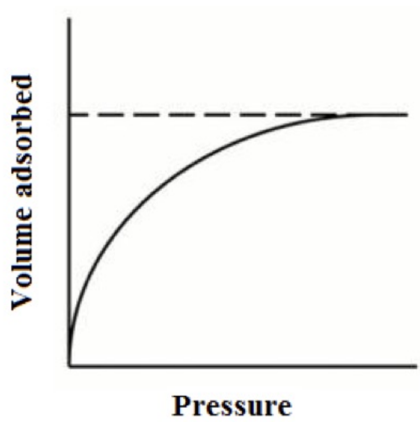

Figure 2.3: Example of a Langmuir isotherm (Goldberg et al., 2007)

The number of adsorbed molecules can be determined by extrapolating back to zero, and the dispersion can be calculated from:

$$D = \frac{v_{\text{ads}} M_m F}{x_m} \tag{2.7}$$

where D is the dispersion, v_{ads} the amount of hydrogen absorbed, M_m the molar mass, F the number of surface atoms covered by one adsorbed molecule and x_m the weight fraction of metal in the catalyst. The v_{ads} can be determined by the equation:

$$v_{\text{ads}} = \frac{V}{V_m} \tag{2.8}$$

where V is the volume absorbed as found in the plot and V_m the volume of one mole of ideal gas at ambient conditions.

Although the Langmuir isotherm is widely used, there are also some limitations as very few chemisorption processes actually follow the Langmuir isotherm. The reason is that real surfaces are heterogeneous, while the Langmuir isotherm assumes a homogeneous surface. Repulsion between neighboring atoms is also neglected in the Langmuir model which is far from reality as well as several types of bonds between absorbed species and the surface.

Some of the common challenges in chemisorption can be that the isotherm does not turn into a linear curve and extrapolation become difficult. In order to account for this, the isotherm is fitted to the Langmuir isotherm to obtain V. Another problem is total adsorption. This happens as not just chemisorption occurs, but also physisorption, and this can be dealt with using the difference between the first total adsorption curve and the second curve obtained after evacuation. The difference between these curves will then show only the strong interactions, i.e., chemisorbed species.

2.2.4 Temperature programmed reduction

Temperature programmed reduction (TPR) is a method used for characterizing metal oxides, alone or on a support (Hurst et al., 1982). The method is based on monitoring a chemical reduction reaction during a linear increase in temperature over time (Chorkendorff and Niemantsverdriet, 2005c). A reactor filled with a catalyst is controlled by a processor, heating the reactor at a rate of 0.1 to $20^{\circ}\mathrm{Cmin}^{-1}$ in a linear manner. Then, a thermal conductivity detector or a mass spectrometer analyzes the composition of the outlet gas. A flow of hydrogen, the reducing agent, diluted in inert argon or nitrogen, is flowed through a catalyst sample at programmed temperatures. Then, the thermal conductivity of the gas stream, time and temperature are monitored, giving information about the total amount of hydrogen reacted, i.e., the degree of reduction. This is measured by a thermal conductivity detector (TCD). The reaction taking place during TPR is illustrated in equation (2.9) and shows how the amount of hydrogen reacted relates to the amount of metal oxides reduced.

$$\mathrm{MxOy} + \mathrm{yH_2} \rightarrow \mathrm{yH_2O} + \mathrm{xM} \tag{2.9}$$

2.2.5 Inductively coupled plasma - mass spectrometry

Inductively Coupled Plasma - Mass Spectrometry (ICP-MS) is an analytical technique used to determine the elemental composition of a sample (Wolf, 2005). The high-temperature ICP source converts the atoms in the sample into ions. Then, the ions are separated and analyzed by the MS. The way in which the ions are produced is by sending a flow of argon gas through the channels of the ICP torch. A radio-frequency (RF) load coil in connection with an RF generator produce oscillating electric and magnetic fields at the end of the ICP torch. Then, as a spark is ignited in the argon flowing through the torch the atoms turn into ions. Subsequently, these ions are trapped in the oscillating fields, causing collisions with other argon ions, creating an argon discharge, or plasma. The sample is then fed to the ICP torch after being converted into an aerosol. As the aerosol sample comes into contact with the plasma the elements turn into gaseous atoms and by the end of the plasma, they are completely ionized. After the sample has been ionized, they are sent to through interface cones that create pressure differences forcing the ions to the MS.

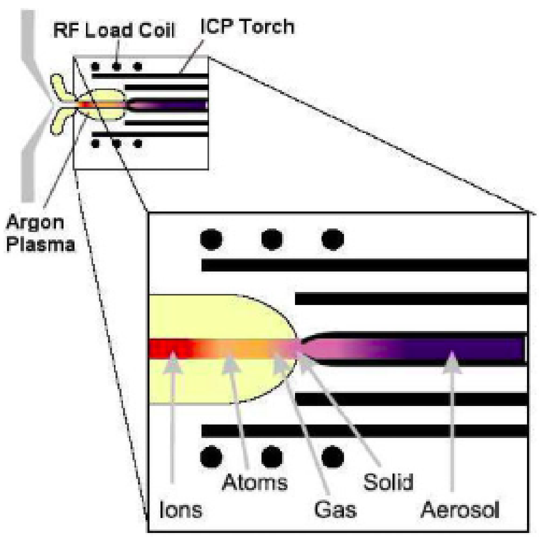

Figure 2.4: The ICP torch displaying its effect of the sample.

2.3 Testing of catalyst

2.3.1 Catalytic activity

There are two terms often used to describe the activity of a Co catalyst, site-time yield (STY) ($\frac{molCO}{molCo \cdot s}$) and turnover frequency (TOF) (Boudart, 1995). These terms were introduced about 70 years ago. The way in which activity normally was reported for heterogeneous catalytic reactions before that time was in terms of arbitrary units such as conversion per unit time at a given temperature. The problem with this way of reporting was that when the areal rates and the number of active sites were excluded from the considerations, the experimental results were impossible to reproduce, even if detailed information about the preparation of catalyst had been provided. STY can be described as ”the number of carbon atoms incorporated into hydrocarbon product molecules per second divided by the total number of surface atoms in the catalyst bed” (Lillebø, 2014). TOF is defined as ”the number of revolutions of the catalytic cycle per unit time” (Boudart, 1995). Therefore, as STY and TOF provide a better scientific foundation they are often preferred. Another way of presenting activity data is per weight of the catalyst, which can be useful in some cases as this proved that cobalt is more active than iron in the catalysis of the FT reaction on weight basis (Gavrilovič, 2018). Another important thing to note is the conversion level of CO. This has a significant effect on the FT reaction rate. As the activity of the FT reaction can be predicted directly from the number of cobalt atoms exposed on the surface, techniques such as CO/H_2-chemisorption, XRD and TEM are useful in order to establish the metal dispersion and predict the catalyst productivity.

2.3.2 Selectivity

The selectivities in the FTS normally included when they are not the main point of investigation can be CH_4-, CO_2-, and C_{5+}-selectivities. The C_{5+}-selectivity will then include all the species except hydrocarbons containing 1, 2, 3, or 4 carbon atoms as well as CO_2.

Chapter 3

Experimental

3.1 Preparation of catalyst

The 20 wt.% Co - 0.5 wt.% Re/$\gamma - Al_2O_3$ catalyst samples in this project were prepared by the incipient wetness impregnation method using mixtures of distilled water and ethylene glycol (EG) in the impregnation solution. These solutions contained, on a mass basis, 40-, 60-, 80-, 95- and 100 wt.% water over EG, which will further be referred to as catalyst CoRe40, CoRe60, CoRe80, CoRe95 and CoRe100, respectively. A 20 wt.% Co - 0.5 wt.% Re/SiO_2 catalyst was also prepared at 100 % water over EG which was called CoRe100-SiO_2. The samples that were post-impregnated with 500 and 1000 ppm K will be further referred to as CoRe80(500ppm), CoRe80(1000ppm), CoRe100(500ppm), CoRe100(1000ppm), and CoRe100(500ppm)-SiO_2 in this section, as these are the nominal values. The catalyst samples were dried and calcined in the same conditions both after initial preparation and after post-impregnation with potassium.

3.1.1 Incipient wetness impregnation

The incipient wetness impregnation (IWI) method was applied for the preparation of all the catalyst samples in this project. The chemicals involved were γ-alumina as support, cobalt nitrate hexahydrate as cobalt precursor, perrhenic acid as rhenium precursor and different solution mixtures of water and ethylene glycol (EG) as IWI solution. Batches of 5-6 g of γ-Al_2O_3, which had been dried for 2 h and sieved to 53-90 µm (for avoiding mass transfer limitations), at impregnation solutions of de-ionized water over EG at 40-, 60-, 80- and 95 wt.% was made. Then, a larger batch of 80- and 100 wt.% water over EG was made for contamination with potassium. First, the liquid absorption capacity of the support material had to be obtained. This point, the IWI point, was found by adding de-ionized water drop by drop onto the support material until it appeared completely saturated. Then, the desired amount of cobalt nitrate hexahydrate and perrhenic acid was mixed in with the different water/EG solutions before being impregnated onto the support. The calculations for the incipient wetness impregnation are shown in appendix C.1. The silica support was first in pellet form so in this case the pellets first had to be crushed in a mortar, sieved to 53-90 µm, calcined at a ramp rate of 5°C/min up to 500°C for 10 h at an air flow of 60-70 mL/min, before being impregnated.

3.1.2 Drying

The samples were prepared in open crystallization beakers, which were subsequently placed inside a ventilated oven at 110°C. The samples were stirred with a glass rod every 15 minutes until they appeared dry. The drying times varied between 1 to 3 h, depending on the weight of the samples, the EG content in the IWI solution and the size of the crystallization beakers.

3.1.3 Calcination

The catalysts were all calcined in an air flow of 60-70 mL/min at 300°C for 16 h in an in-house built calcination setup, as shown in figure 3.1.

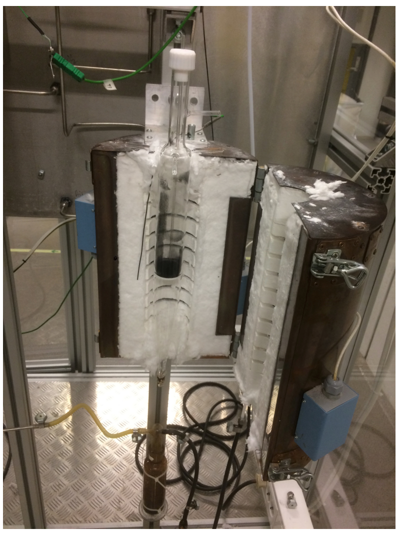

Figure 3.1: The calcination setup with calcinated sample in quartz reactor.

First, the samples were poured into a quartz tube calcination reactor with an inner diameter of 40 mm. The calcination reactors had been thoroughly cleaned before all calcinations. Then, a Teflon lid that had a hole going through it was placed inside the reactor at the "bottleneck", right under the cork, which also had a hole in it. A thin quartz tube was then inserted through the hole in the cork and Teflon lid, reaching right above the catalyst bed. Next, the reactor was placed inside the calcination furnace, as shown in the figure above. Then, a thermocouple was inserted through the hole in the cork and Teflon lid before the furnace was closed. Then, the tube connected to the air mass controller was connected to an opening on the side of the reactor, near the top, while another tube for the outlet was connected to the bottom of the reactor. Finally, a ramping rate of 2 K/min aimed towards a target temperature of 300 °C was set to for 16 h.

3.1.4 Post-impregnation with alkali

The loading of 500 and 1000 ppm K was done using a KNO_3-precursor in a deionized water impregnation solution. The method used for loading the impurities was the incipient wetness impregnation technique, which was described in section 3.1.1. Part of the CoRe80 and CoRe100 catalyst was impregnated with 500 and 1000 ppm K in accord with the calculations in appendix C.2. Finally, the contaminated samples were dried and calcined in the same manner as the other catalysts. The samples will from here on be referred to as CoRe80(500ppm), CoRe80(1000ppm), CoRe100(500ppm) and CoRe100(1000ppm).

3.2 Characterization of catalyst

3.2.1 Nitrogen-physisorption

A Micromeritics TriStar II 3020 apparatus was used for all N_2-physisorption experiments. The catalysts were all physisorbed using nitrogen, providing BET surface area, BJH pore diameter and volume. First, an empty tube reactor was measured. Then, approximately 60 mg catalyst was poured into the empty reactor and then it was weighed again. The reactor was then mounted onto a VacPrep 061 degassing station, where it was first put to vacuum for an hour at room temperature, before being placed with isolation in a furnace at 200°C overnight. The next day the reactor was dismounted from the degassing unit and a cork was quickly inserted. Then, the reactor was weighed before being mounted onto the Micromeritics Tristar II 3020 apparatus. The reactor was lowered into an isolating container containing liquid nitrogen, providing an analysis bath temperature of around -196°C. After the analysis, the reactor was dismounted and a cork was quickly inserted. Finally, the reactor was weighed one last time before it was emptied and cleaned thoroughly. All the weightings were done in order to obtain a more accurate analysis.

3.2.2 X-ray diffraction

A D8 DaVinci-1 X-ray Diffractometer with CuKα radiation was used for all XRD experiments. All the catalysts were tested, providing information about the crystal phases present and estimates of cobalt particle sizes. The catalyst sample was loaded in the grooves of a sample holder before the sample holder was placed in a rack which later went into the XRD apparatus. The actual insertion of the sample holders into the XRD apparatus was done by people responsible for the XRD lab. The analysis was run at 60 min for each catalyst sample, examining a range of 2θ from 10 to 75° at a step size of 0.013° while using X-ray source at 40 kV and 40 mA.

Average particle sizes of Co_3O_4 in the catalysts were estimated using XRD results along with the Scherrer equation, shown in equation (2.6), on the Co_3O_4 peak at 2θ = 36.8°. The assumption that the most intense peak of the (311) phase of Co_3O_4 is sufficient for estimating the particle size with the Scherrer equation was made as well as setting the value of the particle shape constant, K, to 0.89 as this was done by Borg *et al.* Borg et al. (2007). Subsequently, the metallic cobalt particle size was estimated using the relative volume between Co_3O_4 and metallic cobalt, as in equation (3.1) (Schanke et al., 1995).

$$d(\mathrm{Co}^0) = 0.75d(\mathrm{Co_3O_4}) \tag{3.1}$$

3.2.3 Hydrogen-chemisorption

An ASAP 2020 apparatus was used for all H_2-chemisorption experiments. Chemisorption using hydrogen provided information about the catalyst dispersion and particle size. First, a cleaned u-tube quartz reactor was filled with a bit of hand-rolled quartz wool. Then, approximately 200 mg catalyst was poured on top of the quartz wool before another piece of hand-rolled quartz was placed over the catalyst in the reactor, to keep it in place. The filled reactor was then weighed before being cleaned with ethanol on the connection points for leakage prevention. Next, the connections and O-rings for the ASAP 2020 unit was cleaned using ethanol. The reactor was mounted onto the ASAP 2020 apparatus, a thermocouple was placed close to the catalyst bed, and a furnace was raised, isolating the reactor. Then, the reactor was first evacuated at 60°C at a rate of 10°C/min. A leak test was then performed. Then, a flow of H_2 was sent through the reactor at 350°C at a rate of 1°C/min for 600 min. Next, the reactor was evacuated and subsequently leak tested before analysis in a H_2-flow at 40°C at a rate of 10°C/min. After the analysis, helium gas flowed through the reactor in order to obtain atmospheric pressures. The furnace was then lowered and the reactor was dismounted. Subsequently, the reactor was weighed before being emptied and cleaned thoroughly. The weightings were done in order to obtain a more accurate analysis.

The cobalt dispersion was found using H_2-chemisorption results and equation (2.7) under the assumption that two cobalt surface atoms were covered by one hydrogen molecule, F=2. The particle sizes were estimated using equation (3.2) under the assumption that the particles were of spherical geometry and uniform site density of 14.6 atoms per nm^2 (Jones and Bartholomew, 1988).

$$d(\mathrm{Co}^0) = \frac{96.2}{D} \tag{3.2}$$

In equation (3.2), d is the mean particle size of Co_3O_4 (nm) and D the dispersion (%).

3.2.4 Temperature programmed reduction

A BenchCat Hydrid apparatus was used for all the temperature programmed reduction (TPR) experiments. All the catalysts were tested, providing information about the temperatures at which Co_3O_4 is reduced to CoO and CoO to Co. First, a cleaned u-tube quartz reactor was filled with a bit of hand-rolled quartz wool. Then, approximately 100 mg catalyst was poured on top of the quartz wool, before another piece of hand-rolled quartz was placed over the catalyst for keeping the sample in place. The connection points of the filled reactor were then cleaned with acetone for leakage prevention. If the dryerite in the water trap had not been changed during the previous 3 experiments, this was changed using 1 g of fresh dryerite. The reactor was then mounted onto the BenchCat Hydrid apparatus so that the thermocouple resided right above the catalyst bed. Next, a flow of inert gas was used in order to check for stable flow through the reactor. Then, a flow of 7%H_2/Ar flowed through the reactor and a hydrogen detector was used to check for leaks. Then, the analysis was started, using hydrogen in the analysis from ambient temperatures to 650°C. Finally, the reactor was dismounted, emptied and cleaned thoroughly.

3.2.5 ICP-MS

These tests were performed by Syverin Lierhagen, Senior Engineer at the Department of Chemistry. This elemental analysis provided information about the actual loading of Co, Re, K, and Na in the catalyst samples. The catalyst samples were delivered in amounts of 10-20 mg. A solution of 1.5 mL of concentrated HCl, 0.5 mL of concentrated HNO_3, and 0.5 ml of concentrated HF was used to dissolve the samples.

3.3 Testing of catalyst

3.3.1 Fischer-Tropsch Synthesis

The Fischer-Tropsch synthesis was carried out in a 10 mm ID steel tube fixed bed reactor at 210°C, 20 bars and a H_2/CO ratio of 2.1. The samples (1 g) were diluted with inert SiC (20 g, particle size 53-90μm) to improve isothermal conditions along the catalyst bed, loaded over a grid and between quartz wool wads to keep catalyst in place. The reduction was done in-situ in 250 mL/min of H_2. A eurotherm was used to program the ramping rate of 1°C/min up to 350°C, a temperature that was kept for 10 h. Then, after pressurization up to 20 bar, a 250 mL/min flow of syngas containing 31.3 % CO and 3 % N_2 in H_2 was started along with the temperature ramping up to 210°C at a rate of first 20°C/h up to around 205°C, then up to 210°C at a ramping rate of 5°C/h. The reactor setup in the furnace is illustrated in figure 3.2. showing the fixed bed reactor connected to the inlet (location 1) and outlet (location 2) of the Fischer-Tropsch setup. The reactor resides inside the furnace and the flow of syngas enters at the top and product exit at the bottom. The viscous product enter the boiler which in the illustration is hidden by isolation in location 3, while the gas products follow the pipe shown in location 4 before entering the gas chromatograph for product analysis. A flow chart for the whole experimental setup is shown in figure 3.3. Information about the processing of the data is shown in appendix D.5 and calculation procedure in appendix C.3. The GC used for processing the product gases is of the type Agilent Technologies 6890N Network GC System. The STY values were extracted after 24 h on stream, while the selectivities were extracted after 30-45 h on stream at CO conversions around 50 %.

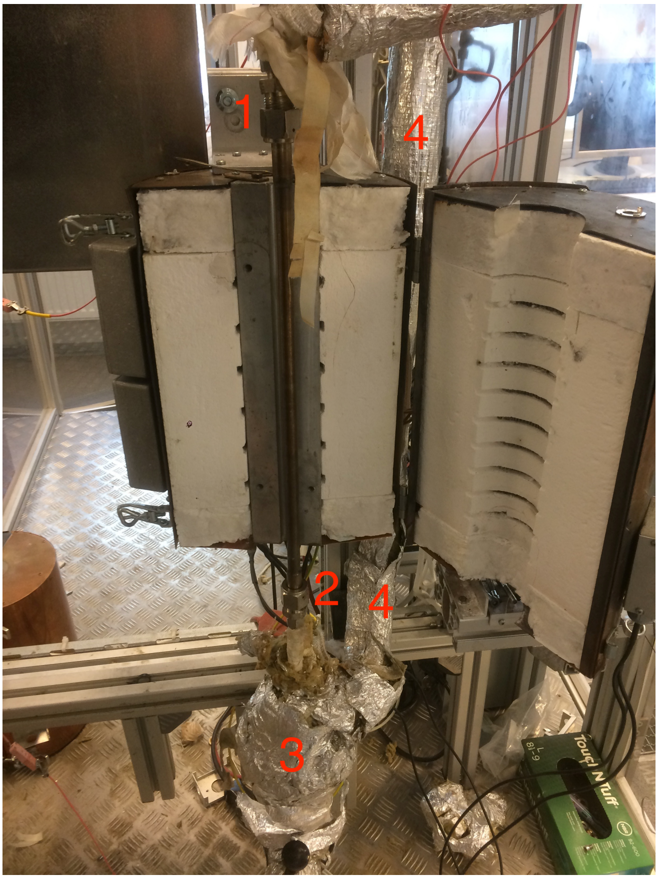

Figure 3.2: Illustration of fixed bed reactor setup in the FT rig.

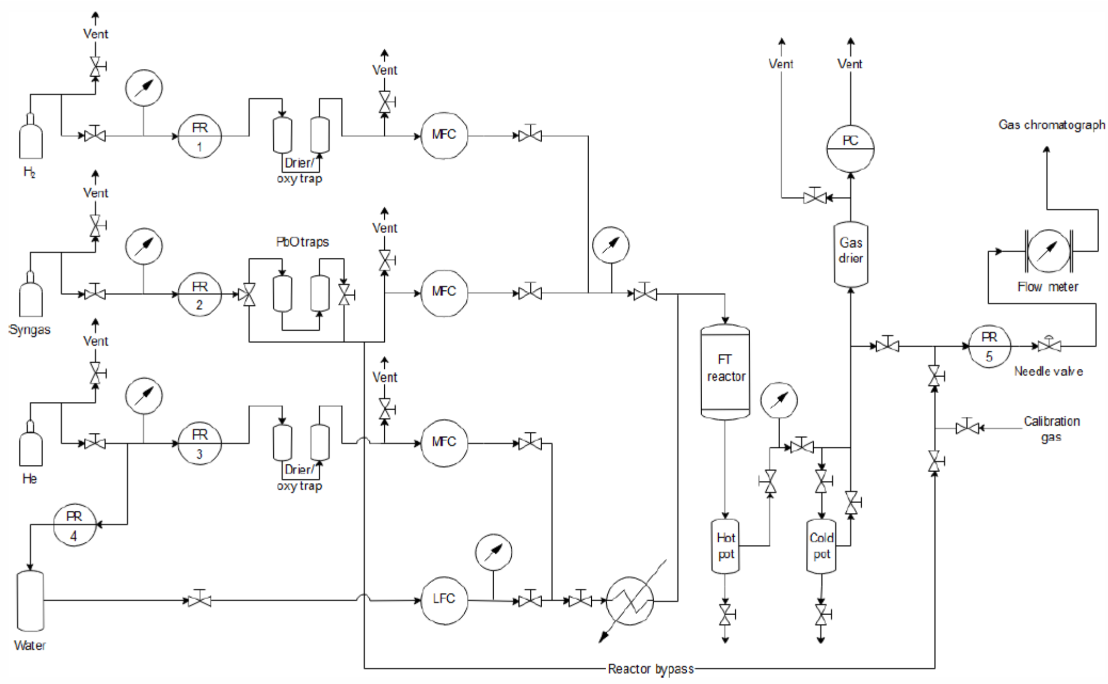

Figure 3.3: Flow chart of experimental Fischer-Tropsch synthesis setup. PR = pressure regulator, MFC = mass-flow controller, LFC = liquid-flow controller, PC = pressure controller. Obtained from the doctoral thesis of Eirik Ø. Pedersen (Pedersen, 2018).

Chapter 4

Results

4.1 Characterization results

4.1.1 ICP-MS

Elemental analysis was performed through inductively coupled plasma - mass spectrometry (ICP-MS). The results from the analysis are given in table 4.1. The obtained composition of the active material was confirmed by ICP-MS results, shown in table 4.1, as the nominal values 20 wt.% Co and 0.5 wt.% Re were matched pretty well with a small deviation of maximum ± 1.74 and ± 0.15 wt.%, respectively. The obtained levels of K on each catalyst is close to the nominal values aimed for, with maximum deviations of ± 51 ppm for 500 ppm and -114 for 1000 ppm. As the catalysts supported by SiO_2 contained significant amounts of Na, Na contents were also included in the table. From here on the catalyst names will be referred to according to the K loading found in this measurement.

4.1.2 Nitrogen-physisorption

N_2-physisorption experiments provided surface areas based on the BET model as well as average pore diameters and pore volumes based on the BJH model. For the catalysts examined, shown in table 4.2, no significant changes in the above-mentioned properties can be reported after addition of ethylene glycol (EG) in the impregnation solution nor after contamination of K. Raw data are provided in appendix D.1

Catalyst	Co [%]	Re [%]	K [ppm]	Na [ppm]
CoRe80(15ppm)	19.6	0.43	15	61
CoRe80(471ppm)	21.74	0.51	471	64
CoRe80(886ppm)	20.04	0.43	886	70
CoRe100(6ppm)	N/A[a]	N/A[a]	6	37
CoRe100(551ppm)	N/A[a]	N/A[a]	551	24
CoRe100(902ppm)	19.6	0.35	902	66
CoRe100(68ppm)-SiO_2	20.81	0.5	68	592
CoRe100(526ppm)-SiO_2	19.59	0.51	526	540

Table 4.1: ICP-MS results providing Co, Re, K, and Na loadings. [a]The reason for the missing results is that the experiment had to be run twice as the catalyst material did not fully dissolve on the first run, and were forgotten on the second run. However, CoRe100(902ppm) and CoRe100(551ppm) both originate from CoRe100(6ppm) and the loadings of Co and Re are therefore most likely the same for all three catalysts.

Catalyst	A_{sp}[a] [m^2/g]	Average pore diameter[b] [nm]	Pore volume[b] [cm^3/g]
γ-Al_2O_3(Dried)	157[A]	14.0[A]	0.63[A]
SiO_2(Calcined)	155	11.6	0.52
CoRe80(15ppm)	143	12.2	0.52
CoRe80(471ppm)	143	12.4	0.53
CoRe80(886ppm)	152	10.6	0.48
CoRe100(6ppm)	145	13.7	0.6
CoRe100(551ppm)	137	12.2	0.46
CoRe100(902ppm)	137	12.4	0.47

[a]Based on BET model
[b]Based on BJH model
[A]The average of two experiments

Table 4.2: Specific surface area, A_{sp}, pore diameter and pore volume estimated through the BET- and BJH model and N_2-physisorption experiments.

4.1.3 XRD

The particle size of Co_3O_4 and Co particles were estimated by XRD measurements. The estimated particle sizes are listed in table 4.3 and show a distinct decrease upon increased (EG) concentration in the impregnation solution. The particle sizes did not change upon the addition of potassium for CoRe80(15ppm), CoRe100(6ppm) or CoRe100(68ppm)-SiO_2, as illustrated in figure 4.4, 4.3 and 4.5, respectively. The XRD profiles are all illustrated in figures 4.1, 4.2, 4.3, 4.4 and 4.5, proving the existence of cubic Co_3O_4, γ-Al_2O_3 and as no signals of SiO_2 were seen, it is most likely amorphous. All the Co_3O_4

peaks increased upon increased EG content in impregnation solution are broadened and less pronounced, while the γ-Al_2O_3 peaks become sharpened and more pronounced.

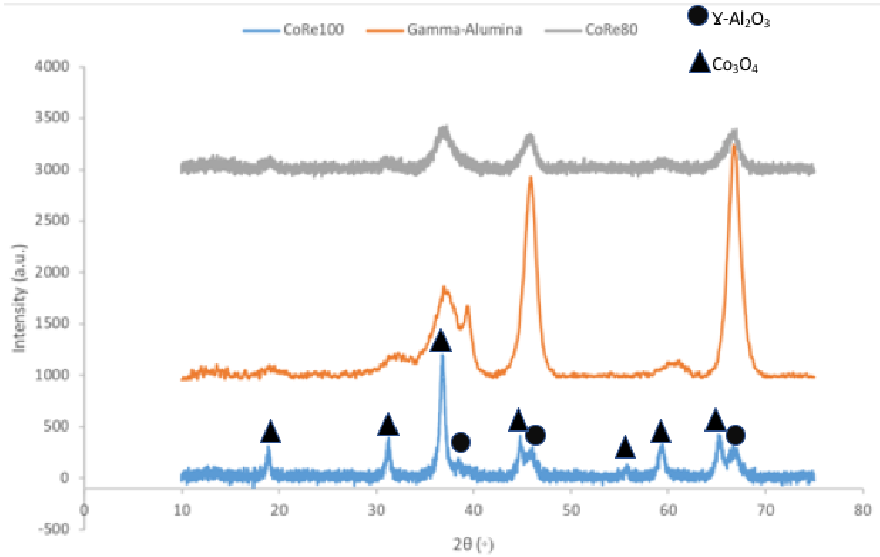

Figure 4.1: XRD results for CoRe80(15ppm), γ-Al_2O_3 and CoRe100(6ppm).

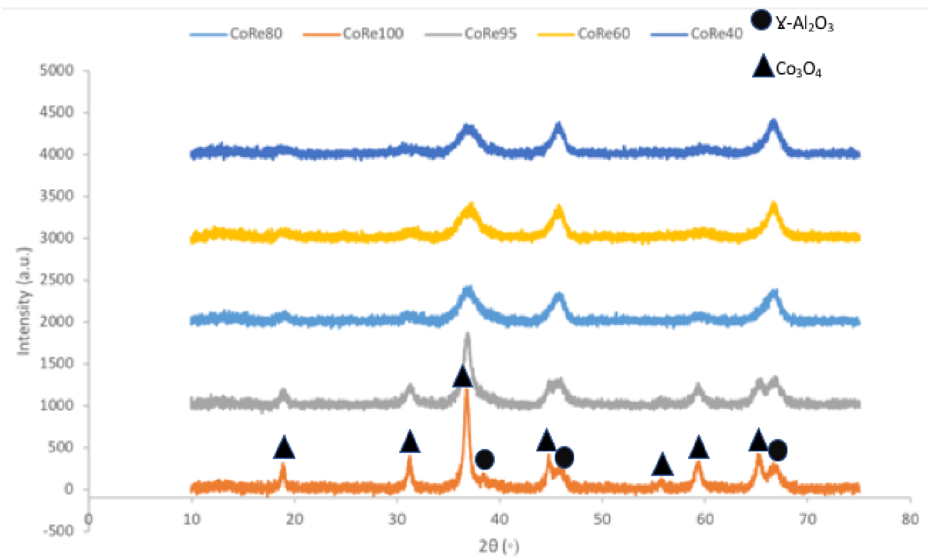

Figure 4.2: XRD results for CoRe40, CoRe60, CoRe80(15ppm), CoRe95 and CoRe100(6ppm).

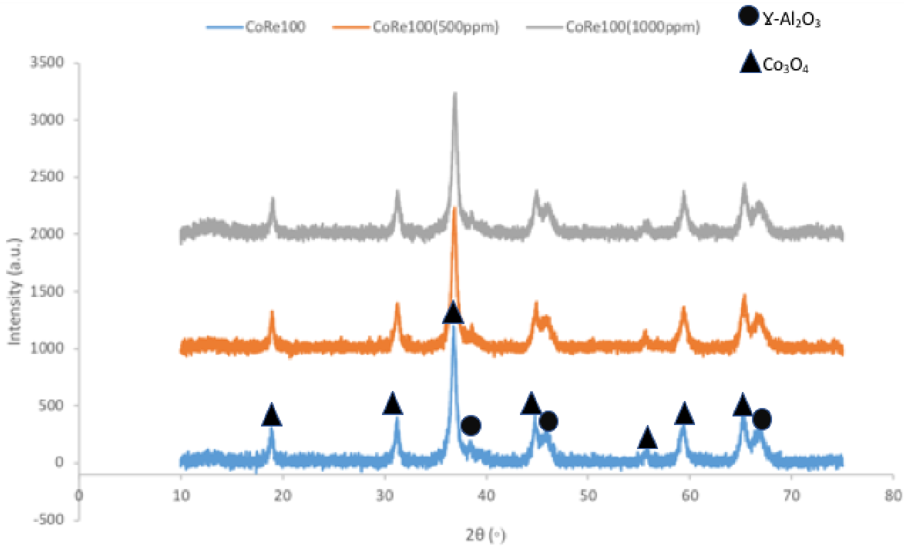

Figure 4.3: XRD results for CoRe100(6ppm), CoRe100(551ppm) and CoRe100(902ppm).

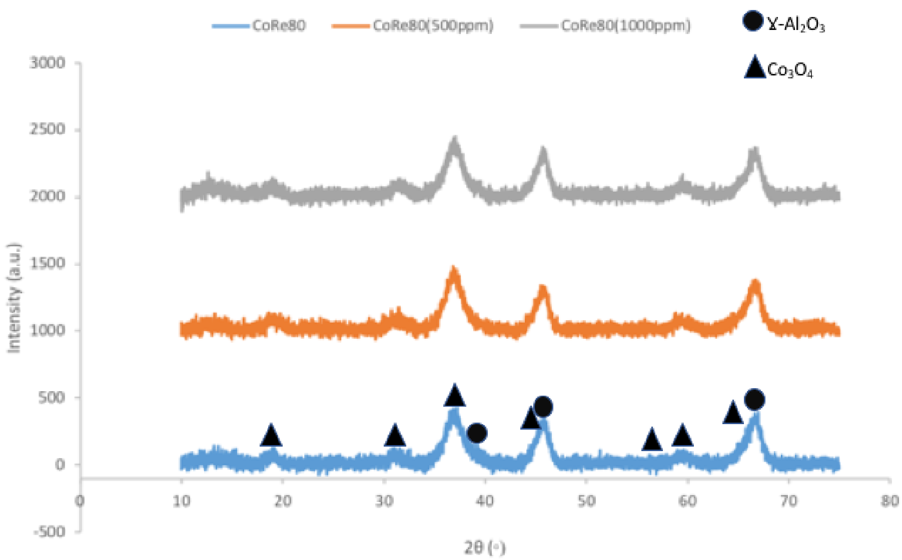

Figure 4.4: XRD results for CoRe80(15ppm), CoRe80(471ppm) and CoRe80(886ppm).

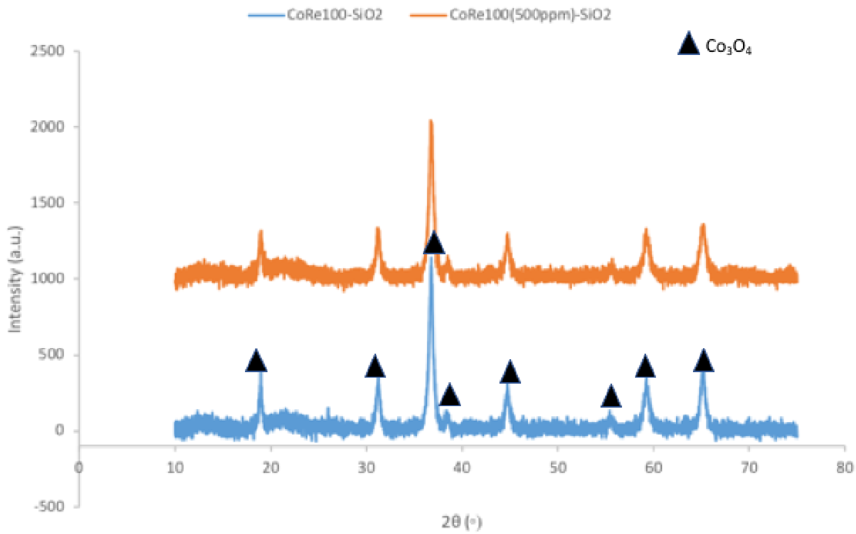

Figure 4.5: XRD results for CoRe100(68ppm)-SiO_2 and CoRe100(526ppm)-SiO_2.

4.1.4 Hydrogen-chemisorption

The dispersion and particle size results found through H_2-chemisorption are provided in table 4.3. Raw data are provided in appendix D.2. There is a clear increase in dispersion upon increased EG in the impregnation solution, indicating smaller Co particles on the surface. The dispersions are not significantly changed after contamination of 500 ppm K on CoRe100(68ppm)-SiO_2 nor after contamination of 500 and 1000 ppm K on CoRe100(6ppm) or CoRe80(15ppm). The Co^0 particle sizes estimated from XRD measurements and H_2-chemisorption measurements are different but have the same trend.

4.1.5 TPR

The TPR profiles are shown in figure 4.6, 4.7, 4.8 and 4.9. TPR profiles showing the reproducibility of CoRe100 and CoRe80 can be found in appendix D.3. The small first peak visible for some of the catalysts in figure 4.6 represent the reduction and removal of residual nitrates from the cobalt precursor. The second peak represents the reduction from Co_3O_4 to CoO. The third peak represents the reduction from CoO to Co^0. As can be seen from figure 4.6, the reduction temperature of the reaction from Co_3O_4 to CoO was slightly decreased upon an increased concentration of EG in impregnation solution, i.e., decreased particle size. However, it should be mentioned that this deviation is small and could be subject to experimental error. The reduction from CoO to Co^0 clearly occur

Catalyst	D^a [%]	$d(Co^0)^a$ [nm]	$d(Co_3O_4)^b$ [nm]	$d(Co^0)^b$ [nm]
CoRe40	13.3	7.2	3.7	2.8
CoRe60	14.1	6.8	3.9	2.9
CoRe80(15ppm)	15.6^B	6.2^B	4.9	3.7
CoRe95	10.1	9.5	9.0	6.8
CoRe100(6ppm)	7.7^A	12.5^A	14.8	11.1
CoRe80(471ppm)	14.3^A	6.7^A	4.6	3.5
CoRe80(886ppm)	15.1	6.4	4.8	3.6
CoRe100(551ppm)	7.7	12.5	15.0	11.3
CoRe100(902ppm)	7.3	13.3	17.2	12.9
CoRe100(68ppm)-SiO_2	8.0	12.1	18.8	14.1
CoRe100(526ppm)-SiO_2	7.6	12.7	17.6	13.2

[a]Found by H_2-chemisorption experiments
[b]Found by XRD experiments
[A]The average of two experiments
[B]The average of three experiments

Table 4.3: Cobalt dispersion, D, and particle size of metallic Co, $d(Co^0)$ were estimated by H_2-chemisorption experiments, (3.2). The Co_3O_4 particle size estimates through XRD measurements and the Scherrer equation are denoted $d(Co_3O_4)$, and the particle size of metallic Co, $d(Co^0)$, were estimated via $d(Co_3O_4)$ and assumptions about the relative molar volumes between Co_3O_4 and Co^0.

at a higher temperature for smaller particles, as CoRe40, CoRe60, CoRe80 and CoRe95 all reside at around 500°C while CoRe100 reside slightly above 400°C. The profiles in figure 4.7, 4.8 and 4.9 all display a slight increase in reduction temperature for both reduction from Co_3O_4 to CoO and from CoO to Co^0, at varying degrees. Here as well it should be mentioned that the error is very small and could be due to experimental error.

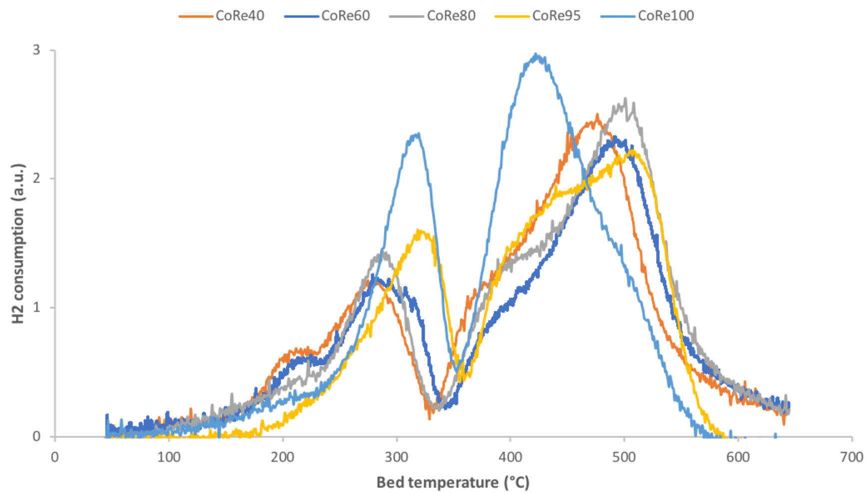

Figure 4.6: TPR curves of CoRe40, CoRe60, CoRe80, CoRe95 and CoRe100.

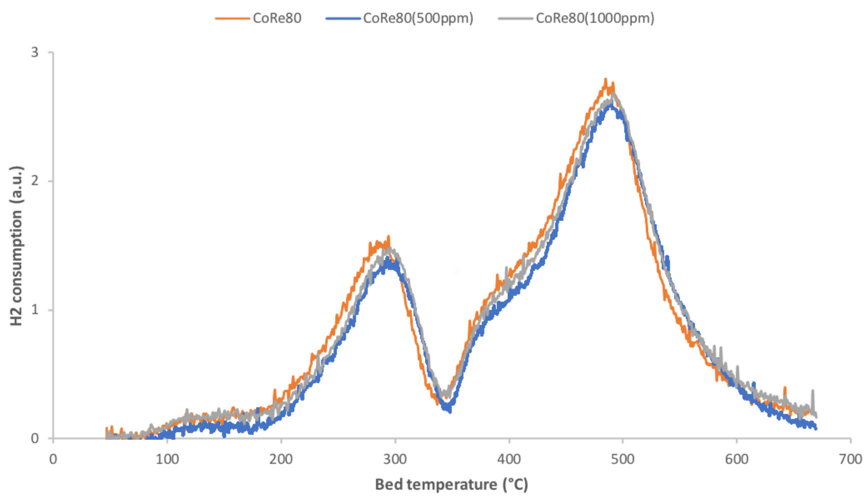

Figure 4.7: TPR curves of CoRe80, CoRe80(471ppm) and CoRe80(886ppm).

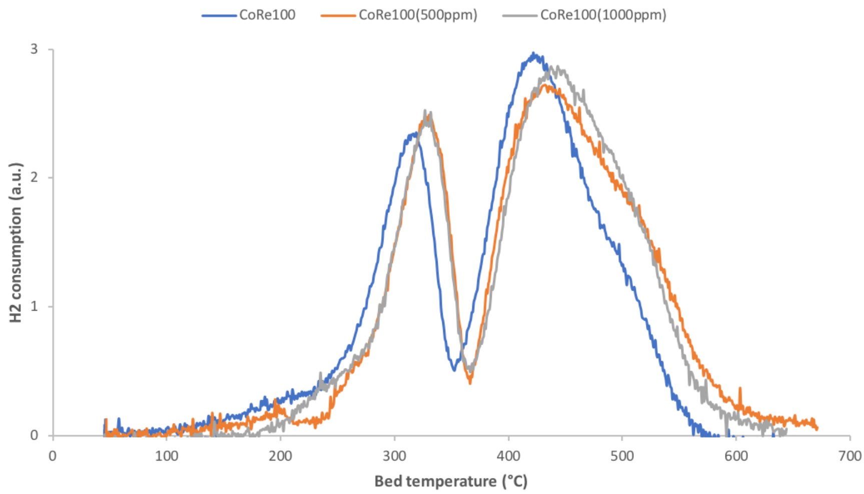

Figure 4.8: TPR curves of CoRe100, CoRe80(551ppm) and CoRe100(1000ppm).

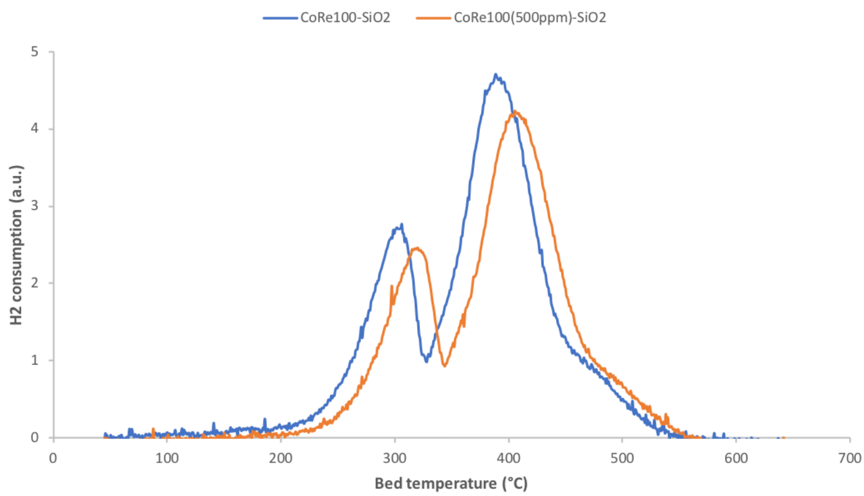

Figure 4.9: TPR curves of CoRe100-SiO_2 and CoRe80(551ppm)-SiO_2.

4.2 Fischer-Tropsch synthesis results

The activity and selectivity results are summarized in table 4.4. The activity is presented as site time yield (STY) (s^{-1}). Additional presentation of this data can be found in appendix D.4.

Catalyst	STY $\times 10^3 [s^{-1}]$	C_{5+}-selectivity [%]	CH_4-selectivity [%]	CO_2-selectivity [%]
CoRe100(6ppm)	54	85.4	7.3	0.16
CoRe100(551ppm)	41	86.6	6.8	0.23
CoRe100(902ppm)	39	86.3	6.7	0.4
CoRe80(15ppm)	27	79.3	10	0.23
CoRe80(471ppm)	22	83.1	9.5	0.39
CoRe80(886ppm)	19	81	9.2	0.55

Table 4.4: STY results after 24 h on stream and selectivity results after 30-45 h on stream at CO conversions around 50 %.

Figure D.36 illustrate the normalized decrease in activity upon increased contamination of catalyst with K. The catalyst containing small Co particles on the surface, CoRe80, decrease at a slightly lower rate than the catalyst containing medium Co particles, CoRe100, after contamination of around 500 ppm K. However, as the catalysts are contaminated from around 500 ppm to around 1000 ppm, CoRe80 display a slightly steeper curve than CoRe100, indicating a slightly more severe deactivation.

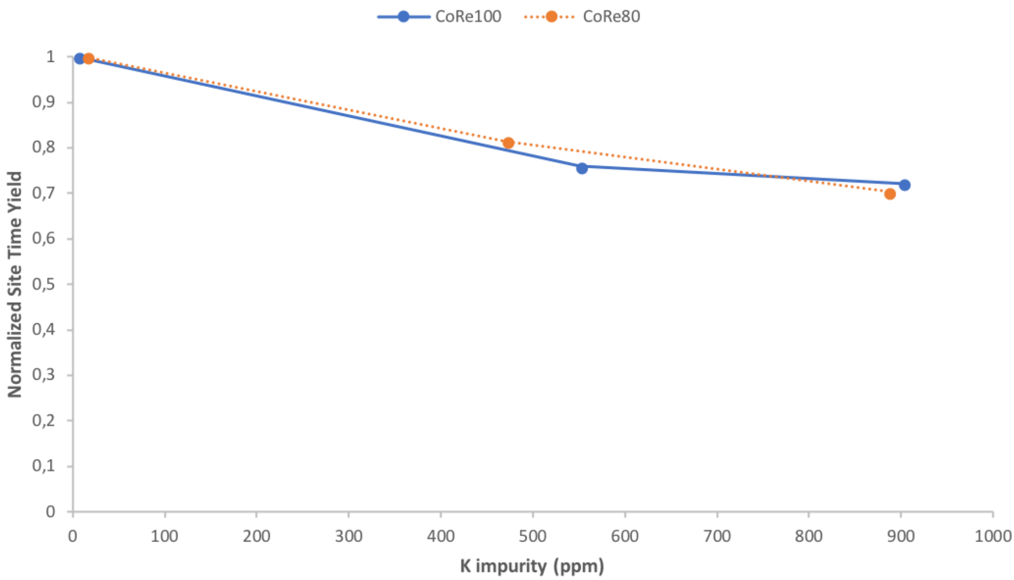

Figure 4.10: Normalized Site Time Yield (STY) after 24 h on stream (TOS) at different K loadings on CoRe100(6ppm) and CoRe80(15ppm).

Chapter 5

Discussion

5.1 Particle size effects

The cobalt particle size was successfully altered without changing the composition of the active material, nor the physical properties of the support material. The XRD results showed that cobalt was present on the calcined catalysts as cubic Co_3O_4, that γ-Al_2O_3 was present on the catalysts with this support, and that amorphous SiO_2 was on the catalysts with this support, after calcination. The ICP-MS results confirmed the loadings of Co, Re, and K on all catalysts. Both the XRD and H_2-chemisorption experiments provide particle size estimates of Co^0 that clearly decrease upon increased EG content of impregnation solution. This further proves the validity of the method used by other authors in the past (Yang et al., 2010; Borg et al., 2008).

The TPR profiles in figure 4.6 all show similar reduction of Co_3O_4 to CoO and CoO to Co^0, but the peaks are shifted. The second peak of the catalysts with smaller particles shift towards slightly lower temperatures, except for CoRe95, while the third peak shift towards significantly higher temperatures. These results indicate a more difficult reduction to the metallic cobalt, which is necessary for obtaining active sites for FT synthesis. A lower degree of reduction have also been reported for cobalt-based FT catalysts of similar particle sizes in previous literature (Yang et al., 2010; Borg et al., 2008; Khodakov et al., 2002). Borg *et al.* reported that the reduction of Co_3O_4 to CoO is independent of cobalt particle size, while a dependence was seen for the reduction of CoO to Co^0 (Borg et al., 2007). This trend is to some extent seen here as well if the reduction deviation of the first peaks is within the error margin of the experiment. The peaks of CoRe40, CoRe60, CoRe80(15ppm) and CoRe95 are clearly broader than the peaks of CoRe100(6ppm). Borg *et al.* previously ascribed this phenomenon to a larger spread in the particle size distribution, as this would indicate a large variation in the degree of interaction between particles and the support, creating shoulders on the reduction peaks (Borg et al., 2007). However, Borg *et al.* later reported that increased EG concentrations lead to more uniformly distributed particles, which is contradictory to the previous statement (Borg et al., 2008). In order to shed more light on the actual particle size distribution, techniques such as TEM could be applied in the future.

Because the catalysts of small particle sizes are clearly harder to reduce, and because the metallic cobalt available is directly proportional to the activity, the dramatic decrease in activity and change in selectivity can be assumed to be at least partially explained by these results. However, the results in this thesis work do not disprove any of the other theories such as a combination of CO-induced surface reconstruction and non-classical structure sensitivity (Bezemer et al., 2006), re-oxidation of metallic cobalt at relevant FT conditions (Wang et al., 2012; Azzam et al., 2014; Fischer et al., 2014) and loss of necessary sites (Ralston et al., 2017; van Helden et al., 2016).

5.2 Potassium effects

500 and 1000 ppm K was successfully added to CoRe100(6ppm) and CoRe80(15ppm), which was confirmed by the ICP-MS. None of the characterization results applied in this work indicated any significant changes of the catalyst upon addition of K, similar to previous literature (Trépanier et al., 2009; Balonek et al., 2010; Eliseev et al., 2013; Borg et al., 2011; Lillebø et al., 2013; Gavrilović et al., 2018). Some of these reports mentioned a slight increase in reduction temperatures, which was seen in CoRe100(68ppm)-SiO_2 to CoRe100(551ppm)-SiO_2 as well, but the deviation is small and as the other profiles show no significant change upon K addition, it is hard to conclude with certainty.

On the other hand, the catalytic performance was dramatically impacted. The C_{5+}-selectivity showed an overall increase for small and medium particles contaminated, but here the results waver, which makes it difficult to confirm whether a significant increase has taken place or not. The CH_4-selectivity and CO_2-selectivity however, portray clear decreasing and increasing trends, respectively, both for small and medium particles. The activity also decreases severely upon increased K loading. These changes in catalytic performance are consistent with previous literature (Trépanier et al., 2009; Balonek et al., 2010; Eliseev et al., 2013; Borg et al., 2011; Lillebø et al., 2013; Gavrilović et al., 2018). One possible explanation as to why the catalytic performance is changed so drastically upon potassium addition is the mobile nature of potassium, allowing it to potentially locate itself onto important catalytic sites (Trépanier et al., 2009; Lillebø et al., 2013; Gavrilović et al., 2018). Another theory is potassium-induced electronic effects, decreasing the concentration of surface H and increasing the CO adsorption and dissociation (Balonek et al., 2010; Borg et al., 2011). None of these theories are disproven by the results found in this thesis work.

5.3 Effect of potassium on catalysts of different cobalt particle sizes

The effect of potassium on Co based FT catalysts was examined on two different particle sizes of cobalt, small and medium. As far as the author is aware, there is no previous literature examining this particular situation. The results presented in figure D.36 indicate no difference in the way medium particles are affected by potassium impurities compared to small particles, and it is therefore suggested that the deactivation mechanism is due to something other than geometric effects. However, in order to be certain of this, investigations of larger particles should also be performed. The theories saying that the effect could be a result of the more specific positioning of mobile potassium species on active FT sites, or of electronic effects induced by potassium, are not disproven by this thesis work. The hypothesis that smaller particles would be more severely deactivated by potassium can be regarded as disproved. This could indicate that the important sites for FT activity are the terrace sites and not the step, kink or edge sites.

Chapter 6

Summary and Conclusion

The effect of K on a 20 wt.% Co - 0.5 wt.% Re/γ-Al_2O_3 catalyst consisting of small and medium cobalt particle sizes were investigated. The particle sizes were adjusted by using different mixtures of ethylene glycol (EG) and deionized water in the impregnation solution. The mass percentages 40-, 60-, 80-, 95-, and 100 %, of water over EG were prepared. The catalysts were initially denoted CoRe40, CoRe60, CoRe80(15ppm), CoRe95 and CoRe100(6ppm). As CoRe40 and CoRe60 showed similar reduction temperatures in TPR measurements, similar Co- and Co_3O_4 particle size estimates in H_2-chemisorption- and XRD measurements as CoRe80(15ppm), and as time was limited, they were not studied in terms of catalytic activity. The catalysts CoRe95, CoRe100(68ppm)-SiO_2 and CoRe100(526ppm)-SiO_2 were not chosen for further activity measurements either mainly due to time limitations.

Decreased cobalt particle sizes lead to a clear decrease in catalytic activity, C_{5+}-selectivity, and an increase in CH_4- and CO_2-selectivity. These effects are ascribed to the lower reducibility of smaller cobalt particles, induced by metal-support interactions. Potassium contaminations lead to severely decreased activities, possibly increased C_{5+}-selectivities, and clear decrease in CH_4- and CO_2-selectivities. These effects are harder to explain but could be because of the more specific positioning of mobile potassium species on active FT sites, or of electronic effects induced by potassium. No difference was seen in the effect of potassium on small particles compared to on medium particles. Therefore, as the hypothesis put forth at the beginning of this work was that smaller particles would be more severely deactivated by potassium is disproved. This could indicate that the important sites for FT activity are not step, kink, or edge sites, but perhaps terrace sites.

Chapter 7

Future work

The deactivation rate of potassium was the same for cobalt catalysts of particle sizes in the range 11.1-12.5 and 3.7-6.2 nm, which perhaps indicate that the FT reaction is not as active at the step edges as first proposed. In order to gain more insight on this subject, it could be beneficial to look at larger particle sizes as well, as these expose more flat surfaces and could give even clearer indications of which sites exhibit the best FT reactivity. The authors recommendation for increasing the particle size is the use of γ-Al_2O_3 with larger average pore diameters than 12-14 nm, as the pore diameter determines the maximum size of the main bulk of the cobalt particles. While on the subject of support material it should be mentioned that the use of SiO_2, TiO_2 or carbon nanofibers could be a better suited support for the comparison of particle size versus potassium effects. These all have weaker metal-support interactions compared to γ-Al_2O_3, which means that the effect of lowered reducibility of small cobalt particles to some degree would be eliminated.

Increased use of density functional theory studies in the investigation of potassium effects on cobalt could shed more light on the subject of potassium deactivation. However, it would also be interesting to see such studies on the deactivation on cobalt from other alkali species as well, as this perhaps could give more clarity on whether the effects are of a more electronic or specific site blocking nature.

Bibliography

Ail, S. S. and Dasappa, S. (2016). Biomass to liquid transportation fuel via fischer tropsch synthesis–technology review and current scenario. *Renewable and sustainable energy reviews*, 58:267–286.

Alam, F., Mobin, S., and Chowdhury, H. (2015). Third generation biofuel from algae. *Procedia Engineering*, **105**:763–768.

Azzam, K., Jacobs, G., Ma, W., and Davis, B. H. (2014). Effect of cobalt particle size on the catalyst intrinsic activity for fischer–tropsch synthesis. *Catalysis letters*, 144(3):389–394.

Balonek, C. M., Lillebø, A. H., Rane, S., Rytter, E., Schmidt, L. D., and Holmen, A. (2010). Effect of alkali metal impurities on co–re catalysts for fischer–tropsch synthesis from biomass-derived syngas. *Catalysis Letters*, **138**(1-2):8–13.

Barrett, E. P., Joyner, L. G., and Halenda, P. P. (1951). The determination of pore volume and area distributions in porous substances. i. computations from nitrogen isotherms. *Journal of the American Chemical Society*, **73**(1):373–380.

Bartholomew, C. H. (2003). History of cobalt catalyst design for fts. In *Proceedings of the National Spring Meeting of the American Institute of Chemical Engineers (AIChE'03)*.

Bezemer, G., Van Laak, A., Van Dillen, A., and De Jong, K. (2004). Cobalt supported on carbon nanofibers-a promising novel fischer-tropsch catalyst. In *Studies in Surface Science and Catalysis*, volume **147**, pages 259–264. Elsevier.

Bezemer, G. L., Radstake, P., Falke, U., Oosterbeek, H., Kuipers, H., Van Dillen, A., and De Jong, K. (2006). Investigation of promoter effects of manganese oxide on carbon nanofiber-supported cobalt catalysts for fischer–tropsch synthesis. *Journal of Catalysis*, **237**(1):152–161.

Borg, Ø., Dietzel, P. D., Spjelkavik, A. I., Tveten, E. Z., Walmsley, J. C., Diplas, S., Eri, S., Holmen, A., and Rytter, E. (2008). Fischer–tropsch synthesis: cobalt particle size and support effects on intrinsic activity and product distribution. *Journal of Catalysis*, **259**(2):161–164.

Borg, Ø., Eri, S., Blekkan, E. A., Storsæter, S., Wigum, H., Rytter, E., and Holmen, A. (2007). Fischer–tropsch synthesis over γ-alumina-supported cobalt catalysts: effect of support variables. *Journal of Catalysis*, **248**(1):89–100.

Borg, Ø., Hammer, N., Enger, B. C., Myrstad, R., Lindvåg, O. A., Eri, S., Skagseth, T. H., and Rytter, E. (2011). Effect of biomass-derived synthesis gas impurity elements on cobalt fischer–tropsch catalyst performance including in situ sulphur and nitrogen addition. *Journal of Catalysis*, **279**(1):163–173.

Boudart, M. (1995). Turnover rates in heterogeneous catalysis. *Chemical Reviews*, 95(3):661–666.

Chen, Q., Svenum, I.-H., Qi, Y., Gavrilovic, L., Chen, D., Holmen, A., and Blekkan, E. A. (2017). Potassium adsorption behavior on hcp cobalt as model systems for the fischer–tropsch synthesis: a density functional theory study. *Physical Chemistry Chemical Physics*, 19(19):12246–12254.

Chorkendorff, I. and Niemantsverdriet, J. (2005a). Solid catalysts. *Concepts of Modern Catalysis and Kinetics*, pages 167–214.

Chorkendorff, I. and Niemantsverdriet, J. (2005b). Solid catalysts. *Concepts of Modern Catalysis and Kinetics*, pages 343–352.

Chorkendorff, I. and Niemantsverdriet, J. (2005c). Solid catalysts. *Concepts of Modern Catalysis and Kinetics*, pages 129–172.

Dayton, D. C., Belle-Oudry, D., and Nordin, A. (1999). Effect of coal minerals on chlorine and alkali metals released during biomass/coal cofiring. *Energy & Fuels*, **13**(6):1203–1211.

Den Breejen, J., Radstake, P., Bezemer, G., Bitter, J., Frøseth, V., Holmen, A., and Jong, K. d. (2009). On the origin of the cobalt particle size effects in fischer- tropsch catalysis. *Journal of the American Chemical Society*, 131(20):7197–7203.

Dry, M. E. (2002). The fischer–tropsch process: 1950–2000. *Catalysis Today*, **71**(3-4):227–241.

Eilers, J., Posthuma, S., and Sie, S. (1990). The shell middle distillate synthesis process (smds). *Catalysis Letters*, **7**(1-4):253–269.

Eliseev, O., Tsapkina, M., Dementeva, O., Davydov, P., Kazakov, A., and Lapidus, A. (2013). Promotion of cobalt catalysts for the fischer-tropsch synthesis with alkali metals. *Kinetics and Catalysis*, **54**(2):207–212.

Fischer, N., Clapham, B., Feltes, T., and Claeys, M. (2014). Cobalt-based fischer–tropsch activity and selectivity as a function of crystallite size and water partial pressure. *ACS Catalysis*, 5(1):113–121.

Gavrilovič, L. (2018). Fischer-tropsch synthesis - influences of aerosol - deposited potassium salts on activity and selectivity of co based catalysts.

Gavrilović, L., Brandin, J., Holmen, A., Venvik, H. J., Myrstad, R., and Blekkan, E. A. (2018). Fischer-tropsch synthesis–investigation of the deactivation of a co catalyst by exposure to aerosol particles of potassium salt. *Applied Catalysis B: Environmental*.

Goldberg, S., Criscenti, L. J., Turner, D. R., Davis, J. A., and Cantrell, K. J. (2007). Adsorption–desorption processes in subsurface reactive transport modeling. *Vadose Zone Journal*, **6**(3):407–435.

Hoek, A. (2005). The shell gtl process: towards a world scale project in qatar. *Chemie Ingenieur Technik*, **77**(8):1172–1172.

Holmen, A. (2002). Heterogen katalyse. *Institutt for kjemisk prosessteknologi, NTNU*.

Hurst, N. W., Gentry, S. J., Jones, A., and McNicol, B. D. (1982). Temperature programmed reduction. *Catalysis Reviews Science and Engineering*, **24**(2):233–309.

Iglesia, E. (1997). Design, synthesis, and use of cobalt-based fischer-tropsch synthesis catalysts. *Applied Catalysis A: General*, **161**(1-2):59–78.

Jones, R. D. and Bartholomew, C. H. (1988). Improved flow technique for measurement of hydrogen chemisorption on metal catalysts. *Applied Catalysis*, **39**:77–88.

Kasthuraiah, K. and Kishore, N. S. (2017). Lignocellulosic biofuels–challenges and potentials. *International Journal of Pharma and Bio Sciences*, **8**(1):376–81.

Khodakov, A. Y. (2009). Fischer-tropsch synthesis: Relations between structure of cobalt catalysts and their catalytic performance. *Catalysis Today*, 144(3-4):251–257.

Khodakov, A. Y., Griboval-Constant, A., Bechara, R., and Zholobenko, V. L. (2002). Pore size effects in fischer tropsch synthesis over cobalt-supported mesoporous silicas. *Journal of Catalysis*, **206**(2):230–241.

Khodakov, A. Y., Lynch, J., Bazin, D., Rebours, B., Zanier, N., Moisson, B., and Chaumette, P. (1997). Reducibility of cobalt species in silica-supported fischer–tropsch catalysts. *Journal of Catalysis*, 168(1):16–25.

Lillebø, A. H. (2014). Conversion of biomass derived synthesis gas into liquid fuels via the fischer-tropsch synthesis process: Effect of alkali and alkaline earth metal impurities and co conversion levels on cobalt based catalysts.

Lillebø, A. H., Patanou, E., Yang, J., Blekkan, E. A., and Holmen, A. (2013). The effect of alkali and alkaline earth elements on cobalt based fischer–tropsch catalysts. *Catalysis Today*, **215**:60–66.

Lok, C. M. (2004). Novel highly dispersed cobalt catalysts for improved fischer-tropsch productivity. In *Studies in surface science and catalysis*, volume 147, pages 283–288. Elsevier.

Martínez, A. and Prieto, G. (2007). Breaking the dispersion-reducibility dependence in oxide-supported cobalt nanoparticles. *Journal of Catalysis*, **245**(2):470–476.

Moulijn, J. A., Makkee, M., and Van Diepen, A. E. (2013). *Chemical process technology*. John Wiley & Sons.

Niemantsverdriet, J. W. (2010). *Spectroscopy in catalysis: an introduction*. John Wiley & Sons.

Nigam, P. S. and Singh, A. (2011). Production of liquid biofuels from renewable resources. *Progress in Energy and Combustion Science*, **37**(1):52–68.

Park, J.-Y., Lee, Y.-J., Karandikar, P. R., Jun, K.-W., Ha, K.-S., and Park, H.-G. (2012). Fischer–tropsch catalysts deposited with size-controlled co3o4 nanocrystals: Effect of co particle size on catalytic activity and stability. *Applied Catalysis A: General*, **411**:15–23.

Pedersen, E. Ø. (2018). Mn promotion effect in co based fischer-tropsch production of light olefins.

Ragauskas, A. J., Williams, C. K., Davison, B. H., Britovsek, G., Cairney, J., Eckert, C. A., Frederick, W. J., Hallett, J. P., Leak, D. J., Liotta, C. L., et al. (2006). The path forward for biofuels and biomaterials. *Science*, **311**(5760):484–489.

Ralston, W. T., Melaet, G., Saephan, T., and Somorjai, G. A. (2017). Evidence of structure sensitivity in the fischer–tropsch reaction on model cobalt nanoparticles by time-resolved chemical transient kinetics. *Angewandte Chemie International Edition*, 56(26):7415–7419.

Richardson, J. (1989). *Principles of catalyst development*. Springer.

Rogelj, J., Den Elzen, M., Höhne, N., Fransen, T., Fekete, H., Winkler, H., Schaeffer, R., Sha, F., Riahi, K., and Meinshausen, M. (2016). Paris agreement climate proposals need a boost to keep warming well below 2 c. *Nature*, **534**(7609):631.

Schanke, D., Vada, S., Blekkan, E., Hilmen, A., Hoff, A., and Holmen, A. (1995). Study of pt-promoted cobalt co hydrogenation catalysts. *Journal of Catalysis*, 156(1):85–95.

Schwarz, J. A., Contescu, C., and Contescu, A. (1995). Methods for preparation of catalytic materials. *Chemical Reviews*, **95**(3):477–510.

Serrano-Ruiz, J. C. and Dumesic, J. A. (2011). Catalytic routes for the conversion of biomass into liquid hydrocarbon transportation fuels. *Energy & Environmental Science*, **4**(1):83–99.

Shahsavari, A. and Akbari, M. (2018). Potential of solar energy in developing countries for reducing energy-related emissions. *Renewable and Sustainable Energy Reviews*, **90**:275–291.

Stranges, A. (2000). Germanys synthetic fuel industry, 1927–1945. In *The German Chemical Industry in the Twentieth Century*, pages 147–216. Springer.

Trépanier, M., Tavasoli, A., Dalai, A. K., and Abatzoglou, N. (2009). Co, ru and k loadings effects on the activity and selectivity of carbon nanotubes supported cobalt catalyst in fischer–tropsch synthesis. *Applied Catalysis A: General*, **353**(2):193–202.

Ullah, K., Sharma, V. K., Ahmad, M., Lv, P., Krahl, J., Wang, Z., et al. (2017). The insight views of advanced technologies and its application in bio-origin fuel synthesis from lignocellulose biomasses waste, a review. *Renewable and Sustainable Energy Reviews*.

van Helden, P., Ciobîcă, I. M., and Coetzer, R. L. (2016). The size-dependent site composition of fcc cobalt nanocrystals. *Catalysis Today*, 261:48–59.

Vannice, M. A. (1975). The catalytic synthesis of hydrocarbons from h2co mixtures over the group viii metals: I. the specific activities and product distributions of supported metals. *Journal of Catalysis*, 37(3):449–461.

Wang, Z.-j., Skiles, S., Yang, F., Yan, Z., and Goodman, D. W. (2012). Particle size effects in fischer–tropsch synthesis by cobalt. *Catalysis today*, 181(1):75–81.

Wolf, R. E. (2005). Introduction to icp-ms. `https://crustal.usgs.gov/laboratories/icpms/intro.html`. Accessed 11.06.2018.

Yang, J., Tveten, E. Z., Chen, D., and Holmen, A. (2010). Understanding the effect of cobalt particle size on fischer- tropsch synthesis: Surface species and mechanistic studies by ssitka and kinetic isotope effect. *Langmuir*, 26(21):16558–16567.

Appendices

A List of chemicals

Table A.1 summarize all the chemicals used during the experimental work of this thesis.

Chemical	Chemical formula	State	Purpose	Producer	Purity [%]
Cobalt(II) nitrate hexahydrate	$Co(NO_3) \cdot 62\,H_2O$	s	Precursor	Sigma-Aldrich	99.999
Puralox SCCa 45/190	γAl_2O_3	s	Support	Sasol Germany GmbH	98
Silicon Oxide	SiO_2	s(pellets)	Support	Alfa Aesar	90
Perrhenic acid solution	HO_4Re	aq	Precursor	Sigma-Aldrich	75-80 wt% in water
Potassium nitrate	KNO_3	s	Precursor	Sigma-Aldrich	99
Ethylene glycol	$HOCH_2CH_2OH$	l	Part of impregnation solution	Sigma-Aldrich	99.5

Table A.1: List of chemicals used in this thesis.

B Weighings

Here all the actual weighings are listed for catalyst synthesis (incipient wetness impregnation), TPR, H_2-chemisorption and N_2-physisorption experiments.

B.1 Incipient wetness impregnation

The actual weigths used during post-impregnation with potassium nitrate are excluded. The amount of potassium on each contaminated catalysts after impregnation and calcination can be found in table 4.1. The measured weights are found in table B.2, B.3, B.4, B.5, B.6, B.7, B.8, and B.9.

Chemical	Weight [g]
Puralox SCCa 45/190 (after drying)	4.851
Deionized water	2.08
Ethylene glycol	4.23
Cobalt(II) nitrate hexahydrate	5.887
Perrhenic acid	0.08

Table B.2: Weighings for preparation of CoRe40

Chemical	Weight [g]
Puralox SCCa 45/190 (after drying)	6.053
Deionized water	4.72134
Ethylene glycol	3.14756
Cobalt(II) nitrate hexahydrate	7.4704
Perrhenic acid	0.05103

Table B.3: Weighings for preparation of CoRe60

Chemical	Weight [g]
Puralox SCCa 45/190 (after drying)	6.0264
Deionized water	7.443
Ethylene glycol	0.392
Cobalt(II) nitrate hexahydrate	7.438
Perrhenic acid	0.051

Table B.4: Weighings for preparation of CoRe95

Chemical	Weight [g]
Puralox SCCa 45/190 (after drying)	6.2146
Deionized water	8.0789
Ethylene glycol	1.616
Cobalt(II) nitrate hexahydrate	7.6698
Perrhenic acid	0.0524

Table B.5: Weighings for preparation of CoRe80(Batch1). This was later combined with CoRe80(Batch2) and is referred to as CoRe80 in the report.

Chemical	Weight [g]
Puralox SCCa 45/190 (after drying)	6.0051
Deionized water	6.245
Ethylene glycol	1.561
Cobalt(II) nitrate hexahydrate	7.411
Perrhenic acid	0.051

Table B.6: Weighings for preparation of CoRe80(Batch2). This was later combined with CoRe80(Batch1) and is referred to as CoRe80 in the report.

Chemical	Weight [g]
Puralox SCCa 45/190 (after drying)	10.63
Deionized water	13.819
Ethylene glycol	0
Cobalt(II) nitrate hexahydrate	13.119238
Perrhenic acid	0.08963

Table B.7: Weighings for preparation of CoRe100(Batch1).

Chemical	Weight [g]
Puralox SCCa 45/190 (dried and sieved)	24.753
Deionized water	32.1789
Ethylene glycol	0
Cobalt(II) nitrate hexahydrate	30.5494
Perrhenic acid	0.2087

Table B.8: Weighings for preparation of CoRe100(Batch2). This is later called only CoRe100.

Chemical	Weight [g]
Silicon dioxide (dried and sieved)	10.979
Deionized water	19.7622
Ethylene glycol	0
Cobalt(II) nitrate hexahydrate	13.32
Perrhenic acid	0.093

Table B.9: Weighings for preparation of CoRe100-SiO_2

B.2 TPR

The neglected TPR results are included as they make it easier to interpret the chronological order of the lab journal. All the actual weighings are listed in table B.10.

Catalyst	Weight [mg]
CoRe40	102.5
CoRe60	101.0
CoRe80(Batch1)	99.6
CoRe100(Batch1)	102.5
CoRe80(Batch2)	100.0
CoRe95(neglected)	0.1
CoRe100(500ppm)(neglected)	101.8
CoRe100(Batch2)	105.4
CoRe80(500ppm)(neglected)	103.0
CoRe80(Batch1and2)(neglected)	102.4
CoRe100(1000ppm)(neglected)	103.2
CoRe80(1000ppm)Test1(neglected)	100.8
CoRe80(1000ppm)Test2(neglected)	101.6
CoRe100(500ppm)Test2(neglected)	104.1
CoRe100-SiO_2	103.4
CoRe100(500ppm)-SiO_2(neglected)	101.5
CoRe100-SiO_2Test2	100.8
CoRe100(Batch2)(neglected)	101.7
CoRe80	100.4
CoRe80(500ppm)	101.3
CoRe80(1000ppm)	99.9
CoRe100	100.9
CoRe100(500ppm)	101.3
CoRe100(1000ppm)	101.9
CoRe95	101.3

Table B.10: Weighings for temperature programmed reduction.

B.3 Hydrogen-chemisorption

Equation 7.1 was used to account for potential impurities initially present in the catalyst bed. w(corr) is the correlated weight actually used in the chemisorption software, w(in) the initial weigth of the catalyst, W(in) the weight of catalyst, quartz wool and reactor initially, while W(fin) is the weight of the catalyst, quartz wool and reactor after analysis. The weights are all listed in B.11.

$$w(corr) = \frac{w(in)W(fin)}{W(in)} \tag{7.1}$$

Catalyst	W(in) [mg]	W(fin) [mg]	w(in) [mg]	w(corr) [mg]
CoRe40	18638.0	18616.9	199.9	199.7
CoRe60	19564.6	19497.1	200.3	199.6
CoRe80(Batch1)	19510.0	19415.9	204.6	203.6
CoRe95	19664.0	19519.8	208.0	206.5
CoRe80(Batch1)	19698.5.0	19579.0	207.7	206.4
CoRe100(Batch1)	19638.6	19615.7	204.4	204.2
CoRe80(Batch1)Test2	19640.8	19427.1	204.5	202.3
CoRe80(500ppm)	19512.0	19478.5	201.3	201.0
CoRe80(500ppm)Test2	19573.2	19553.5	204.4	204.2
CoRe100(500ppm)	19665.0	19529.9	200.6	199.2
CoRe100(Batch2)	19008.1	18963.9	204.0	203.5
CoRe80(1000ppm)	19600.6	19575.0	200.8	200.5
CoRe100-SiO_2	19239.6	19220.1	201.3	201.1
CoRe100(500ppm)-SiO_2	19276.2	19263.8	200.7	200.6
CoRe100(1000ppm)	19221.7	19183.5	201.5	201.1

Table B.11: Weighings for H_2-chemisorption.

B.4 Nitrogen-physisorption

As the only weights used here was the initially weighed out catalyst, these are the only weights included in table B.12

B.5 Fischer-Tropsch synthesis

Weights of catalyst and silicon carbide (SiC) loaded in reactor before Fischer-Tropsch synthesis are shown in table B.13

Catalyst	Weight [mg]
CoRe80	62.3
CoRe80(500ppm)	57.7
CoRe100	60.1
γ-Al_2O_3Test1	69.5
γ-Al_2O_3Test2	67.0
CoRe100(500ppm)	61.6
CoRe100(1000ppm)	63.7
CoRe80(1000ppm)	63.4
SiO_2 (calcined)	60.1

Table B.12: Weighings for N_2-physisorption.

Catalyst	Catalyst weight [g]	SiC weight [g]
CoRe100	1.0185	20.0829
CoRe80	1.0003	20.0335
CoRe80(500ppm)	1.0026	20.0183
CoRe100(500ppm)	1.0005	19.9985
CoRe80(1000ppm)	1.0006	20.0128
CoRe100(1000ppm)	1.0004	20.0026

Table B.13: Weighings for Fischer-Tropsch synthesis.

C Calculations

C.1 Incipient wetness impregnation with calculations of metal loading

The calculations for preparation of 20 wt.% Co - 0.5 wt.% Re catalysts supported on γ-Al_2O_3 by incipient wetness impregnation (IWI) started by finding the liquid absorption capacity, or IWI point, as shown in equation (7.2).

$$\frac{m_{H_2O}}{m_{\gamma-Al_2O_3}} = 1.3 \tag{7.2}$$

Here, m_{H_2O} is the mass of water and $m_{\gamma-Al_2O_3}$ the mass of the alumina support being impregnated. Then, as the IWI-point was established, corresponding mass percentages of $(\frac{m_{H_2O}}{m_{H_2O}+m_{EG}})100\%$ = 40-, 60-, 80-, 95- or 100 was prepared so the total mass of the water/EG mixture amounted to the necessary weight for an IWI-point of around 1.3, i.e., replacing the term m_{H_2O} in equation (7.2). Then, in order to get 20 wt.% Co using a $Co(NH_2)_2 \cdot 6\,H_2O$-precursor, equations (7.3) and (7.4) were used:

$$m_{Co} = m_{\gamma-Al_2O_3}\frac{20\%}{80\%} \tag{7.3}$$

$$m_{Co(NH_2)_2 \cdot 6\,H_2O} = m_{Co}\frac{M_{Co(NH_2)_2 \cdot 6\,H_2O}}{M_{Co}} \tag{7.4}$$

where $M_{Co(NH_2)_2 \cdot 6\,H_2O}$ and M_{Co} is the molar mass of the respective species, while the value of $m_{Co(NH_2)_2 \cdot 6\,H_2O}$ was added to the impregnation solution. The same procedure was followed when adding the 0.5 wt.% Re by the precursor $HReO_4$ according to the equations below:

$$m_{Re} = m_{\gamma-Al_2O_3}\frac{0.5\%}{80\%} \tag{7.5}$$

$$m_{HReO_4} = m_{Re}\frac{M_{HReO_4}}{M_{Re}} \tag{7.6}$$

where M_{HReO_4} and M_{Re} is the molar mass of the respective species and m_{HReO_4} (perrhenic acid) was added to the impregnation solution as well. After the solution was well mixed in a beaker, a dropwise addition onto the support was performed until all of the impregnation solution was used up.

The same procedure was followed upon loading of 20 wt.% Co - 0.5 wt.% Re catalysts supported on SiO_2, the only difference was the IWI point. The IWI point found for the SiO_2 support was around 1.8.

C.2 Loading of and 500 and 1000 ppm K

The same procedure (incipient wetness impregnation) was followed when loading the catalysts with K contaminations, only here the impregnation solution was distilled water and a potassium precursor KNO_3. Also, due to the increased difficulty of measuring out the small amounts of KNO_3 necessary for 500 and 1000 ppm K in an impregnation solution meant for catalysts of 5-15 g, a mixture of 0.5 L distilled water and the necessary amount of precursor for 500 and 1000 ppm K and satisfying the IWI-point was made. The IWI-point was found to be around 1.1. An amount of potassium precursor KNO_3 that added up to 500 and 1000 ppm K on the basis of the weight of the catalyst sample being impregnated was dissolved in distilled water and impregnated on the catalyst sample. The calculations based on 5 g catalyst and 500 ppm K are shown below.

For 5 g catalyst and an IWI-point of around 1.1, the mass of the impregnation solution is as in equation (7.7)

$$\mathrm{m(solution)} = 5\mathrm{g} \times 1.1 = 5.5\mathrm{g} \tag{7.7}$$

Where 5.5 g of water amounts to 5.5 mL as we assume the density of water to be 1. Then, the mass of potassium adding up to 500 ppm based on 5 g catalyst can be found through equation (7.8).

$$500\mathrm{ppm\ (K)} = \frac{5\mathrm{g}}{10^6} \times 500 = 2.5 \times 10^{-3}\mathrm{g\ (K)} \tag{7.8}$$

Then, the amount of KNO_3 this adds up to can be found by equation (7.9).

$$\mathrm{m_{KNO_3}} = 2.5 \times 10^{-3}\mathrm{g\ (K)}\frac{\mathrm{M_{KNO_3}}}{\mathrm{M_K}} = 6.46 \times 10^{-3} g(\mathrm{KNO3}) \tag{7.9}$$

Where $\mathrm{M_{KNO_3}}$ and $\mathrm{M_K}$ is the molar mass of the respective species. Then, the amount of moles this adds up to can be found through equation (7.10)

$$\mathrm{n_{KNO_3}} = \frac{\mathrm{m_{KNO_3}}}{\mathrm{M_{KNO_3}}} = 6.39 \times 10^{-5} mol \tag{7.10}$$

Then the amount of moles can be divided by the mass of IWI-solution, finding the necessary concentration through equation (7.11)

$$\mathrm{C_{KNO_3}} = \frac{\mathrm{n_{KNO_3}}}{\mathrm{m(solution)}} = 11.62 \times 10^{-3} \mathrm{mol/L} \tag{7.11}$$

Then, a mixture of 0.5 L distilled water and $\mathrm{KNO_3}$ at the concentration $\mathrm{C_{KNO_3}}$ was prepared using equation (7.12).

$$\mathrm{m_{KNO_3}} = \mathrm{M_{KNO_3}} \times \mathrm{C_{KNO_3}} \times 0.5L = 0.587\mathrm{g(KNO_3)} \tag{7.12}$$

Finally, 5.5 g of the 0.5 L solution was used for impregnating the 5 g catalyst and 500 ppm K was obtained.

The same calculation procedure was followed upon impregnation of 1000 ppm K, where the only change was changing the value of 500 ppm to 1000 ppm.

C.3 Site time yield and selectivities

Site time yield

The site-time yield (STY) was calculated through the MATLAB script presented in appendix D.5. The input is the signal from the gas chromatograph Agilent Technologies 6890N Network GC System. The output of the calculations are presented in an example in appendix D.6.

First, equation 7.13 was used in order to calculate the CO conversion:

$$X = 1 - \frac{F_{xh}^{CO}}{F_{feed,av}^{CO}} = 1 - \frac{\left(\frac{A_{CO}}{A_{\mathrm{N_2}}}\right)_{xh}}{\left(\frac{A_{CO}}{A_{\mathrm{N_2}}}\right)_{feed,av}} \tag{7.13}$$

where X (%) is the CO conversion, F_{xh}^{CO} the flow of CO going into the GC at hour x, $F_{feed,av}^{CO}$ the average flow of CO in the feed analysis going into the GC, A_{CO} the area of the CO signal registered by the GC, and A_{N_2} the area of the N_2 signal registered by the GC. xh represents the hour, x, at which the value is valid for, while feed, av represents the average of the feed values registered during a feed analysis.

Then, in order to calculate the STY value, an equation for the reaction rate, r ($\frac{mL_{CO}}{g_{cat}s}$), have to be defined.

$$r = \frac{F \cdot Y_{\text{CO}} \cdot X}{W} \tag{7.14}$$

In equation 7.14, F ($\frac{mL}{s}$) is the flow rate of syngas, Y_{CO} (%) the CO-content of the syngas, X (%) the CO conversion and W (g) the weight of the cobalt catalyst. The STY can then be calculated using equation 7.15

$$\text{STY} = \frac{\text{r} \cdot \text{M}_{\text{CO}}}{\text{V}_{\text{m}} \cdot 3600 \cdot \frac{\text{X}_{\text{m}}}{100}\frac{\text{D}}{100}} \tag{7.15}$$

where STY is the site time yield ($\frac{molCO}{molCo \cdot s}$), r is the reaction rate calculated from equation 7.14, M_{CO} ($\frac{g_{CO}}{mol_{CO}}$) the molecular mass of CO, V_m ($\frac{mL}{mol}$) the volumetric flow per mole of syngas, X_m ($\frac{g_{\text{CO}}}{g_{cat}}$) the metal loading, and D ($\frac{mol_{\text{Co}(Surface)}}{mol_{\text{Co}}}$) the cobalt dispersion.

Selectivities

The first step towards finding the selectivity towards CH_4, $S_{\text{CH}_4,xh}$, was by using equation 7.16 to find the flow of CH_4 at hour x:

$$F_{\text{CH}_4,xh} = \frac{F_{\text{N}_2} RRF_{\text{CH}_4} A_{\text{CH}_4,xh}}{A_{\text{N}_2,xh}} \tag{7.16}$$

where $F_{CH4,xh}$ is the flow of CH_4 at hour x, $F_{N2,xh}$ the flow of N_2 at hour x, RRF_{CH_4} the relative response factor obtained from the thermal conductivity detector (TCD) of the GC calibration data, $A_{\text{CH}_4,xh}$ the area of the CH_4 signal registered by the GC at hour x, and $A_{\text{N}_2,xh}$ the area of the CH_4 signal registered by the GC at hour x. Then, using equation 7.17, the CH_4-selectivity is found:

$$S_{\mathrm{CH_4},xh} = \frac{F_{\mathrm{CH_4,\,xh}}}{F_{\mathrm{CO}}X_{\mathrm{CO},xh}}; \tag{7.17}$$

where $S_{\mathrm{CH_4},xh}$ is the CH_4-selectivity (%), $F_{\mathrm{CO},xh}$ the flow of CO at hour x, and $X_{\mathrm{CO},xh}$ the CO conversion at hour x.

The same procedure was followed when calculating the selectivity towards CO_2, $S_{\mathrm{CO_2},xh}$. Equation 7.18 to find the flow of CH_4 at hour x:

$$F_{\mathrm{CO_2},xh} = \frac{F_{\mathrm{N_2}}RRF_{\mathrm{CO_2}}A_{\mathrm{CO_2},xh}}{A_{\mathrm{N_2},xh}} \tag{7.18}$$

where $F_{CO2,xh}$ is the flow of CO_2 at hour x, $F_{N2,xh}$ the flow of N_2 at hour x, $RRF_{\mathrm{CO_2}}$ the relative response factor obtained from the thermal conductivity detector (TCD) of the GC calibration data, $A_{\mathrm{CO_2},xh}$ the area of the CO_2 signal registered by the GC at hour x, and $A_{\mathrm{N_2},xh}$ the area of the CO_2 signal registered by the GC at hour x. Then, using equation 7.19, the CH_4-selectivity is found:

$$S_{\mathrm{CO_2},xh} = \frac{F_{\mathrm{CO_2,\,xh}}}{F_{\mathrm{CO}}X_{\mathrm{CO},xh}}; \tag{7.19}$$

where $S_{\mathrm{CO_2},xh}$ is the CO_2-selectivity (%), $F_{\mathrm{CO},xh}$ the flow of CO at hour x, and $X_{\mathrm{CO},xh}$ the CO conversion at hour x.

The C_{5+}-selectivity at hour x, $S_{C_{5+},xh}$, can be found by using equation 7.20:

$$S_{C_{5+},xh} = 1 - \left(S_{\mathrm{CH_4},xh} + S_{C2,xh} + S_{C3,xh} + S_{C4,xh} + S_{\mathrm{CO_2},xh}\right) \tag{7.20}$$

where $S_{C2,xh}$, $S_{C3,xh}$, and $S_{C4,xh}$ is the selectivities towards C2, C3 and C4 products calculated by the same procedure as the CH_4- and CO_2-selectivities. C2 products include ethane and ethene, C3 products include propane and propene, while C4 products include n-butane, i-butane, 1-butene, i-butene, cis-2-butene, and trans-2-butene.

D Raw data and additional results

D.1 Nitrogen-physisorption raw data

The following figures display the isotherm plots, pore volume distribution plots and summary reports for all catalysts ran in N_2-physisorption experiments.

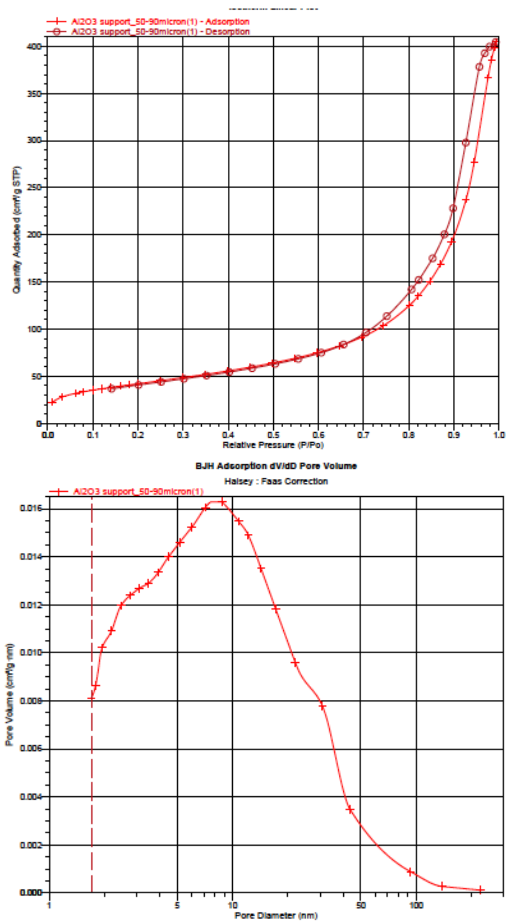

Figure D.1: Isotherm plot and pore volume distribution plot for γ-Al_2O_3Test1. Tested during the spring of 2018.

Summary Report

Surface Area

Single point surface area at P/Po = 0.299968138: 148.0851 m^2/g

BET Surface Area: 152.6408 m^2/g

Langmuir Surface Area: 244.2323 m^2/g

t-Plot External Surface Area: 154.6971 m^2/g

BJH Adsorption cumulative surface area of pores between 1.7000 nm and 300.0000 nm diameter: 174.656 m^2/g

BJH Desorption cumulative surface area of pores between 1.7000 nm and 300.0000 nm diameter: 190.9058 m^2/g

Pore Volume

Single point adsorption total pore volume of pores less than 82.1365 nm diameter at P/Po = 0.975851799: 0.566844 cm^3/g

t-Plot micropore volume: -0.002463 cm^3/g

BJH Adsorption cumulative volume of pores between 1.7000 nm and 300.0000 nm diameter: 0.615360 cm^3/g

BJH Desorption cumulative volume of pores between 1.7000 nm and 300.0000 nm diameter: 0.628484 cm^3/g

Pore Size

Adsorption average pore width (4V/A by BET): 14.85432 nm

BJH Adsorption average pore diameter (4V/A): 14.0930 nm

BJH Desorption average pore diameter (4V/A): 13.1685 nm

Figure D.2: Summary report for γ-Al_2O_3Test1. Tested during the spring of 2018.

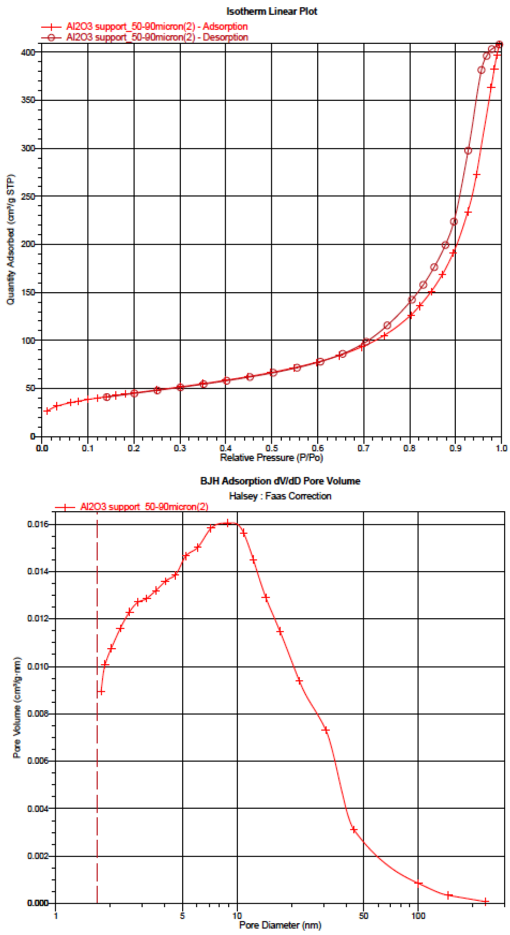

Figure D.3: Isotherm plot and pore volume distribution plot for γ-Al_2O_3Test2. Tested during the spring of 2018.

Summary Report

Surface Area

Single point surface area at P/Po = 0.300496949: 157.2850 m^2/g

BET Surface Area: 160.9991 m^2/g

Langmuir Surface Area: 255.1280 m^2/g

t-Plot Micropore Area: 9.0198 m^2/g

t-Plot External Surface Area: 151.9793 m^2/g

BJH Adsorption cumulative surface area of pores between 1.7000 nm and 300.0000 nm diameter: 172.268 m^2/g

BJH Desorption cumulative surface area of pores between 1.7000 nm and 300.0000 nm diameter: 187.5273 m^2/g

Pore Volume

Single point adsorption total pore volume of pores less than 88.1637 nm diameter at P/Po = 0.977537714: 0.561662 cm^3/g

t-Plot micropore volume: 0.003627 cm^3/g

BJH Adsorption cumulative volume of pores between 1.7000 nm and 300.0000 nm diameter: 0.621221 cm^3/g

BJH Desorption cumulative volume of pores between 1.7000 nm and 300.0000 nm diameter: 0.634966 cm^3/g

Pore Size

Adsorption average pore width (4V/A by BET): 13.95442 nm

BJH Adsorption average pore diameter (4V/A): 14.4246 nm

BJH Desorption average pore diameter (4V/A): 13.5440 nm

Figure D.4: Summary report for γ-Al_2O_3Test2. Tested during the spring of 2018.

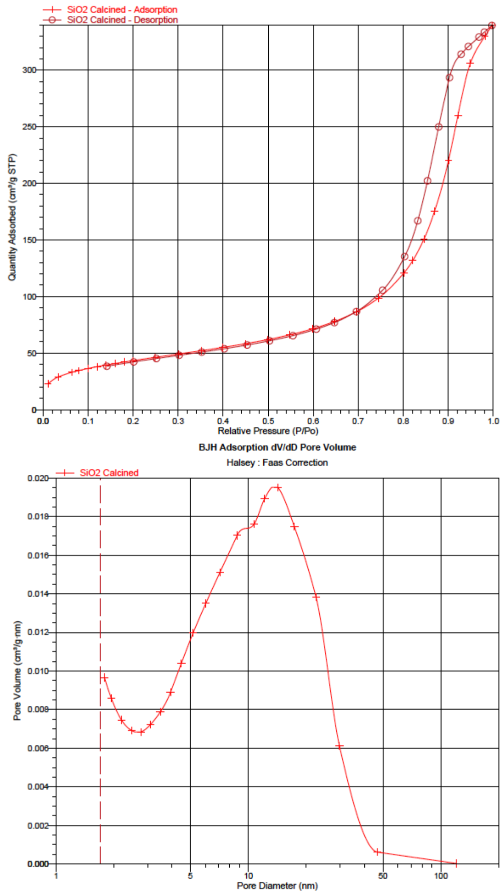

Figure D.5: Isotherm plot and pore volume distribution plot for calcined SiO_2. Tested during the spring of 2018.

Summary Report

Surface Area

Single point surface area at P/Po = 0.300960388: 149.8763 m²/g

BET Surface Area: 154.5378 m²/g

Langmuir Surface Area: 246.3938 m²/g

t-Plot Micropore Area: 0.4821 m²/g

t-Plot External Surface Area: 154.0558 m²/g

BJH Adsorption cumulative surface area of pores
between 1.7000 nm and 300.0000 nm diameter: 158.806 m²/g

BJH Desorption cumulative surface area of pores
between 1.7000 nm and 300.0000 nm diameter: 178.5028 m²/g

Pore Volume

Single point adsorption total pore volume of pores
less than 107.7482 nm diameter at P/Po = 0.981696464: 0.510607 cm³/g

t-Plot micropore volume: -0.000261 cm³/g

BJH Adsorption cumulative volume of pores
between 1.7000 nm and 300.0000 nm diameter: 0.507889 cm³/g

BJH Desorption cumulative volume of pores
between 1.7000 nm and 300.0000 nm diameter: 0.519156 cm³/g

Pore Size

Adsorption average pore width (4V/A by BET): 13.21636 nm

BJH Adsorption average pore diameter (4V/A): 12.7927 nm

BJH Desorption average pore diameter (4V/A): 11.6336 nm

Figure D.6: Summary report for calcined SiO_2. Tested during the spring of 2018.

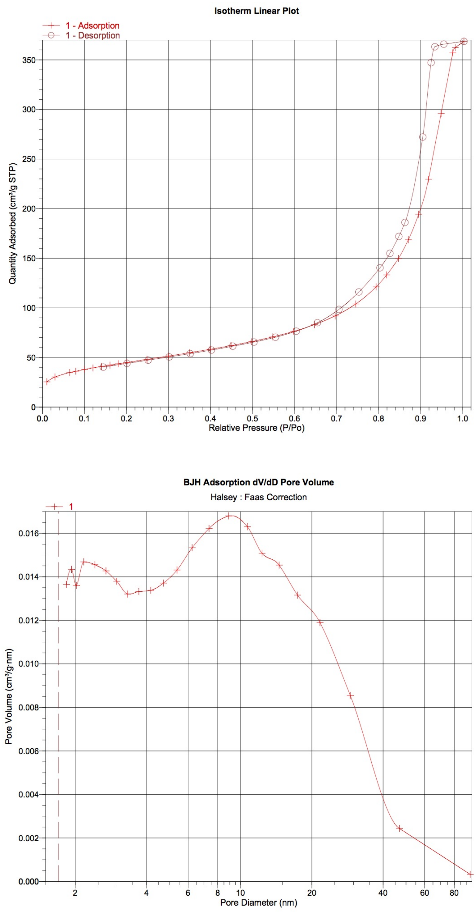

Figure D.7: Isotherm plot and pore volume distribution plot for CoRe100. Tested during the fall of 2017.

Summary Report

Surface Area

Single point surface area at p/p° = 0,299746214: 156,7334 m^2/g

BET Surface Area: 145,0316 m^2/g

BJH Adsorption cumulative surface area of pores
between 17,000 Å and 3 000,000 Å width: 155.436 m^2/g

BJH Desorption cumulative surface area of pores
between 17,000 Å and 3 000,000 Å width: 175,0508 m^2/g

Pore Volume

Single point adsorption total pore volume of pores
less than 850,154 Å width at p/p° = 0,976341896: 0,552381 cm^3/g

BJH Adsorption cumulative volume of pores
between 17,000 Å and 3 000,000 Å width: 0,579370 cm^3/g

BJH Desorption cumulative volume of pores
between 17,000 Å and 3 000,000 Å width: 0,597433 cm^3/g

Pore Size

Adsorption average pore diameter (4V/A by BET): 152,3478 Å

BJH Adsorption average pore width (4V/A): 149,095 Å

BJH Desorption average pore width (4V/A): 136,517 Å

Figure D.8: Summary report for CoRe100. Tested during the fall of 2017.

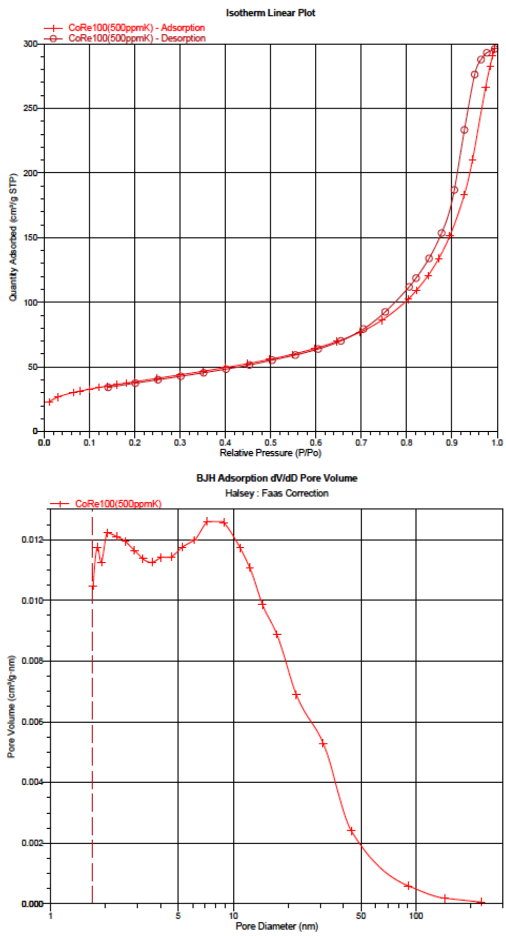

Figure D.9: Isotherm plot and pore volume distribution plot for CoRe100(500ppm). Tested during the spring of 2018.

Summary Report

Surface Area

Single point surface area at P/Po = 0.300120590: 133.7249 m^2/g

BET Surface Area: 136.8632 m^2/g

Langmuir Surface Area: 216.7988 m^2/g

t-Plot Micropore Area: 7.9910 m^2/g

t-Plot External Surface Area: 128.8721 m^2/g

BJH Adsorption cumulative surface area of pores between 1.7000 nm and 300.0000 nm diameter: 141.115 m^2/g

BJH Desorption cumulative surface area of pores between 1.7000 nm and 300.0000 nm diameter: 151.2609 m^2/g

Pore Volume

Single point adsorption total pore volume of pores less than 77.9486 nm diameter at P/Po = 0.974524189: 0.412009 cm^3/g

t-Plot micropore volume: 0.003322 cm^3/g

BJH Adsorption cumulative volume of pores between 1.7000 nm and 300.0000 nm diameter: 0.449087 cm^3/g

BJH Desorption cumulative volume of pores between 1.7000 nm and 300.0000 nm diameter: 0.461712 cm^3/g

Pore Size

Adsorption average pore width (4V/A by BET): 12.04149 nm

BJH Adsorption average pore diameter (4V/A): 12.7297 nm

BJH Desorption average pore diameter (4V/A): 12.2097 nm

Figure D.10: Summary report for CoRe100(500ppm). Tested during the spring of 2018.

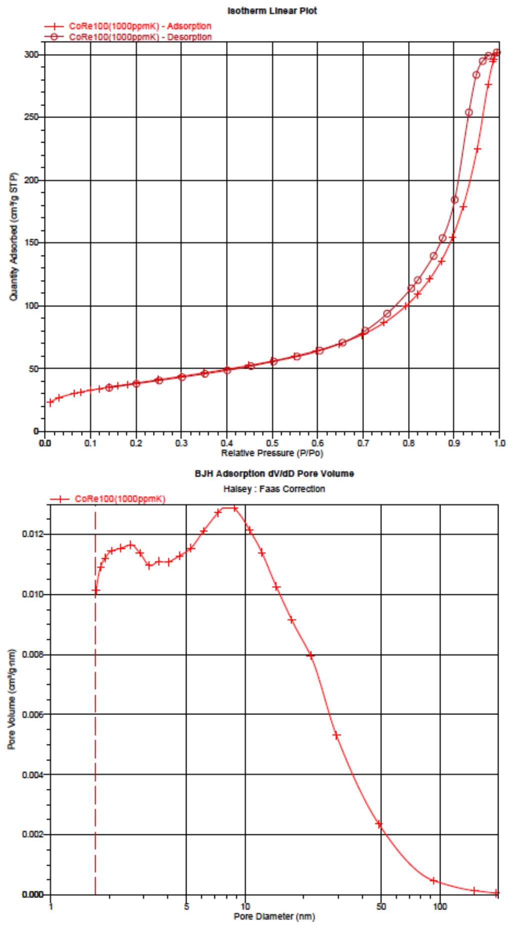

Figure D.11: Isotherm plot and pore volume distribution plot for CoRe100(1000ppm). Tested during the spring of 2018.

Summary Report

Surface Area

Single point surface area at P/Po = 0.300425864: 133.9955 m^2/g

BET Surface Area: 137.0637 m^2/g

Langmuir Surface Area: 217.1186 m^2/g

t-Plot Micropore Area: 8.7664 m^2/g

t-Plot External Surface Area: 128.2973 m^2/g

BJH Adsorption cumulative surface area of pores
between 1.7000 nm and 300.0000 nm diameter: 141.753 m^2/g

BJH Desorption cumulative surface area of pores
between 1.7000 nm and 300.0000 nm diameter: 151.6413 m^2/g

Pore Volume

Single point adsorption total pore volume of pores
less than 78.9914 nm diameter at P/Po = 0.974868133: 0.427683 cm^3/g

t-Plot micropore volume: 0.003766 cm^3/g

BJH Adsorption cumulative volume of pores
between 1.7000 nm and 300.0000 nm diameter: 0.458150 cm^3/g

BJH Desorption cumulative volume of pores
between 1.7000 nm and 300.0000 nm diameter: 0.470375 cm^3/g

Pore Size

Adsorption average pore width (4V/A by BET): 12.48128 nm

BJH Adsorption average pore diameter (4V/A): 12.9281 nm

BJH Desorption average pore diameter (4V/A): 12.4076 nm

Figure D.12: Summary report for CoRe100(1000ppm). Tested during the spring of 2018.

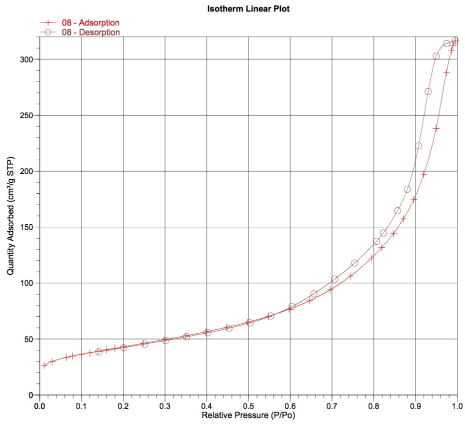

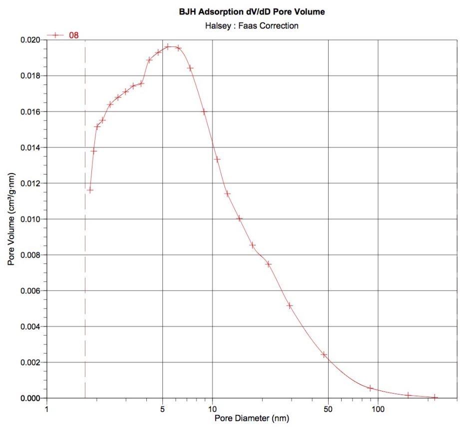

Figure D.13: Isotherm plot and pore volume distribution plot for CoRe80. Tested during the fall of 2017.

Summary Report

Surface Area

Single point surface area at p/p° = 0,299479569: 150,9156 m²/g

BET Surface Area: 142,9977 m²/g

BJH Adsorption cumulative surface area of pores
between 17,000 Å and 3 000,000 Å width: 156,232 m²/g

BJH Desorption cumulative surface area of pores
between 17,000 Å and 3 000,000 Å width: 169,7634 m²/g

Pore Volume

Single point adsorption total pore volume of pores
less than 768,795 Å width at p/p° = 0,973773757: 0,445732 cm³/g

BJH Adsorption cumulative volume of pores
between 17,000 Å and 3 000,000 Å width: 0,509924 cm³/g

BJH Desorption cumulative volume of pores
between 17,000 Å and 3 000,000 Å width: 0,518617 cm³/g

Pore Size

Adsorption average pore diameter (4V/A by BET): 124,6822 Å

BJH Adsorption average pore width (4V/A): 130,556 Å

BJH Desorption average pore width (4V/A): 122,198 Å

Figure D.14: Summary report for CoRe80. Tested during the fall of 2017.

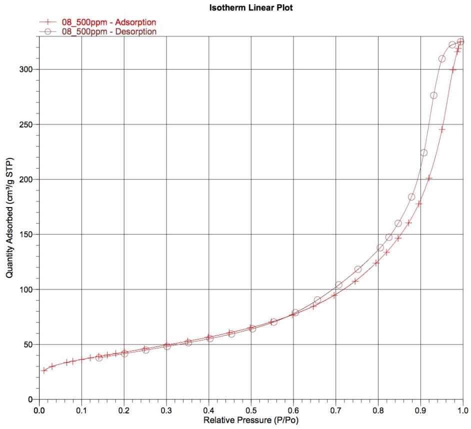

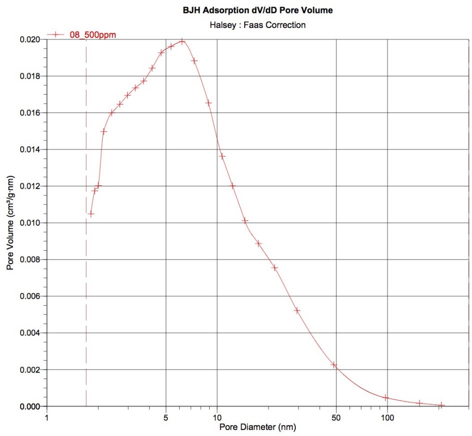

Figure D.15: Isotherm plot and pore volume distribution plot for CoRe80(500ppm K). Tested during the fall of 2017.

Summary Report

Surface Area

Single point surface area at p/p° = 0,300005881: 150,8347 m²/g

BET Surface Area: 143,2248 m²/g

BJH Adsorption cumulative surface area of pores
between 17,000 Å and 3 000,000 Å width: 158.583 m²/g

BJH Desorption cumulative surface area of pores
between 17,000 Å and 3 000,000 Å width: 172,9881 m²/g

Pore Volume

Single point adsorption total pore volume of pores
less than 838,853 Å width at p/p° = 0,976014787: 0,463308 cm³/g

BJH Adsorption cumulative volume of pores
between 17,000 Å and 3 000,000 Å width: 0,524992 cm³/g

BJH Desorption cumulative volume of pores
between 17,000 Å and 3 000,000 Å width: 0,534754 cm³/g

Pore Size

Adsorption average pore diameter (4V/A by BET): 129,3934 Å

BJH Adsorption average pore width (4V/A): 132,437 Å

BJH Desorption average pore width (4V/A): 123,852 Å

Figure D.16: Summary report for CoRe80(500ppm). Tested during the fall of 2017.

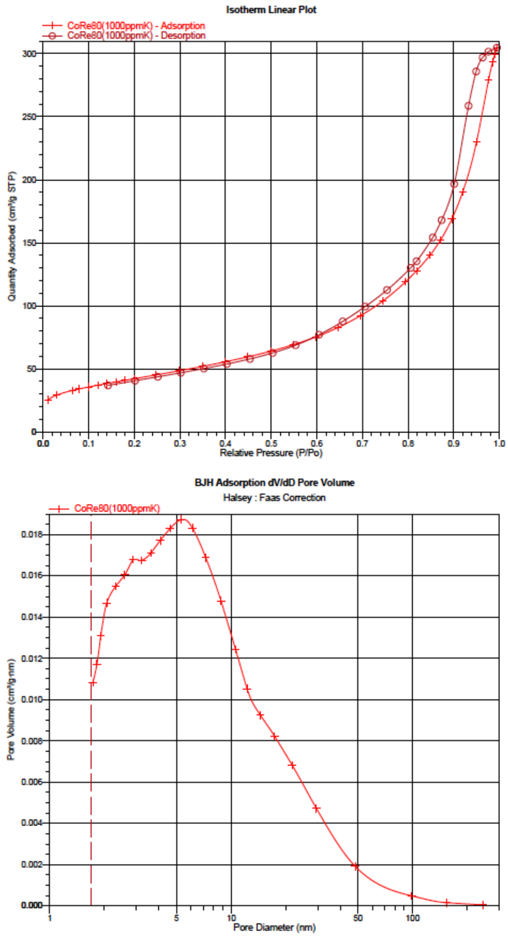

Figure D.17: Isotherm plot and pore volume distribution plot for CoRe80(1000ppm). Tested during the spring of 2018.

Summary Report

Surface Area

Single point surface area at P/Po = 0.299214020: 148.2113 m^2/g

BET Surface Area: 151.9207 m^2/g

Langmuir Surface Area: 241.6311 m^2/g

t-Plot Micropore Area: 4.7557 m^2/g

t-Plot External Surface Area: 147.1650 m^2/g

BJH Adsorption cumulative surface area of pores between 1.7000 nm and 300.0000 nm diameter: 170.069 m^2/g

BJH Desorption cumulative surface area of pores between 1.7000 nm and 300.0000 nm diameter: 180.0205 m^2/g

Pore Volume

Single point adsorption total pore volume of pores less than 85.4798 nm diameter at P/Po = 0.976816825: 0.432150 cm^3/g

t-Plot micropore volume: 0.001042 cm^3/g

BJH Adsorption cumulative volume of pores between 1.7000 nm and 300.0000 nm diameter: 0.467976 cm^3/g

BJH Desorption cumulative volume of pores between 1.7000 nm and 300.0000 nm diameter: 0.475531 cm^3/g

Pore Size

Adsorption average pore width (4V/A by BET): 11.37831 nm

BJH Adsorption average pore diameter (4V/A): 11.0067 nm

BJH Desorption average pore diameter (4V/A): 10.5662 nm

Figure D.18: Summary report for CoRe80(1000ppm). Tested during the spring of 2018.

D.2 Hydrogen-chemisorption raw data

The following figures show the line fit plots from the H_2-chemisorption experiments as well as the analysis summaries of all catalysts.

Analysis Summary

Element	Percent of Sample Weight (%)	Atomic Weight	Stoichiometry Factor	Atomic Cross-Sectional Area (nm²)	Density (cm³/g)
cobalt	20.000	58.933	2.000	0.0662	8.900

Analysis Results

Metal Dispersion: 13.3219 %
Metallic Surface Area: 18.0264 m²/g sample
Metallic Surface Area: 90.1321 m²/g metal
Crystallite Size (6.000 V / A): 7.47966 nm
Y-Intercept Quantity Adsorbed: 5.0667 ± 0.0703 cm³/g STP
Slope: 0.002577 ± 0.000177
Correlation Coefficient: 9.93024E-01

Difference Results

Metal Dispersion: 9.3394 %
Metallic Surface Area: 12.6375 m²/g sample
Metallic Surface Area: 63.1877 m²/g metal
Crystallite Size (6.000 V / A): 10.66912 nm
Y-Intercept Quantity Adsorbed: 3.5521 ± 0.0446 cm³/g STP
Slope: 0.001550 ± 0.000112
Correlation Coefficient: 9.92242E-01

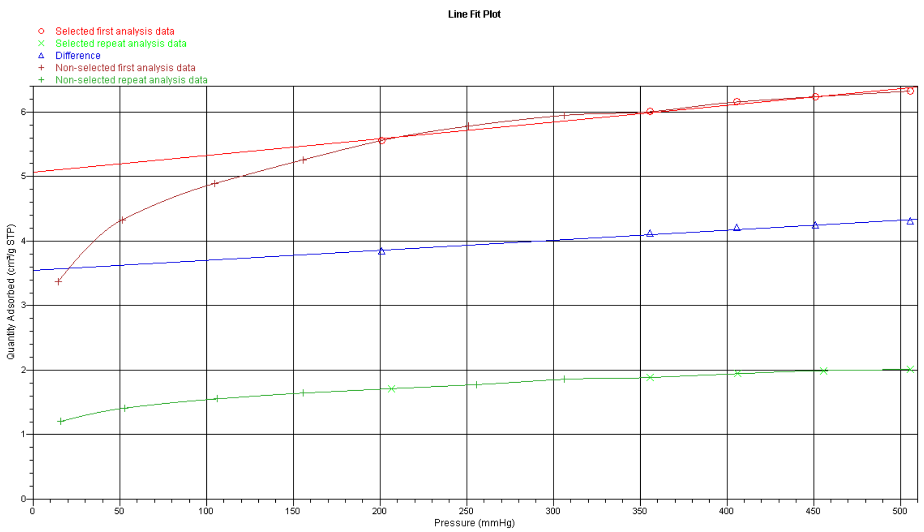

Figure D.19: Analysis summary and line fit plots from the H_2-chemisorption for CoRe40. Tested during the fall of 2017.

Analysis Summary

Element	Percent of Sample Weight (%)	Atomic Weight	Stoichiometry Factor	Atomic Cross-Sectional Area (nm^2)	Density (cm^3/g)
cobalt	20.000	58.933	2.000	0.0662	8.900

Analysis Results

Metal Dispersion: 14.0890 %
Metallic Surface Area: 19.0644 m^2/g sample
Metallic Surface Area: 95.3219 m^2/g metal
Crystallite Size (6.000 V / A): 7.07243 nm
Y-Intercept Quantity Adsorbed: 5.3585 ± 0.0497 cm^3/g STP
Slope: 0.002165 ± 0.000127
Correlation Coefficient: 9.94880E-01

Difference Results

Metal Dispersion: 9.9218 %
Metallic Surface Area: 13.4256 m^2/g sample
Metallic Surface Area: 67.1280 m^2/g metal
Crystallite Size (6.000 V / A): 10.04287 nm
Y-Intercept Quantity Adsorbed: 3.7736 ± 0.0581 cm^3/g STP
Slope: 0.001131 ± 0.000148
Correlation Coefficient: 9.75138E-01

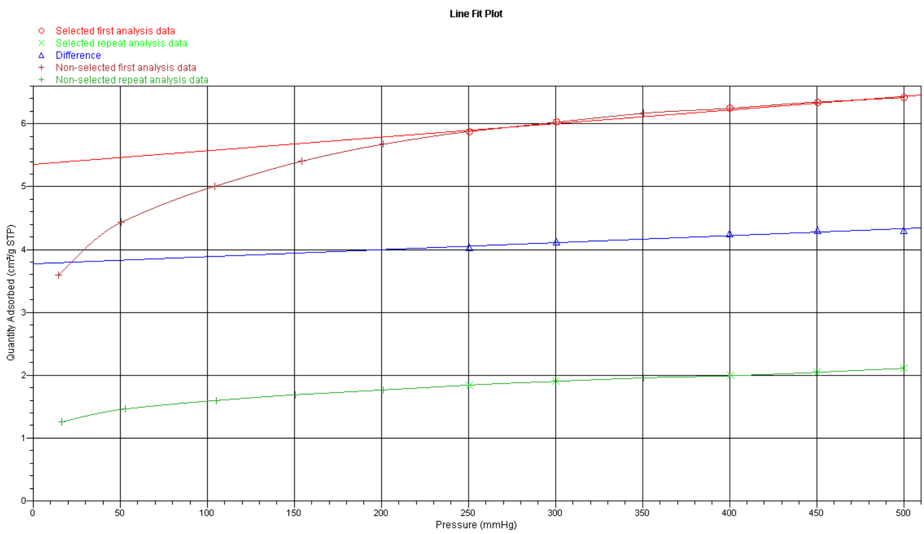

Figure D.20: Analysis summary and line fit plots from the H_2-chemisorption for CoRe60. Tested during the fall of 2017.

Analysis Summary

Element	Percent of Sample Weight (%)	Atomic Weight	Stoichiometry Factor	Atomic Cross-Sectional Area (nm²)	Density (cm³/g)
cobalt	20.000	58.933	2.000	0.0662	8.900

Analysis Results

Metal Dispersion: 15.1528 %
Metallic Surface Area: 20.5038 m²/g sample
Metallic Surface Area: 102.5191 m²/g metal
Crystallite Size (6.000 V / A): 6.57592 nm
Y-Intercept Quantity Adsorbed: 5.7631 ± 0.0432 cm³/g STP
Slope: 0.002330 ± 0.000120
Correlation Coefficient: 9.96027E-01

Difference Results

Metal Dispersion: 11.0132 %
Metallic Surface Area: 14.9024 m²/g sample
Metallic Surface Area: 74.5119 m²/g metal
Crystallite Size (6.000 V / A): 9.04764 nm
Y-Intercept Quantity Adsorbed: 4.1887 ± 0.0496 cm³/g STP
Slope: 0.001290 ± 0.000138
Correlation Coefficient: 9.83281E-01

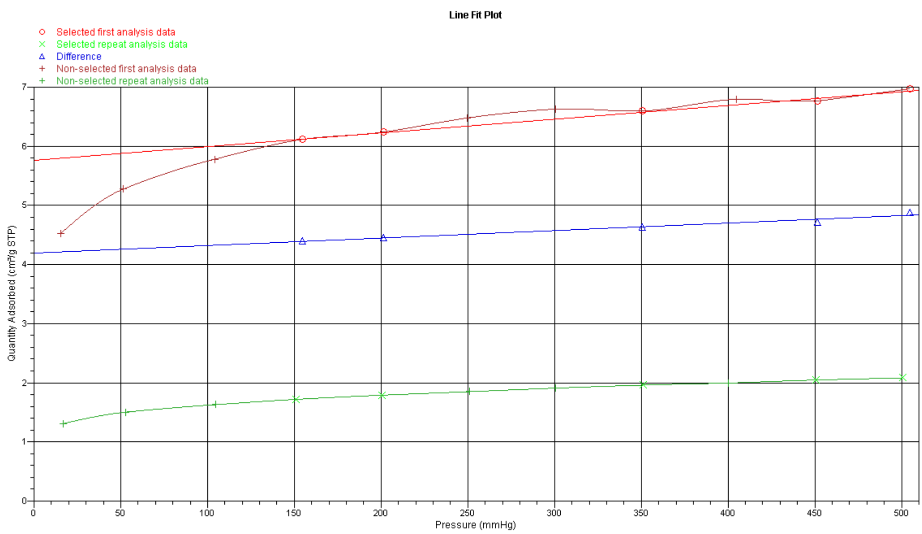

Figure D.21: Analysis summary and line fit plots from the H_2-chemisorption for CoRe80(Batch1). Tested during the fall of 2017.

Analysis Summary

Element	Percent of Sample Weight (%)	Atomic Weight	Stoichiometry Factor	Atomic Cross-Sectional Area (nm²)	Density (cm³/g)
cobalt	20.000	58.933	2.000	0.0662	8.900

Analysis Results

Metal Dispersion: 16.0988 %
Metallic Surface Area: 21.7839 m²/g sample
Metallic Surface Area: 108.9196 m²/g metal
Crystallite Size (6.000 V / A): 6.18949 nm
Y-Intercept Quantity Adsorbed: 6.1229 ± 0.0333 cm³/g STP
Slope: 0.002021 ± 0.000086
Correlation Coefficient: 9.96363E-01

Difference Results

Metal Dispersion: 11.7934 %
Metallic Surface Area: 15.9581 m²/g sample
Metallic Surface Area: 79.7903 m²/g metal
Crystallite Size (6.000 V / A): 8.44912 nm
Y-Intercept Quantity Adsorbed: 4.4854 ± 0.0336 cm³/g STP
Slope: 0.000997 ± 0.000087
Correlation Coefficient: 9.84985E-01

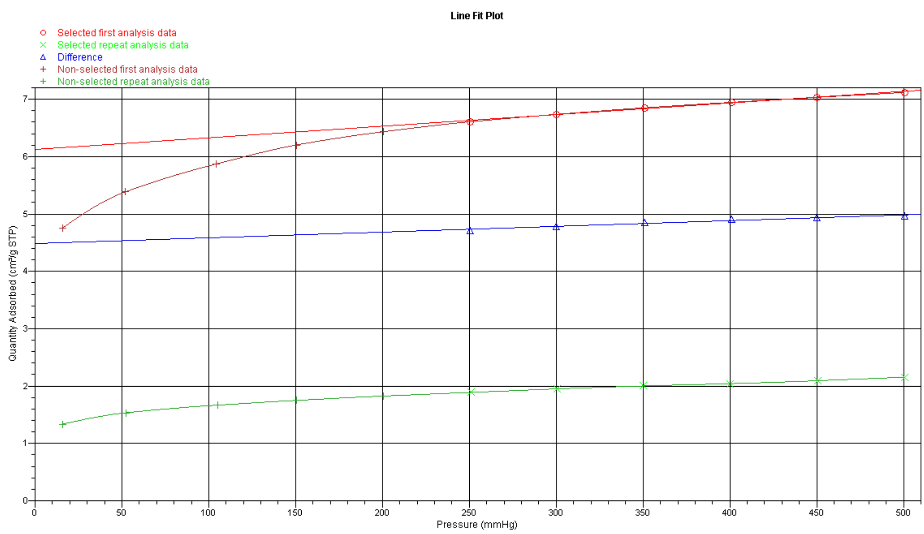

Figure D.22: Analysis summary and line fit plots from the H_2-chemisorption for CoRe80(Batch2). Tested during the fall of 2017.

Analysis Summary

Element	Percent of Sample Weight (%)	Atomic Weight	Stoichiometry Factor	Atomic Cross-Sectional Area (nm^2)	Density (cm^3/g)
cobalt	20.000	58.933	2.000	0.0662	8.900

Analysis Results

Metal Dispersion: 15.6423 %
Metallic Surface Area: 21.1662 m^2/g sample
Metallic Surface Area: 105.8308 m^2/g metal
Crystallite Size (6.000 V / A): 6.37014 nm
Y-Intercept Quantity Adsorbed: 5.9492 ± 0.0392 cm^3/g STP
Slope: 0.001567 ± 0.000096
Correlation Coefficient: 9.94358E-01

Difference Results

Metal Dispersion: 11.4427 %
Metallic Surface Area: 15.4836 m^2/g sample
Metallic Surface Area: 77.4179 m^2/g metal
Crystallite Size (6.000 V / A): 8.70803 nm
Y-Intercept Quantity Adsorbed: 4.3520 ± 0.0392 cm^3/g STP
Slope: 0.000614 ± 0.000096
Correlation Coefficient: 9.64896E-01

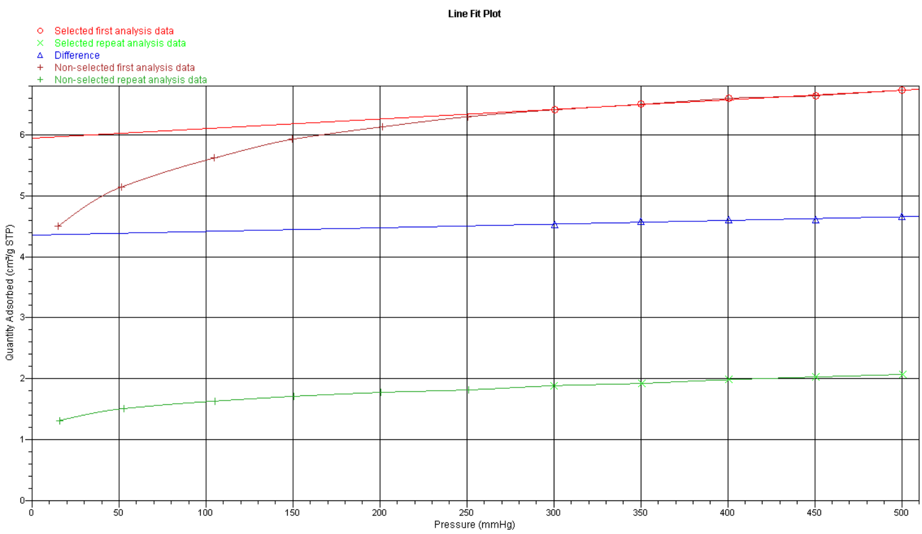

Figure D.23: Analysis summary and line fit plots from the H_2-chemisorption for CoRe80(Batch1and2). Tested during the fall of 2017.

Analysis Summary

Element	Percent of Sample Weight (%)	Atomic Weight	Stoichiometry Factor	Atomic Cross-Sectional Area (nm^2)	Density (cm^3/g)
cobalt	20.000	58.933	2.000	0.0662	8.900

Analysis Results

Metal Dispersion: 10.0629 %
Metallic Surface Area: 13.6165 m^2/g sample
Metallic Surface Area: 68.0823 m^2/g metal
Crystallite Size (6.000 V / A): 9.90209 nm
Y-Intercept Quantity Adsorbed: 3.8272 ± 0.0294 cm^3/g STP
Slope: 0.001270 ± 0.000081
Correlation Coefficient: 9.90070E-01

Difference Results

Metal Dispersion: 7.1958 %
Metallic Surface Area: 9.7369 m^2/g sample
Metallic Surface Area: 48.6846 m^2/g metal
Crystallite Size (6.000 V / A): 13.84744 nm
Y-Intercept Quantity Adsorbed: 2.7368 ± 0.0263 cm^3/g STP
Slope: 0.000478 ± 0.000072
Correlation Coefficient: 9.47797E-01

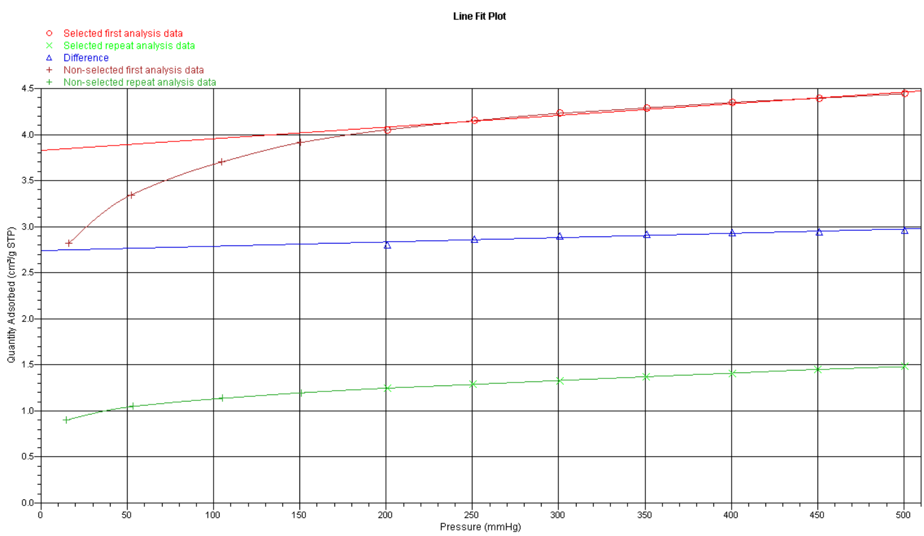

Figure D.24: Analysis summary and line fit plots from the H_2-chemisorption for CoRe95. Tested during the fall of 2017.

Analysis Summary

Element	Percent of Sample Weight (%)	Atomic Weight	Stoichiometry Factor	Atomic Cross-Sectional Area (nm^2)	Density (cm^3/g)
cobalt	20.000	58.933	2.000	0.0662	8.900

Analysis Results

Metal Dispersion: 7.7364 %
Metallic Surface Area: 10.4685 m^2/g sample
Metallic Surface Area: 52.3423 m^2/g metal
Crystallite Size (6.000 V / A): 12.87977 nm
Y-Intercept Quantity Adsorbed: 2.9424 ± 0.0132 cm^3/g STP
Slope: 0.000843 ± 0.000034
Correlation Coefficient: 9.96733E-01

Difference Results

Metal Dispersion: 5.8336 %
Metallic Surface Area: 7.8937 m^2/g sample
Metallic Surface Area: 39.4685 m^2/g metal
Crystallite Size (6.000 V / A): 17.08092 nm
Y-Intercept Quantity Adsorbed: 2.2187 ± 0.0174 cm^3/g STP
Slope: 0.000533 ± 0.000045
Correlation Coefficient: 9.85887E-01

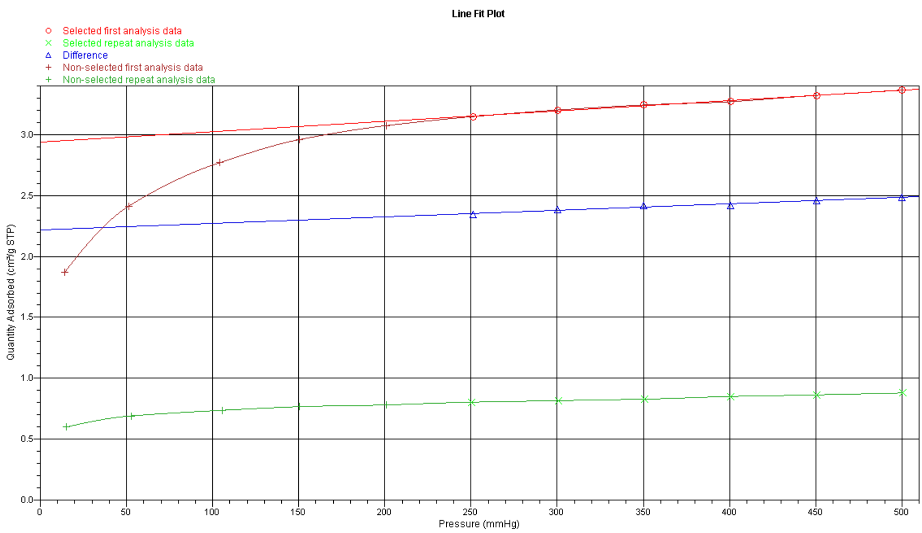

Figure D.25: Analysis summary and line fit plots from the H_2-chemisorption for CoRe100(Batch1). Tested during the fall of 2017.

Analysis Summary

Element	Percent of Sample Weight (%)	Atomic Weight	Stoichiometry Factor	Atomic Cross-Sectional Area (nm^2)	Density (cm^3/g)
cobalt	20.000	58.933	2.000	0.0662	8.900

Analysis Results

Metal Dispersion: 7.7412 %
Metallic Surface Area: 10.4749 m^2/g sample
Metallic Surface Area: 52.3747 m^2/g metal
Crystallite Size (6.000 V / A): 12.87181 nm
Y-Intercept Quantity Adsorbed: 2.9442 ± 0.0203 cm^3/g STP
Slope: 0.001271 ± 0.000054
Correlation Coefficient: 9.96373E-01

Difference Results

Metal Dispersion: 5.3397 %
Metallic Surface Area: 7.2253 m^2/g sample
Metallic Surface Area: 36.1265 m^2/g metal
Crystallite Size (6.000 V / A): 18.66104 nm
Y-Intercept Quantity Adsorbed: 2.0308 ± 0.0174 cm^3/g STP
Slope: 0.000494 ± 0.000046
Correlation Coefficient: 9.82729E-01

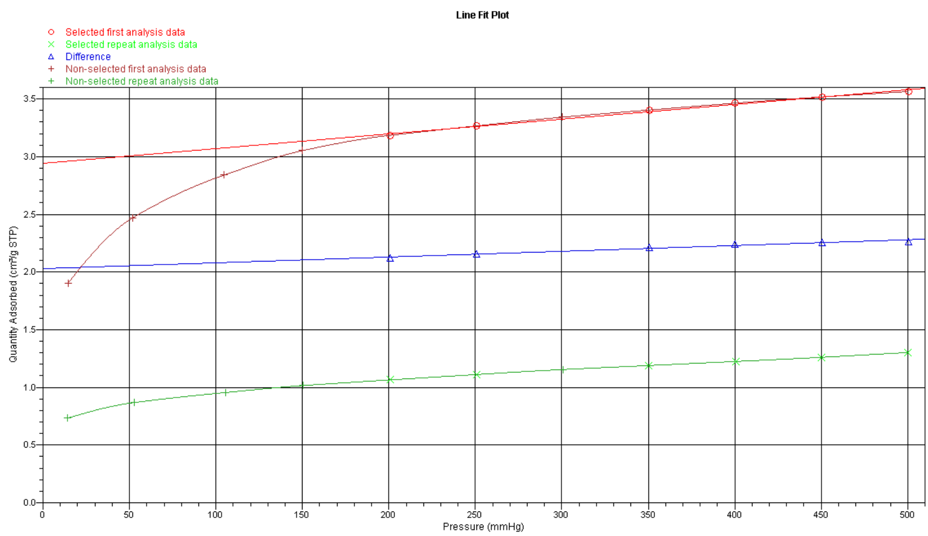

Figure D.26: Analysis summary and line fit plots from the H_2-chemisorption for CoRe100(Batch2). Tested during the fall of 2017.

Analysis Summary

Element	Percent of Sample Weight (%)	Atomic Weight	Stoichiometry Factor	Atomic Cross-Sectional Area (nm^2)	Density (cm^3/g)
cobalt	20.000	58.933	2.000	0.0662	8.900

Analysis Results

Metal Dispersion:	7.7332 %
Metallic Surface Area:	10.4641 m^2/g sample
Metallic Surface Area:	52.3204 m^2/g metal
Crystallite Size (6.000 V / A):	12.88516 nm
Y-Intercept Quantity Adsorbed:	2.9412 ± 0.0081 cm^3/g STP
Slope:	0.001047 ± 0.000021
Correlation Coefficient:	9.99192E-01

Difference Results

Metal Dispersion:	5.3727 %
Metallic Surface Area:	7.2700 m^2/g sample
Metallic Surface Area:	36.3501 m^2/g metal
Crystallite Size (6.000 V / A):	18.54623 nm
Y-Intercept Quantity Adsorbed:	2.0434 ± 0.0052 cm^3/g STP
Slope:	0.000289 ± 0.000014
Correlation Coefficient:	9.95648E-01

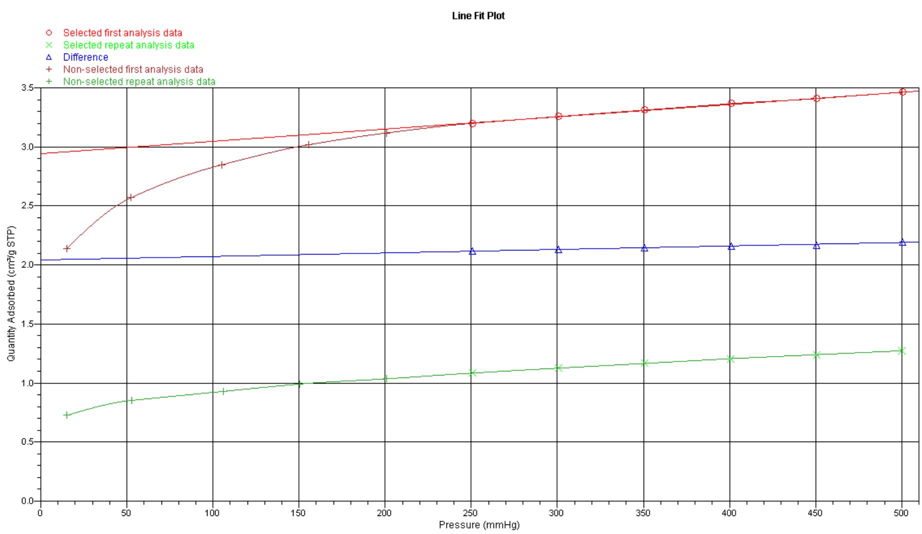

Figure D.27: Analysis summary and line fit plots from the H_2-chemisorption for CoRe100(500ppm). Tested during the fall of 2017.

Sample: CoRe100(1000ppm)
Operator: JS
File: C:\...\JONASS\000-448.SMP

Started:	02.06.2018 15:04:01	Analysis Gas:	H2
Completed:	03.06.2018 16:36:48	Analysis Temp:	40.0 °C
Report Time:	04.06.2018 10:54:25	Equilibration Interval:	24 s
Sample Mass:	0.2011 g	Low Pressure Dose:	None
Measured free space:	17.8022 cm³	Smoothed Pressures:	No
Automatic Degas:	No		

Analysis Summary

Element	Percent of Sample Weight (%)	Atomic Weight	Stoichiometry Factor	Atomic Cross-Sectional Area (nm²)	Density (cm³/g)
cobalt	20.000	58.933	2.000	0.0662	8.900

Analysis Results

Metal Dispersion: 7.2560 %
Metallic Surface Area: 9.8184 m²/g sample
Metallic Surface Area: 49.0920 m²/g metal
Crystallite Size (6.000 V / A): 13.73252 nm
Y-Intercept Quantity Adsorbed: 2.7597 ± 0.0133 cm³/g STP
Slope: 0.000694 ± 0.000038
Correlation Coefficient: 9.96975E-01

Difference Results

Metal Dispersion: 4.8335 %
Metallic Surface Area: 6.5404 m²/g sample
Metallic Surface Area: 32.7021 m²/g metal
Crystallite Size (6.000 V / A): 20.61512 nm
Y-Intercept Quantity Adsorbed: 1.8383 ± 0.0658 cm³/g STP
Slope: 0.000102 ± 0.000190
Correlation Coefficient: 3.54911E-01

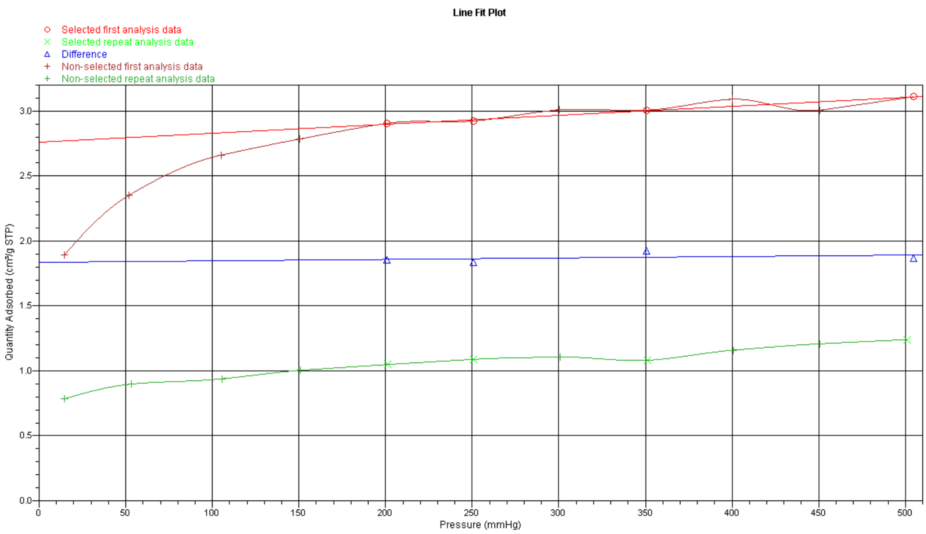

Figure D.28: Analysis summary and line fit plots from the H_2-chemisorption for CoRe100(1000ppm). Tested during the spring of 2018.

Analysis Summary

Element	Percent of Sample Weight (%)	Atomic Weight	Stoichiometry Factor	Atomic Cross-Sectional Area (nm²)	Density (cm³/g)
cobalt	20.000	58.933	2.000	0.0662	8.900

Analysis Results

Metal Dispersion: 13.9161 %
Metallic Surface Area: 18.8304 m²/g sample
Metallic Surface Area: 94.1518 m²/g metal
Crystallite Size (6.000 V / A): 7.16033 nm
Y-Intercept Quantity Adsorbed: 5.2927 ± 0.0434 cm³/g STP
Slope: 0.001741 ± 0.000111
Correlation Coefficient: 9.93978E-01

Difference Results

Metal Dispersion: 9.9126 %
Metallic Surface Area: 13.4131 m²/g sample
Metallic Surface Area: 67.0656 m²/g metal
Crystallite Size (6.000 V / A): 10.05221 nm
Y-Intercept Quantity Adsorbed: 3.7701 ± 0.0407 cm³/g STP
Slope: 0.000909 ± 0.000104
Correlation Coefficient: 9.80975E-01

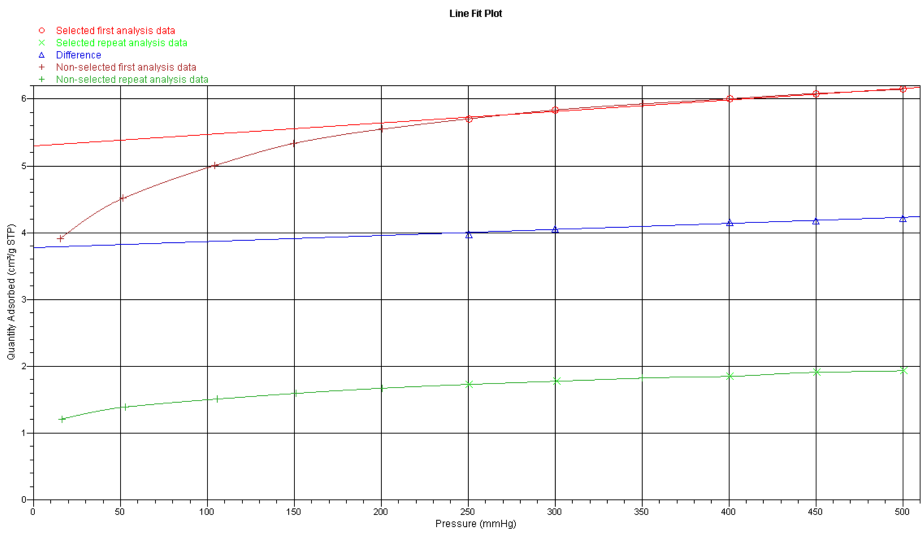

Figure D.29: Analysis summary and line fit plots from the H_2-chemisorption for CoRe80(500ppm)Test1. Tested during the fall of 2017.

Analysis Summary

Element	Percent of Sample Weight (%)	Atomic Weight	Stoichiometry Factor	Atomic Cross-Sectional Area (nm^2)	Density (cm^3/g)
cobalt	20.000	58.933	2.000	0.0662	8.900

Analysis Results

Metal Dispersion: 14.7062 %
Metallic Surface Area: 19.8995 m^2/g sample
Metallic Surface Area: 99.4973 m^2/g metal
Crystallite Size (6.000 V / A): 6.77563 nm
Y-Intercept Quantity Adsorbed: 5.5932 ± 0.0355 cm^3/g STP
Slope: 0.001804 ± 0.000092
Correlation Coefficient: 9.94831E-01

Difference Results

Metal Dispersion: 10.5470 %
Metallic Surface Area: 14.2716 m^2/g sample
Metallic Surface Area: 71.3579 m^2/g metal
Crystallite Size (6.000 V / A): 9.44755 nm
Y-Intercept Quantity Adsorbed: 4.0114 ± 0.0257 cm^3/g STP
Slope: 0.000871 ± 0.000067
Correlation Coefficient: 9.88456E-01

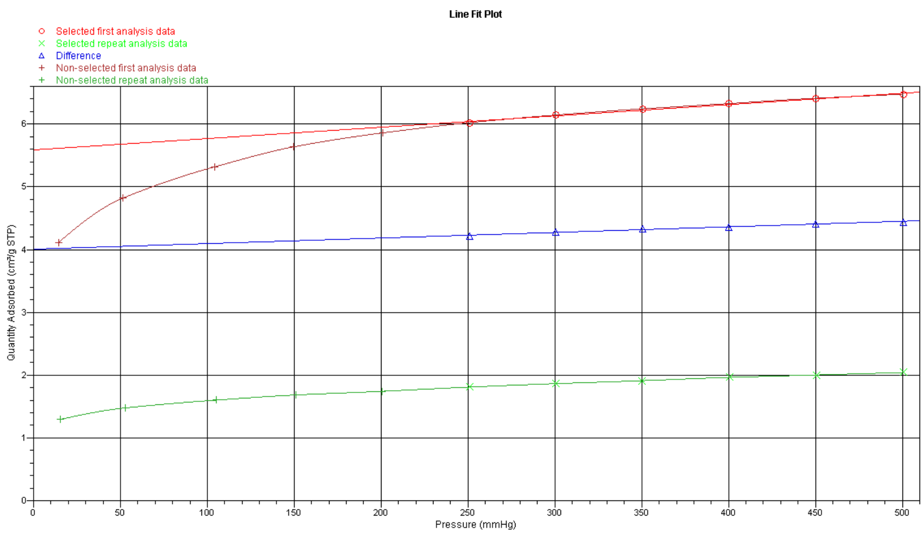

Figure D.30: Analysis summary and line fit plots from the H_2-chemisorption for CoRe80(500ppm)Test2. Tested during the fall of 2017.

Analysis Summary

Element	Percent of Sample Weight (%)	Atomic Weight	Stoichiometry Factor	Atomic Cross-Sectional Area (nm^2)	Density (cm^3/g)
cobalt	20.000	58.933	2.000	0.0662	8.900

Analysis Results

Metal Dispersion:	15.0636 %
Metallic Surface Area:	20.3831 m^2/g sample
Metallic Surface Area:	101.9155 m^2/g metal
Crystallite Size (6.000 V / A):	6.61487 nm
Y-Intercept Quantity Adsorbed:	5.7291 ± 0.0421 cm^3/g STP
Slope:	0.002167 ± 0.000109
Correlation Coefficient:	9.94943E-01

Difference Results

Metal Dispersion:	10.7018 %
Metallic Surface Area:	14.4810 m^2/g sample
Metallic Surface Area:	72.4052 m^2/g metal
Crystallite Size (6.000 V / A):	9.31090 nm
Y-Intercept Quantity Adsorbed:	4.0702 ± 0.0456 cm^3/g STP
Slope:	0.001115 ± 0.000118
Correlation Coefficient:	9.78189E-01

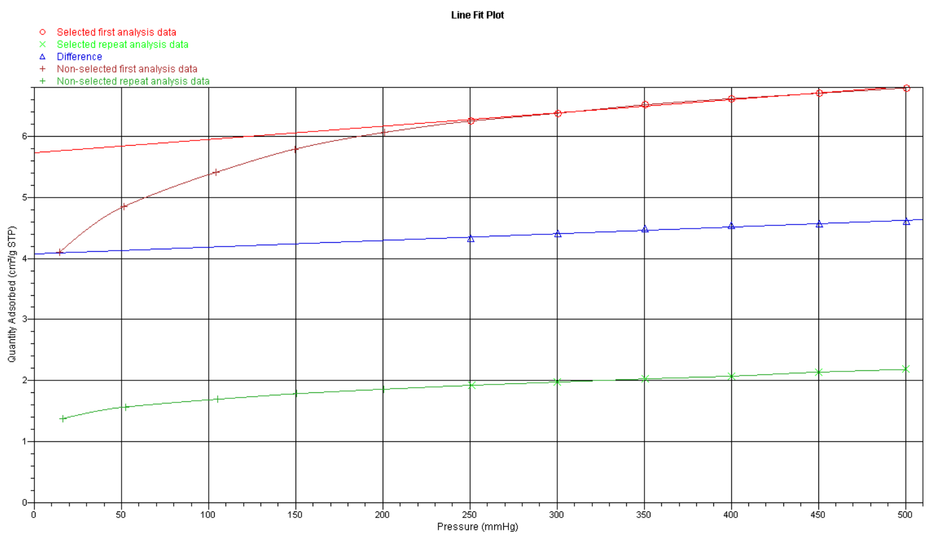

Figure D.31: Analysis summary and line fit plots from the H_2-chemisorption for CoRe80(1000ppm). Tested during the spring of 2018.

Analysis Summary

Element	Percent of Sample Weight (%)	Atomic Weight	Stoichiometry Factor	Atomic Cross-Sectional Area (nm^2)	Density (cm^3/g)
cobalt	15.000	58.933	2.000	0.0662	8.900

Analysis Results

Metal Dispersion: 7.9627 %
Metallic Surface Area: 8.0810 m^2/g sample
Metallic Surface Area: 53.8734 m^2/g metal
Crystallite Size (6.000 V / A): 12.51372 nm
Y-Intercept Quantity Adsorbed: 2.2714 ± 0.0066 cm^3/g STP
Slope: 0.000762 ± 0.000018
Correlation Coefficient: 9.98586E-01

Difference Results

Metal Dispersion: 4.2952 %
Metallic Surface Area: 4.3590 m^2/g sample
Metallic Surface Area: 29.0600 m^2/g metal
Crystallite Size (6.000 V / A): 23.19880 nm
Y-Intercept Quantity Adsorbed: 1.2252 ± 0.0120 cm^3/g STP
Slope: 0.000087 ± 0.000033
Correlation Coefficient: 7.64225E-01

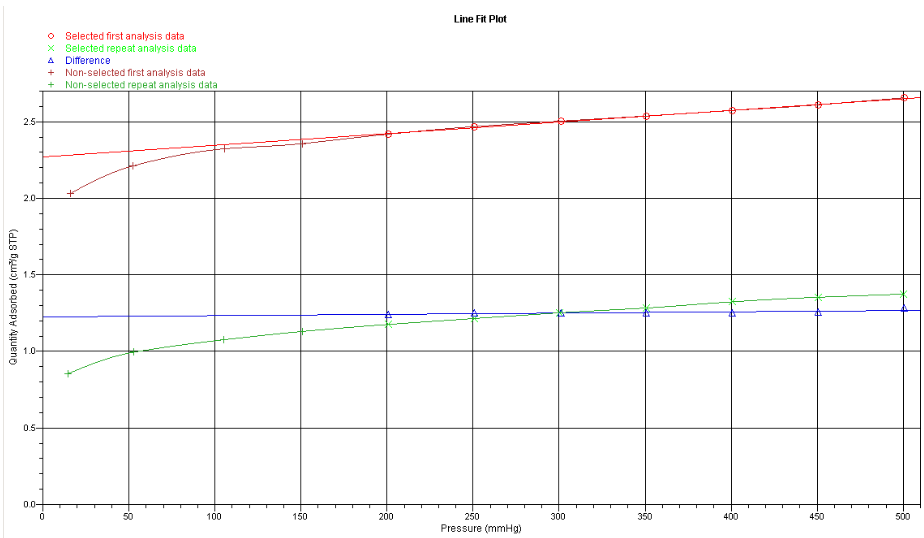

Figure D.32: Analysis summary and line fit plots from the H_2-chemisorption for CoRe100(68ppm)-SiO_2. Tested during the spring of 2018.

Analysis Summary

Element	Percent of Sample Weight (%)	Atomic Weight	Stoichiometry Factor	Atomic Cross-Sectional Area (nm^2)	Density (cm^3/g)
cobalt	15.000	58.933	2.000	0.0662	8.900

Analysis Results

Metal Dispersion: 7.5886 %
Metallic Surface Area: 7.7013 m^2/g sample
Metallic Surface Area: 51.3422 m^2/g metal
Crystallite Size (6.000 V / A): 13.13066 nm
Y-Intercept Quantity Adsorbed: 2.1646 ± 0.0210 cm^3/g STP
Slope: 0.001026 ± 0.000066
Correlation Coefficient: 9.91934E-01

Difference Results

Metal Dispersion: 3.9966 %
Metallic Surface Area: 4.0559 m^2/g sample
Metallic Surface Area: 27.0394 m^2/g metal
Crystallite Size (6.000 V / A): 24.93237 nm
Y-Intercept Quantity Adsorbed: 1.1400 ± 0.0201 cm^3/g STP
Slope: 0.000197 ± 0.000063
Correlation Coefficient: 8.43320E-01

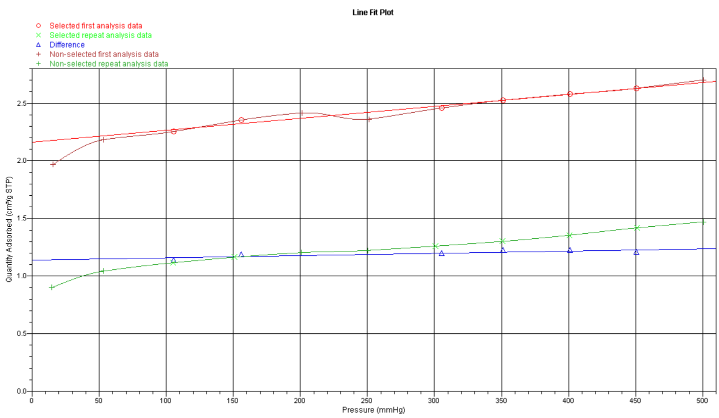

Figure D.33: Analysis summary and line fit plots from the H_2-chemisorption for CoRe100(526ppm)-SiO_2. Tested during the spring of 2018.

D.3 Additional TPR results

The figures D.34 and D.35 illustrate the reproducibility of the catalysts upon TPR experiments.

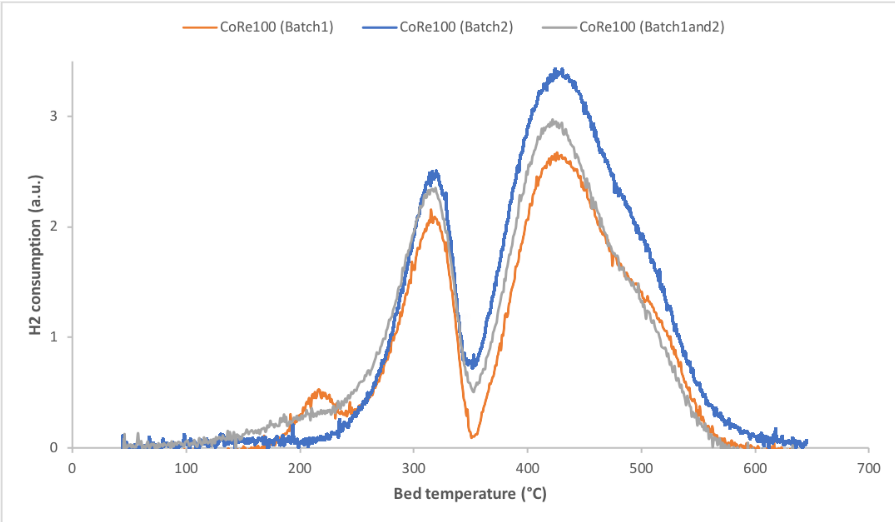

Figure D.34: TPR curves of CoRe100 showing reproducibility.

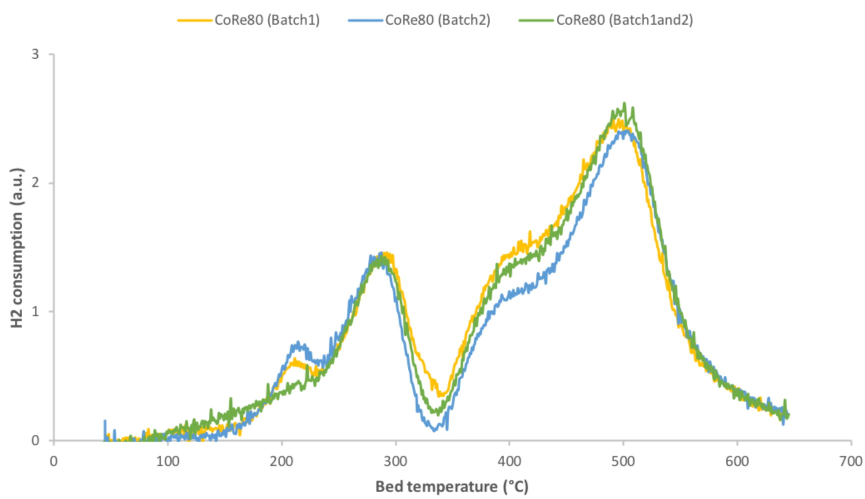

Figure D.35: TPR curves of CoRe80 showing reproducibility.

D.4 Additional Fischer-Tropsch synthesis results

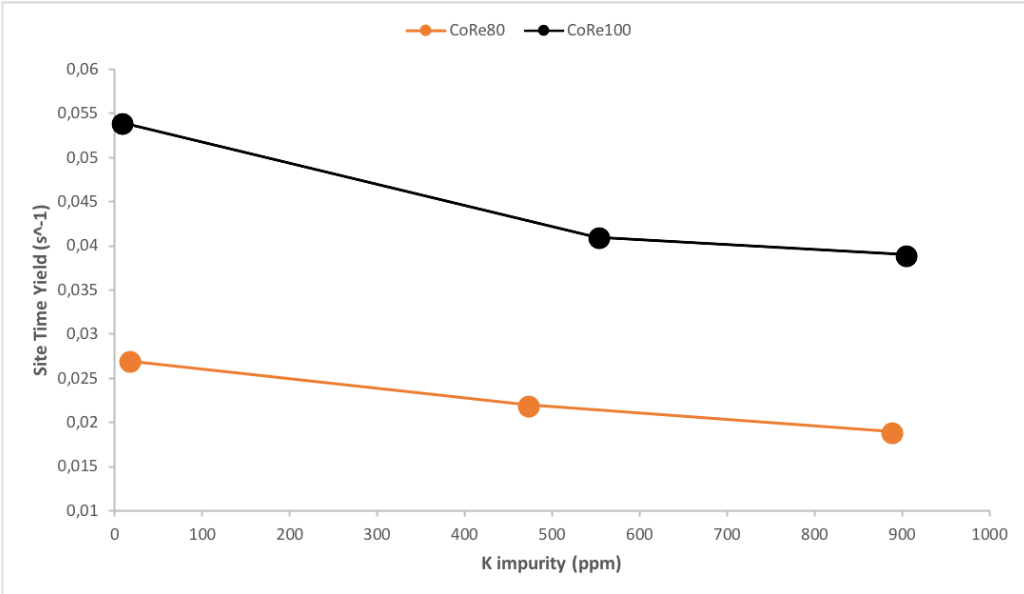

Figure D.36: Site Time Yield (STY) after 24 h on stream for CoRe catalysts of medium and small cobalt particle sizes (CoRe100 and CoRe80, respectively) at different K loadings.

The activity and selectivity results were all produced through processing of GC data in the MATLAB code, shown in section D.5. An example of the result is shown for CoRe80(500ppm) in section D.6

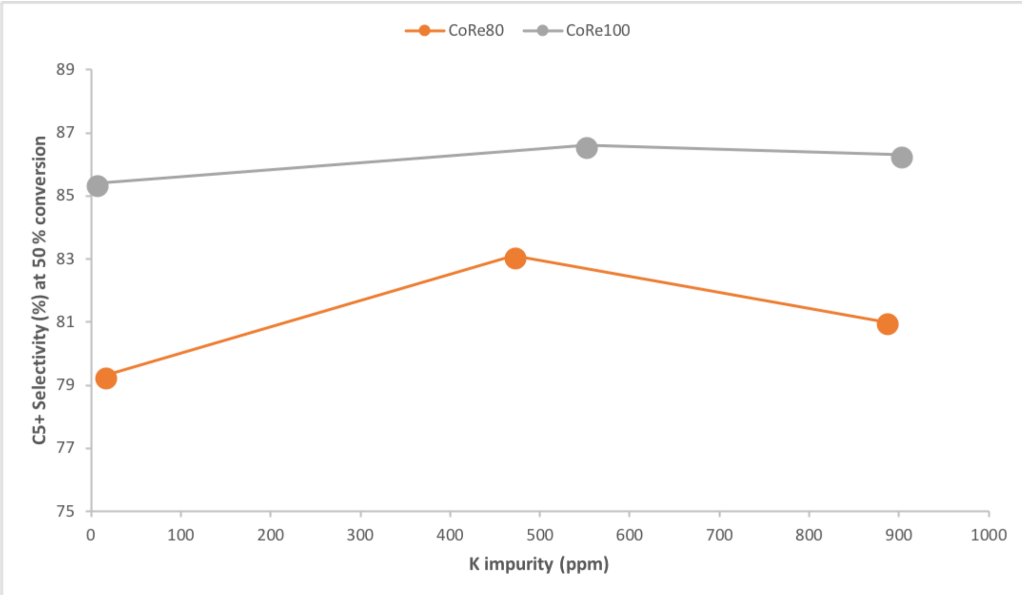

Figure D.37: C_{5+}-selectivity after 30-45 h on stream for CoRe catalysts of medium and small cobalt particle sizes (CoRe100 and CoRe80, respectively) at different K loadings.

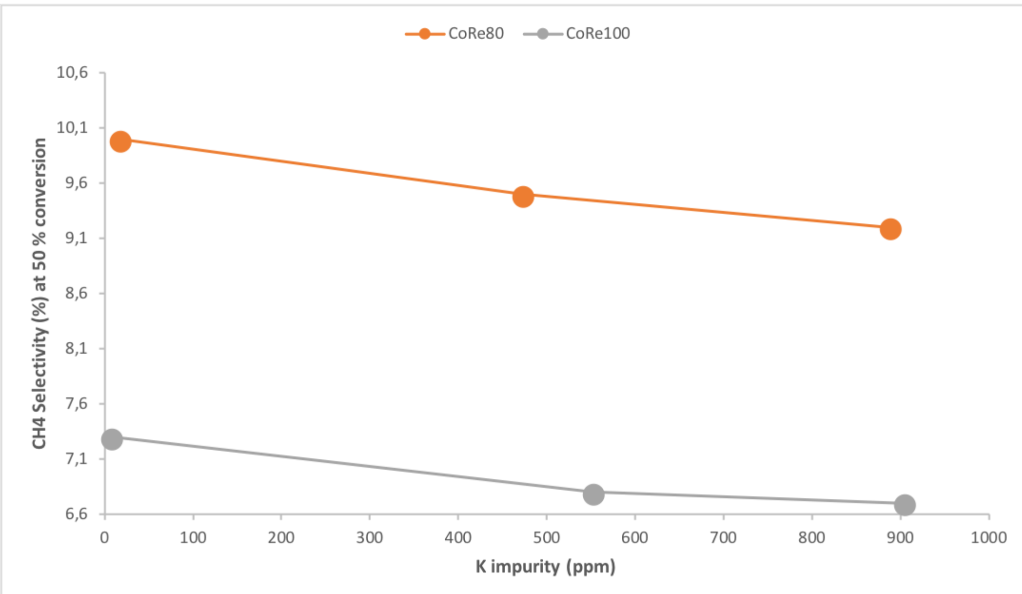

Figure D.38: CH_4-selectivity after 30-45 h on stream for CoRe catalysts of medium and small cobalt particle sizes (CoRe100 and CoRe80, respectively) at different K loadings.

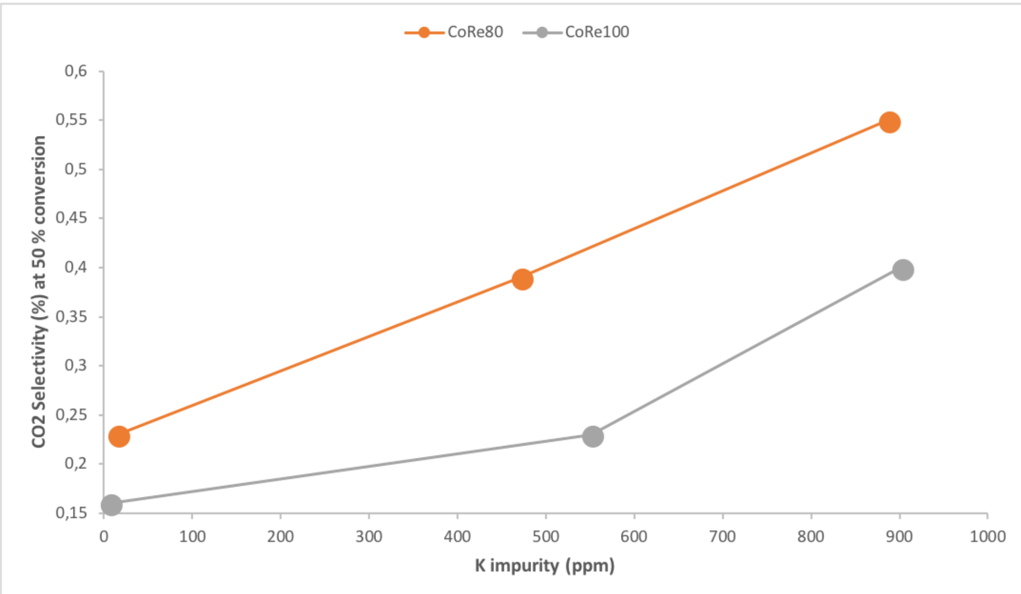

Figure D.39: CO_2-selectivity after 30-45 h on stream for CoRe catalysts of medium and small cobalt particle sizes (CoRe100 and CoRe80, respectively) at different K loadings.

D.5 MATLAB code producing activity results

MATLAB code used for processing the data obtained from the gas chromatograph. The following MATLAB code illustrate how the activity data for CoRe80(500ppm) was processed.

```
clear all
close all
fclose('all');
clc

% %%%%%%%%%%%%%%%%%%%%%%%%%%%%%%%%%%%%%%%%%%%%%%%%%%%%%%%%%%%%%%%%%%%%%%%%%%%%%%%%%%%%%%%%%%%%%%%%%%%%%%%%
%%%%%%%%%%%%%%%%%%%%%%%%%%%%%%%%%%%%%%%%%%%%%%%%%%%%%%     INPUT PARAMETERS     %%%%%%%%%%%%%%%%%%%%%%%%%%%%%%%%%%%%%%%%%%%%%%%%%%%%%%%%%%%%%%%%%%%%%%%%%%%
% %%%%%%%%%%%%%%%%%%%%%%%%%%%%%%%%%%%%%%%%%%%%%%%%%%%%%%%%%%%%%%%%%%%%%%%%%%%%%%%%%%%%%%%%%%%%%%%%%%%%%%%%%%%%%


% INFO:
Catalyst_Name = 'CoRe80(500ppmK)';
SynGasBottle = 'AGA751';

% Catalyst Properties
m_cat = 1.0026;                                    % Mass of catalyst [g]
m_SiC = 20.0183;                                   % Mass of SiC [g]
x_m = 20;                      % Active Metal fraction in catalyst [%]
D = 15;                                       % Catalyst Dispersion [%]

% SynGas Properties
Y_N2 = 3;                                          % N2 mole fraction [%]
Y_CO = 31.3;                                       % CO mole fraction [%]

```

```
% Measurements
N_FEED = 22;                                                        % No. of feed analyses
N_REAC = 35;                                                        % No. of reactor analyses

% Report
WriteReport = 1;                                  % Write ExCel report? 1=Yes/0=No
ConPlot = 1;                              % Plot conversion vs. time? 1=Yes/0=No
TarCon = 50;                  % Conversion at which selectivity is compared [%]

% Experiment Matrix:
% No. of rows = No. of reaction steps
% Columns 1-6) Start-time: dd mm yy hh min sec
% 7) First injection no. in step, i.e. running injection # + 1
% 8-11) Feeds: 8) Syngas 9) CO 10) H2 11) CO2 12) H2O(l) [mL/min]
% 13) T [C]
% 14) P [bar a]

ExpMat = [27 2 18 12 39 0 1 298.3 0 0 0 0 210 20;
          28 2 18 14 9 0 26 99.92 0 0 0 0 210 20;
          28 2 18 20 22 0 32 101.1 0 0 0 0 210 20;
          28 2 18 21 22 0 33 103.44 0 0 0 0 210 20;
          28 2 18 22 25 0 34 105.79 0 0 0 0 210 20];
% %%%%%%%%%%%%%%%%%%%%%%%%%%%%%%%%%%%%%%%%%%%%%%%%%%%%%%%%%%%%%%%%%%%%%%%%%%%%%%%%%%%%%%%%%%%%%%%%%%
%%%%%%%%%%%%%%%%%%%%%%%%%%% END OF INPUT PARAMETERS %%%%%%%%%%%%%%%%%%%%%%%%%%%%%%%%
% %%%%%%%%%%%%%%%%%%%%%%%%%%%%%%%%%%%%%%%%%%%%%%%%%%%%%%%%%%%%%%%%%%%%%%%%%%%%%%%%%%%%%%%%%%%%%%%%%%

% %%%%%%%%%%%%%%%%%%%%%%%%%%%%%%%%%%%%%%%%%%%%%%%%%%%%%%%%%%%%%%%%%%%%%%%%%%%%%%%%%%%%%%%%%%%%%%%%%%
```

```
%%%%%%%%%%%%%%%%%%%% CONSTANTS & PRELIMINARY CALCULATIONS %%%%%%%%%%%%%%%%%%%%%%%%
% %%%%%%%%%%%%%%%%%%%%%%%%%%%%%%%%%%%%%%%%%%%%%%%%%%%%%%%%%%%%%%%%%%%%%%%%%%%%%%%%%%%%%%%%%%%%%%%%%%%%%%%%%%%%%%%

% Sort analysis folders
if N_FEED > 0
    warning('off','MATLAB:MKDIR:DirectoryExists');
    feedfolder = dir('FT-FODE*');
    feedfolder = num2str(feedfolder.name);
    mkdir Feed
end
if N_REAC > 0
    reakfolder = dir('FT-REAK*');
    reakfolder = num2str(reakfolder.name);
    mkdir Reactor
end

% Start Date
Date = [num2str(ExpMat(1,1)) '.' num2str(ExpMat(1,2)) '.20' num2str(ExpMat(1,3))];

% Physical Constants
V_m = 24465;                % Ideal gas molar volume (1 atm, 25 C) [mL/mol]
% V_m = 22414:              % Ideal gas molar volume (1 atm,  0 C) [mL/mol]
% V_m = 24790:              % Ideal gas molar volume (1 bar, 25 C) [mL/mol]
% V_m = 22711:              % Ideal gas molar volume (1 bar,  0 C) [mL/mol]

M_Co  = 58.93319;                            % Molar mass of Cobalt [g/mol]
M_H2O = 18.01528;                             % Molar mass of Water [g/mol]
rho_H2O = 0.9970479;                     % Density of Water (25 C) [g/cm^3]
```

```
% rho_H2O = 0.999972;                    % Density of
    Water  (4 C) [g/cm^3]

% No. of reaction steps
N_STEP = size(ExpMat,1);

% SynGas Mole fractions [N2 CO H2]
Y_Syn = [Y_N2;Y_CO;(100-Y_N2-Y_CO)]/100;

% Gas Feed rates [mL/min]
F0_N2   = ExpMat(:,8)*Y_Syn(1);
F0_CO   = ExpMat(:,8)*Y_Syn(2)+ExpMat(:,9);
F0_H2   = ExpMat(:,8)*Y_Syn(3)+ExpMat(:,10);
F0_CO2  = ExpMat(:,11);
F0_H2O  = ExpMat(:,12)*rho_H2O*V_m/M_H2O;
F0_T    = F0_N2 + F0_CO + F0_H2 + F0_CO2 + F0_H2O;

% Feed Gas Mole Fractions [N2 CO H2 CO2 H2O]
Y(:,1)  = F0_N2./F0_T;
Y(:,2)  = F0_CO./F0_T;
Y(:,3)  = F0_H2./F0_T;
Y(:,4)  = F0_CO2./F0_T;
Y(:,5)  = F0_H2O./F0_T;

% GHSV [mL total gas flow/gcat h]
GHSV = F0_T*60/m_cat;

% Leap year correction
Year = ExpMat(1,3)+2000;
if mod(Year,4) ~= 0
    leapyear = 0;
elseif mod(Year,100) ~= 0
    leapyear = 1;
elseif mod(Year,400) ~= 0
    leapyear = 0;
else
    leapyear = 1;
end

% Assign month correction
```

```
if  ismember(ExpMat(1,2),[1 3 5 7 8 10 12])
    dayfac = 31;
elseif ismember(ExpMat(1,2),[4 6 9 11])
    dayfac = 30;
else
    dayfac = 28+leapyear;
end

%%%%%%%%%%%%%%%%%%%%%%%%%%%%%%%%%%%%%%%%%%%%%%%%%%%%%%%%%%%%%%%%%%%%%%%%%%%%%%%%%%%%%%%%%%%%%%%%%%%
%%%%%%%%%%%%%%%%%%%%%%%%%%%%%%%%%% GC Calibration Data %%%%%%%%%%%%%%%%%%%%%%%%%%%%%%%%%%%%%%%%
%%%%%%%%%%%%%%%%%%%%%%%%%%%%%%%%%%%%%%%%%%%%%%%%%%%%%%%%%%%%%%%%%%%%%%%%%%%%%%%%%%%%%%%%%%%%%%%%%%%

%%%%%%%%%%%%%%%%%%%%%%%%%%%%%%%%%%%%%%%%%%%%
% Relative response factors
%%%%%%%%%%%%%%%%%%%%%%%%%%%%%%%%%%%%%%%%%%%%

% TCD
RRF_H2  = 35.90545705;
RRF_CO  = 0.997845877;
RRF_CH4 = 1.316560478;
RRF_CO2 = 0.888951609;

% FID
RRF_C2 = 1/2;                                           % Ethane/Ethene
RRF_C3 = 1/3;  % Propane/Propene
RRF_C4 = 1/4;                              % n/i-Butane,1/cis/trans/i-Butene
RRF_C5 = 1/5;                            % n/i-Pentane,1/i-Pentene,C5-olefin?
RRF_C6 = 1/6;                                                 % n-Hexane/1-Hexene
```

```
RRF_C7 = 1/7;                                                    % n-Heptane/i-Heptene

% %%%%%%%%%%%%%%%%%%%%%%%%%%%%%%%%%%%%%%%%%%%%%%%%%%%%%%%%%%%%%%%%%%%%%%%%%%%
%%%%%%%%%%%%%%%%%%%%%%%%%%%%%%%%%%%%        FEED ANALYSIS        %%%%%%%%%%%%%%%%%%%%%%%%%%%%%%%%%%%%%%%%
% %%%%%%%%%%%%%%%%%%%%%%%%%%%%%%%%%%%%%%%%%%%%%%%%%%%%%%%%%%%%%%%%%%%%%%%%%%%

cd(feedfolder)
for i = 1:N_FEED
    Dig = floor(log10(i))+1;
     if Dig == 1;
        Temp1 = sprintf('001F010%i.D/Report.TXT',i);
        Temp2 = sprintf('../Feed/001F010%i.D/',i);
        Temp3 = sprintf('../Feed/001F010%i.D/Report.TXT',i);
     elseif Dig == 2;
        Temp1 = sprintf('001F01%i.D/Report.TXT',i);
        Temp2 = sprintf('../Feed/001F01%i.D/',i);
        Temp3 = sprintf('../Feed/001F01%i.D/Report.TXT',i);
     end

     % Sort
     mkdir(Temp2)

     % Read report file
        unicode2ascii(Temp1,Temp3)          % Converts report to ASCII format
        fid = fopen(Temp3,'r');                               % Open report file
        C = textscan(fid,'%s','Delimiter','\n');          % Scans text to cell
        fclose(fid);                                          % Close report file

```

```
    % Search for CO - Syntax
    % L_CO = strfind(C{1}, 'CO ');            % Empty or
        nonempty lines w/CO
    % L_CO = find(~cellfun('isempty', L_CO));              %
        Returns line no.
    % L_CO = C{1}{L_CO}
                                                  % Returns line

        A_CO(i) = str2num(C{1}{~cellfun('isempty', strfind
            (C{1}, 'CO '))}(14:23));
        A_H2(i) = str2num(C{1}{~cellfun('isempty', strfind
            (C{1}, 'H2 '))}(14:23));
        A_N2(i) = str2num(C{1}{~cellfun('isempty', strfind
            (C{1}, 'N2 '))}(14:23));
        CO_N2(i) = A_CO(i)/A_N2(i);
        H2_N2(i) = A_H2(i)/A_N2(i);
end
cd ..

A_CO_raw = A_CO;
A_H2_raw = A_H2;
A_N2_raw = A_N2;

clear A_CO A_H2 A_N2

%%%%%%%%%%%%%%%%%%%%%%%%%%%%%%%%%%%%%%%%%%%%%
%%%% Remove outlying values
%%%%%%%%%%%%%%%%%%%%%%%%%%%%%%%%%%%%%%%%%%%%%

OK = 0;

while OK == 0;
    OK = 1;
    CO_N2_d = abs(CO_N2-mean(CO_N2));
    [d1,d2] = max(CO_N2_d);
    if d1 > 1.5*std(CO_N2)
            CO_N2(d2) = [ ];
            OK = 0;
    end

```

```
        H2_N2_d = abs(H2_N2-mean(H2_N2));
        [d1,d2] = max(H2_N2_d);
        if H2_N2_d(d2) > 1.5*std(H2_N2)
                H2_N2(d2) = [ ];
                OK = 0;
        end


end


% %%%%%%%%%%%%%%%%%%%%%%%%%%%%%%%%%%%%%%%%%%%%%%%%%%%%%%%%%%%%%%%%%%%%%%%%%%%%%%%%%%%%%%%%%%%%%%%%
%%%%%%%%%%%%%%%%%%%%%%%%%%%%%%%%%%%%          REACTOR ANALYSIS          %%%%%%%%%%%%%%%%%%%%%%%%%%%%%%%%%%%%%%%%%%%%
% %%%%%%%%%%%%%%%%%%%%%%%%%%%%%%%%%%%%%%%%%%%%%%%%%%%%%%%%%%%%%%%%%%%%%%%%%%%%%%%%%%%%%%%%%%%%%%%%

if N_REAC == 0
        break
end

cd(reakfolder)
for i = 2:N_REAC


        %%%%%%%%%%%%%%%%%%%%%%%%%%%%%%%%%%%%%%%%%%%
        % Identify Reaction Step
        %%%%%%%%%%%%%%%%%%%%%%%%%%%%%%%%%%%%%%%%%%%

        for k = 1:N_STEP
                if i >= ExpMat(k,7)
                        CurrStep = k;
                end
        end

        %%%%%%%%%%%%%%%%%%%%%%%%%%%%%%%%%%%%%%%%%%%%%%%%%%%%%%%%%%%%%%%%%%%%%%%%%%%%%%%%%%%%%%%%%%%%
        % Determine report file name and convert to ASCII
        %%%%%%%%%%%%%%%%%%%%%%%%%%%%%%%%%%%%%%%%%%%%%%%%%%%%%%%%%%%%%%%%%%%%%%%%%%%%%%%%%%%%%%%%%%%%
```

```
    Dig = floor(log10(i))+1;
     if Dig == 1;
         Temp1 = sprintf('001F010%i.D/Report.TXT',i);
         Temp2 = sprintf('../Reactor/001F010%i.D/',i);
         Temp3 = sprintf('../Reactor/001F010%i.D/Report.TXT
             ',i);
     elseif Dig == 2;
         Temp1 = sprintf('001F01%i.D/Report.TXT',i);
         Temp2 = sprintf('../Reactor/001F01%i.D/',i);
         Temp3 = sprintf('../Reactor/001F01%i.D/Report.TXT'
             ,i);
     end

    % Sort
     mkdir(Temp2)

    %%%%%%%%%%%%%%%%%%%%%%
    % Read report file
    %%%%%%%%%%%%%%%%%%%%%%
         unicode2ascii(Temp1,Temp3)
         fid = fopen(Temp3,'r');
         C = textscan(fid,'%s','Delimiter','\n');
         fclose(fid);

    %%%%%%%%%%%%%%%%%%%%%%%%%%
    % Find injection time
    %%%%%%%%%%%%%%%%%%%%%%%%%%

    t_line = C{1}{~cellfun('isempty', strfind(C{1}, '
       Injection Date'))};
    t_month = t_line(22:24);
    Months = 'JanFebMarAprMayJunJulAugSepOctNovDec';
    for j = 1:12
        if t_month == Months(3*j-2:3*j);
            t_month = j;
        end
    end

    t_inj = [str2double(t_line(19:20))
```

```
            t_month
            str2num(t_line(26:27))
            str2num(t_line(30:31))
            str2num(t_line(33:34))
            str2num(t_line(36:37))]';                    % [
               dd mm yy hh mm ss]

    %%%%%%%%%%%%%%%%%%%%%%%%%%%%%%%%%
    % Convert to time on stream [h]
    %%%%%%%%%%%%%%%%%%%%%%%%%%%%%%%%%

    TOS(i) = (t_inj - ExpMat(1,1:6))*[24 dayfac*24 (365+
       leapyear)*24 1 1/60 1/3600]';
    TOStep(i) = (t_inj - ExpMat(CurrStep,1:6))*[24 dayfac
       *24 (365+leapyear)*24 1 1/60 1/3600]';

    %%%%%%%%%%%%%%%%
    % Find GC Areas
    %%%%%%%%%%%%%%%%

%       % Search for CO syntax:
%        L_CO = strfind(C{1}, '1-Buten')
%        L_CO = find(~cellfun('isempty', L_CO))
%        L_CO = C{1}{L_CO}
%        A_CO = str2num(L_CO(13:24))

     %%%%%%%%%%%%%%%%%%%%
     % TCD Calculations
     %%%%%%%%%%%%%%%%%%%%
        A_N2(i) = str2num(C{1}{~cellfun('isempty',strfind(
           C{1},'N2'))}(14:23));
        A_CO(i) = str2num(C{1}{~cellfun('isempty',strfind(
           C{1},'CO  '))}(14:23));
        A_H2(i) = str2num(C{1}{~cellfun('isempty',strfind(
           C{1},'H2  '))}(14:23));

        temp = str2num(C{1}{~cellfun('isempty',strfind(C
           {1},'CH4'))}(11:23));
        if isempty(temp)
            temp = 0;
```

```
        end
        A_CH4(i)=temp;

        temp = str2num(C{1}{~cellfun('isempty',strfind(C{1},'CO2'))}(11:23));
        if isempty(temp)
            temp = 0;
        end
        A_CO2(i)=temp;

    %%%%%%%%%%%%%
    % Conversion
    %%%%%%%%%%%%%
        F_N2 = F0_N2(CurrStep);
        F_CO = F0_CO(CurrStep);
        F_H2 = F0_H2(CurrStep);

    if any(ExpMat(:,9))
    F_COo = (A_CO(i)/A_N2(i))*F_N2*RRF_CO;
    X_CO(i) = 1 - F_COo/F_CO;
    else
    X_CO(i) = 1 - (A_CO(i)/A_N2(i))/mean(CO_N2);
    end

    if any(ExpMat(:,10))
    F_H2o = (A_H2(i)/A_N2(i))*F_N2*RRF_H2;
    X_H2(i) = 1 - F_H2o/F_H2;
    else
    X_H2(i) = 1 - (A_H2(i)/A_N2(i))/mean(H2_N2);
    end

    %%%%%%%%%%%%%%%%
    % Reaction Rate
    %%%%%%%%%%%%%%%%
        R(i) = GHSV(CurrStep)*Y(CurrStep,2)*X_CO(i); % [mL CO/g cat h]

    %%%%%%%%%%%%%%%%%%
    % Site-time yield
    %%%%%%%%%%%%%%%%%%
```

```
        STY(i) = R(i)*M_Co/(V_m*3600*(x_m/100)*(D/100));
            % [s^-1]

    %%%%%%%%%%%%%%%%%%%
    % Selectivities
    %%%%%%%%%%%%%%%%%%%

        % CH4
        F_CH4(i) = F_N2*RRF_CH4*A_CH4(i)/A_N2(i);
        S_CH4(i) = F_CH4(i)/(F_CO*X_CO(i));
        % CO2
        F_CO2(i) = F_N2*RRF_CO2*A_CO2(i)/A_N2(i);
        S_CO2(i) = F_CO2(i)/(F_CO*X_CO(i));

    %%%%%%%%%%%%%%%%%%%%%%%
    % FID Calculations
    %%%%%%%%%%%%%%%%%%%%%%%

        % Methane
        temp = str2num(C{1}{~cellfun('isempty',strfind(C
            {1},'Metan'))}(11:23));
        if isempty(temp)
            temp = 0;
        end
        A_C1(i)=temp;

        % Ethane
        temp = str2num(C{1}{~cellfun('isempty',strfind(C
            {1},'Etan'))}(11:23));
        if isempty(temp)
            temp = 0;
        end
        A_C2p(i)=temp;

        % Ethene
        temp = str2num(C{1}{~cellfun('isempty',strfind(C
            {1},'Eten'))}(9:23));
        if isempty(temp)
            temp = 0;
        end
```

```
        A_C2o(i)=temp;

        % Propane
        temp = str2num(C{1}{~cellfun('isempty',strfind(C{1},'Propan'))}(9:23));
        if isempty(temp)
            temp = 0;
        end
        A_C3p(i)=temp;

        % Propene
        temp = str2num(C{1}{~cellfun('isempty',strfind(C{1},'Propen'))}(9:23));
        if isempty(temp)
            temp = 0;
        end
        A_C3o(i)=temp;

        % n-Butane
        temp = str2num(C{1}{~cellfun('isempty',strfind(C{1},'  n-Butan'))}(9:23));
        if isempty(temp)
            temp = 0;
        end
        A_C4np(i)=temp;

        % i-Butane
        temp = str2num(C{1}{~cellfun('isempty',strfind(C{1},'i-Butan'))}(9:23));
        if isempty(temp)
            temp = 0;
        end
        A_C4ip(i)=temp;

        % 1-Butene
        temp = str2num(C{1}{~cellfun('isempty',strfind(C{1},'1-Buten'))}(13:23));
        if isempty(temp)
            temp = 0;
        end
```

```
A_C4no(i)=temp;

% i-Butene
temp = str2num(C{1}{~cellfun('isempty',strfind(C{1},'i-Buten'))}(13:23));
 if isempty(temp)
     temp = 0;
end
A_C4io(i)=temp;

% cis-2-Butene
temp = str2num(C{1}{~cellfun('isempty',strfind(C{1},'cis-2-Buten'))}(13:23));
 if isempty(temp)
     temp = 0;
end
A_C4co(i)=temp;

% trans-2-Butene
temp = str2num(C{1}{~cellfun('isempty',strfind(C{1},'trans-2-Buten'))}(13:23));
 if isempty(temp)
     temp = 0;
end
A_C4to(i)=temp;

% n-Pentane
temp = str2num(C{1}{~cellfun('isempty',strfind(C{1},'n-Pentan'))}(13:23));
 if isempty(temp)
     temp = 0;
end
A_C5np(i)=temp;

% i-Pentane
temp = str2num(C{1}{~cellfun('isempty',strfind(C{1},'i-Pentan'))}(13:23));
  if isempty(temp)
     temp = 0;
end
```

```
        A_C5ip(i)=temp;

        % 1-Pentene
        temp = str2num(C{1}{~cellfun('isempty',strfind(C
            {1},'1-Penten'))}(13:23));
        if isempty(temp)
            temp = 0;
        end
        A_C5no(i)=temp;

        % i-Pentene
        temp = str2num(C{1}{~cellfun('isempty',strfind(C
            {1},'i-Penten'))}(13:23));
        if isempty(temp)
            temp = 0;
        end
        A_C5io(i)=temp;

        % C5 olefins
        C5_Lines = find(~cellfun('isempty', strfind(C{1},
            'C5-olefin?')));
        A_C5o(i) = 0;
        for k = 1:length(C5_Lines)
            temp = str2num(C{1}{C5_Lines(k)}(13:24));
            if isempty(temp)
                temp = 0;
            end
            A_C5o(i)=A_C5o(i)+temp;
        end

        % n-Hexane
        temp = str2num(C{1}{~cellfun('isempty',strfind(C
            {1},'n-Heksan'))}(13:23));
        if isempty(temp)
            temp = 0;
        end
        A_C6np(i)=temp;

        % 1-Hexene
```

```
        temp = str2num(C{1}{~cellfun('isempty',strfind(C{1},' 1-Heksen'))}(13:23));
        if isempty(temp)
            temp = 0;
        end
        A_C6no(i)=temp;

        % n-Heptane
        temp = str2num(C{1}{~cellfun('isempty',strfind(C{1},' n-Heptan'))}(13:23));
        if isempty(temp)
            temp = 0;
        end
        A_C7np(i)=temp;

        % 1-Heptene
        temp = str2num(C{1}{~cellfun('isempty',strfind(C{1},' 1-Hepten'))}(13:23));
        if isempty(temp)
            temp = 0;
        end
        A_C7no(i)=temp;

    %%%%%%%%%%%%%%%%%%%%%%%%%%%%%%
    % Species Selectivities
    %%%%%%%%%%%%%%%%%%%%%%%%%%%%%%

        F_CO   = F0_CO(CurrStep);

        % Ethane
        F_C2p(i) = F_CH4(i)*RRF_C2*A_C2p(i)/A_C1(i);
        S_C2p(i) = F_C2p(i)*2/(F_CO*X_CO(i));

        % Ethene
        F_C2o(i) = F_CH4(i)*RRF_C2*A_C2o(i)/A_C1(i);
        S_C2o(i) = F_C2o(i)*2/(F_CO*X_CO(i));

        % Propane
        F_C3p(i) = F_CH4(i)*RRF_C3*A_C3p(i)/A_C1(i);
        S_C3p(i) = F_C3p(i)*3/(F_CO*X_CO(i));
```

```
% Propene
F_C3o(i) = F_CH4(i)*RRF_C3*A_C3o(i)/A_C1(i);
S_C3o(i) = F_C3o(i)*3/(F_CO*X_CO(i));

% n-Butane
F_C4np(i) = F_CH4(i)*RRF_C4*A_C4np(i)/A_C1(i);
S_C4np(i) = F_C4np(i)*4/(F_CO*X_CO(i));

% i-Butane
F_C4ip(i) = F_CH4(i)*RRF_C4*A_C4ip(i)/A_C1(i);
S_C4ip(i) = F_C4ip(i)*4/(F_CO*X_CO(i));

% 1-Butene
F_C4no(i) = F_CH4(i)*RRF_C4*A_C4no(i)/A_C1(i);
S_C4no(i) = F_C4no(i)*4/(F_CO*X_CO(i));

% i-Butene
F_C4io(i) = F_CH4(i)*RRF_C4*A_C4io(i)/A_C1(i);
S_C4io(i) = F_C4io(i)*4/(F_CO*X_CO(i));

% cis-2-Butene
F_C4co(i) = F_CH4(i)*RRF_C4*A_C4co(i)/A_C1(i);
S_C4co(i) = F_C4co(i)*4/(F_CO*X_CO(i));

% trans-2-Butene
F_C4to(i) = F_CH4(i)*RRF_C4*A_C4to(i)/A_C1(i);
S_C4to(i) = F_C4to(i)*4/(F_CO*X_CO(i));

% n-Pentane
F_C5np(i) = F_CH4(i)*RRF_C5*A_C5np(i)/A_C1(i);
S_C5np(i) = F_C5np(i)*5/(F_CO*X_CO(i));

% i-Pentane
F_C5ip(i) = F_CH4(i)*RRF_C5*A_C5ip(i)/A_C1(i);
S_C5ip(i) = F_C5ip(i)*5/(F_CO*X_CO(i));

% 1-Pentene
F_C5no(i) = F_CH4(i)*RRF_C5*A_C5no(i)/A_C1(i);
S_C5no(i) = F_C5no(i)*5/(F_CO*X_CO(i));
```

```
        % i-Pentene
        F_C5io(i) = F_CH4(i)*RRF_C5*A_C5io(i)/A_C1(i);
        S_C5io(i) = F_C5io(i)*5/(F_CO*X_CO(i));

        % C5-olefin
        F_C5o(i) = F_CH4(i)*RRF_C5*A_C5o(i)/A_C1(i);
        S_C5o(i) = F_C5o(i)*5/(F_CO*X_CO(i));

        % n-Hexane
        F_C6np(i) = F_CH4(i)*RRF_C6*A_C6np(i)/A_C1(i);
        S_C6np(i) = F_C6np(i)*6/(F_CO*X_CO(i));

        % 1-Hexene
        F_C6no(i) = F_CH4(i)*RRF_C6*A_C6no(i)/A_C1(i);
        S_C6no(i) = F_C6no(i)*6/(F_CO*X_CO(i));

        % n-Heptane
        F_C7np(i) = F_CH4(i)*RRF_C7*A_C7np(i)/A_C1(i);
        S_C7np(i) = F_C7np(i)*7/(F_CO*X_CO(i));

        % 1-Heptene
        F_C7no(i) = F_CH4(i)*RRF_C7*A_C7no(i)/A_C1(i);
        S_C7no(i) = F_C7no(i)*7/(F_CO*X_CO(i));


    % %%%%%%%%%%%%%%%%%%%%%%%%%%%%%%%%%%%%%%%%%%%%%%%%%%%%%%%%%%%%%%%%%%%%%%%%%%%%%%%%%%%%
    %%%%%%%%%%%%%%%%%%%%%%%%%%%%%%% OTHER DATA FOR REPORT %%%%%%%%%%%%%%%%%%%%%%%%%%%%%%%%%%%%%%
    % %%%%%%%%%%%%%%%%%%%%%%%%%%%%%%%%%%%%%%%%%%%%%%%%%%%%%%%%%%%%%%%%%%%%%%%%%%%%%%%%%%%%

    T(i) = ExpMat(CurrStep,13);
    P(i) = ExpMat(CurrStep,14);
    Y_Feed(i,:) = Y(CurrStep,:)*100;
    GHSV_Feed(i) = GHSV(CurrStep);

end
```

```
cd ..
        %%%%%%%%%%%%%%%%%%%%%%%%%%%%%%%%%%%%%%%%%%%%%
        % Total Carbon Selectivities
        %%%%%%%%%%%%%%%%%%%%%%%%%%%%%%%%%%%%%%%%%%%%%
            S_C1 = S_CH4;
            S_C2 = S_C2p+S_C2o;
            S_C3 = S_C3p+S_C3o;
            S_C4 = S_C4np+S_C4ip+S_C4no+S_C4io+S_C4co+S_C4to;
            S_C5 = S_C5np+S_C5ip+S_C5no+S_C5io+S_C5o;
            S_C5plus = 1 - (S_C1+S_C2+S_C3+S_C4+S_CO2);

        %%%%%%%%%%%%%%%%%%%%%%%%%%%%%%%%%%%%
        % Other Selectivities
        %%%%%%%%%%%%%%%%%%%%%%%%%%%%%%%%%%%%
            S_LO = S_C2o+S_C3o+S_C4no;
            S_LOplus = S_C2o+S_C3o+S_C4no+S_C4io+S_C4co+S_C4to
                ;

        %%%%%%%%%%%%%%%%%%%%%%%%%%%%%%%%%%%%%%%%%%%%
        % a-Olefin/n-Paraffin ratio
        %%%%%%%%%%%%%%%%%%%%%%%%%%%%%%%%%%%%%%%%%%%%
            OP2 = S_C2o./S_C2p;
            OP3 = S_C3o./S_C3p;
            OP4 = S_C4no./S_C4np;
            OP5 = S_C5no./S_C5np;
            OP6 = S_C6no./S_C6np;
            OP7 = S_C7no./S_C7np;
        %%%%%%%%%%%%%%%%%%%%%%%%%%%%%%%%%%%%%%%%%%%%
        % FT-Selectivity (w/o CO2)
        %%%%%%%%%%%%%%%%%%%%%%%%%%%%%%%%%%%%%%%%%%%%
            FT_Corr = 1./(1-S_CO2);
            S_C1_FT   = S_C1.*FT_Corr;
            S_C2o_FT  = S_C2o.*FT_Corr;
            S_C2p_FT  = S_C2p.*FT_Corr;
            S_C3o_FT  = S_C3o.*FT_Corr;
            S_C3p_FT  = S_C3p.*FT_Corr;
            S_C4no_FT = S_C4no.*FT_Corr;
            S_C4np_FT = S_C4np.*FT_Corr;
            S_C5no_FT = S_C5no.*FT_Corr;
            S_C5np_FT = S_C5np.*FT_Corr;
```

```
            S_C2_FT = S_C2.*FT_Corr;
            S_C3_FT = S_C3.*FT_Corr;
            S_C4_FT = S_C4.*FT_Corr;
            S_C5_FT = S_C5.*FT_Corr;
            S_C5plus_FT = S_C5plus.*FT_Corr;
            S_LO_FT = S_LO.*FT_Corr;
            S_LOplus_FT = S_LOplus.*FT_Corr;


%%%%%%%%%%%%%%%%%%%%%%%%%%%%%%%%%%%%%%%%%%%%%%%%%%%%%%%%%%%%%%%%%%%%%%%%%%%%%%%%%
%%%%%%%%%%%%%%%%%%%%%%%%%%%%%%%%%%%%%%%%% WRITE TO REPORT %%%%%%%%%%%%%%%%%%%%%%%%%%%%%%%%%%%%%%%%%
%%%%%%%%%%%%%%%%%%%%%%%%%%%%%%%%%%%%%%%%%%%%%%%%%%%%%%%%%%%%%%%%%%%%%%%%%%%%%%%%%

if WriteReport == 1

PrintArray1 = [[1:N_REAC]' TOS' TOStep' T' P' Y_Feed
    GHSV_Feed' X_CO'*100 X_H2'*100 R' STY'];
PrintArray2 = [[1:N_REAC]' TOS' TOStep' S_CH4'*100 S_C2o
    '*100 S_C2p'*100 S_C2'*100 S_C3o'*100 S_C3p'*100 S_C3
    '*100 S_C4no'*100 S_C4np'*100 S_C4'*100 S_C5no'*100
    S_C5np'*100 S_C5'*100 S_C5plus'*100 S_LO'*100 S_LOplus
    '*100 S_CO2'*100];
PrintArray3 = [[1:N_REAC]' TOS' TOStep' S_C1_FT'*100
    S_C2o_FT'*100 S_C2p_FT'*100 S_C2_FT'*100 S_C3o_FT'*100
    S_C3p_FT'*100 S_C3_FT'*100 S_C4no_FT'*100 S_C4np_FT
    '*100 S_C4_FT'*100 S_C5no_FT'*100 S_C5np_FT'*100
    S_C5_FT'*100 S_C5plus_FT'*100 S_LO_FT'*100 S_LOplus_FT
    '*100];
PrintArray4 = [[1:N_REAC]' TOS' TOStep' OP2' OP3' OP4' OP5
    ' OP6' OP7'];
PrintArray5 = [[1:N_REAC]' A_H2' A_N2' A_CO' A_CH4' A_CO2'
     A_C1' A_C2p' A_C2o' A_C3p' A_C3o' A_C4ip' A_C4np'
    A_C4to' A_C4no' A_C4io' A_C4co' A_C5ip' A_C5np' A_C5io'
     A_C5no' A_C5o' A_C6np' A_C6no' A_C7np' A_C7no'];
PrintArray6 = [[1:N_FEED]' A_H2_raw' A_N2_raw' A_CO_raw'];
```

```matlab

xlsheets({'Conditions and Activity','Carbon Selectivity','FT Selectivity','Olefin Paraffin Ratio','Raw Data','Feed Analysis'},'ExpReport')

% Headers
TopHeader = {'Catalyst:' Catalyst_Name ''; 'SynGas Bottle No:' SynGasBottle ''; 'Date:' Date ''; 'Catalyst mass:' m_cat 'g'; 'Co content:' x_m '%'; 'Dispersion:' D '%'};
Header1    = {'Injection no.' 'Time on stream' '' 'T' 'P' 'Inlet Composition' '' '' '' '' 'GHSV' 'Conversion' '' 'Reaction Rate' 'Site-time Yield';
              '' 'Total' 'Step' '' '' 'N2' 'CO' 'H2' 'CO2' 'H2O' 'Total' 'CO' 'H2' '' '';
              '' '[h]' '[h]' '[C]' '[bar]' '[mol%]' '' '' '' '' '[mL SynGas/g_cat*h]' '[%]' '' '[mL CO/g_cat*h]' '[s^-1]'};
Header2    = {'Injection no.' 'Time on stream' '' 'Carbon Selectivity [%]' '' '' '' '' '' '' '' '' '' '' '' '' '' '' '' '';
              '' 'Total' 'Step' 'CH4' 'C2' '' '' 'C3' '' '' 'C4' '' '' 'C5' '' '' 'C5+' 'C2-4 a-olefins' 'C2-4 total olefins' 'CO2';
              '' '[h]' '[h]' '' 'a-Olefin' 'n-Paraffin' 'Total' 'a-Olefin' 'n-Paraffin' 'Total' 'a-Olefin' 'n-Paraffin' 'Total' 'a-Olefin' 'n-Paraffin' 'Total' '' '' '' ''};
Header3    = {'Injection no.' 'Time on stream' '' 'FT Selectivity [%]' '' '' '' '' '' '' '' '' '' '' '' '' '' '' '';
              '' 'Total' 'Step' 'CH4' 'C2' '' '' 'C3' '' '' 'C4' '' '' 'C5' '' '' 'C5+' 'C2-4 a-olefins' 'C2-4 total olefins';
              '' '[h]' '[h]' '' 'a-Olefin' 'n-Paraffin' 'Total' 'a-Olefin' 'n-Paraffin' 'Total' 'a-Olefin' 'n-Paraffin' 'Total' 'a-Olefin' 'n-Paraffin' 'Total' '' '' ''};
Header4    = {'Injection no.' 'Time on stream' '' 'a-Olefin/n-Paraffin Ratio' '' '' '' '' '';
```

```
              '' 'Total' 'Step' 'Carbon no.' '' '' '' '' '';
              '' '[h]' '[h]' '2' '3' '4' '5' '6' '7'};
Header5    = {'Injection no.' 'GC Areas' '' '' '' '' '' '' '' '' '' '' '' '' '' '' '' '' '' '' '' '' '' '' '' '';
              '' 'TCD [uV*s]' '' '' '' '' 'FID [pA*s]' '' '' '' '' '' '' '' '' '' '' '' '' '' '' '' '' '' '' '';
              '' 'H2' 'N2' 'CO' 'CH4' 'CO2' 'Methane' 'Ethane' 'Ethene' 'Propane' 'Propene' 'i-Butane' 'n-Butane' 'trans-2-Butene' '1-Butene' 'i-Butene' 'cis-2-Butene' 'i-Pentane' 'n-Pentane' 'i-Pentene' '1-Pentene' 'C5-olefin?(agg.)' 'n-Hexane' '1-Hexene' 'n-Heptane' '1-Heptene'};
Header6    = {'Injection no.' 'GC Areas' '' '';
              '' 'TCD [uV*s]' '' '';
              '' 'H2' 'N2' 'CO'};


xlswrite('ExpReport.xlsx',TopHeader,'Conditions and Activity','A1')
xlswrite('ExpReport.xlsx',TopHeader,'Carbon Selectivity','A1')
xlswrite('ExpReport.xlsx',TopHeader,'FT Selectivity','A1')
xlswrite('ExpReport.xlsx',TopHeader,'Olefin Paraffin Ratio','A1')
xlswrite('ExpReport.xlsx',TopHeader,'Raw Data','A1')
xlswrite('ExpReport.xlsx',TopHeader,'Feed Analysis','A1')


xlswrite('ExpReport.xlsx',Header1,'Conditions and Activity','A8')
xlswrite('ExpReport.xlsx',Header2,'Carbon Selectivity','A8')
xlswrite('ExpReport.xlsx',Header3,'FT Selectivity','A8')
xlswrite('ExpReport.xlsx',Header4,'Olefin Paraffin Ratio','A8')
xlswrite('ExpReport.xlsx',Header5,'Raw Data','A8')
xlswrite('ExpReport.xlsx',Header6,'Feed Analysis','A8')

```

```
xlswrite('ExpReport.xlsx',PrintArray1,'Conditions and Activity','A11')
xlswrite('ExpReport.xlsx',PrintArray2,'Carbon Selectivity','A11')
xlswrite('ExpReport.xlsx',PrintArray3,'FT Selectivity','A11')
xlswrite('ExpReport.xlsx',PrintArray4,'Olefin Paraffin Ratio','A11')
xlswrite('ExpReport.xlsx',PrintArray5,'Raw Data','A11')
xlswrite('ExpReport.xlsx',PrintArray6,'Feed Analysis','A11')

end

if ConPlot == 1
    hold on
    plot(TOS,X_CO*100,'ko-')
    axis([0 4*ceil((max(TOS)+1)/4) 0 5*ceil(max(X_CO*20))])
    xlabel('Time on stream [h]')
    ylabel('CO conversion [%]')
    set(gca,'XTick',0:4:4*ceil((max(TOS)+1)/4),'YTick',0:5:5*ceil(max(X_CO*20)))
    CurrCon = round(X_CO(N_REAC)*100,2);
    [TempX,TempY] = ds2nfu([TOS(N_REAC) TOS(N_REAC)],[100*X_CO(N_REAC)-5 100*X_CO(N_REAC)]);
    annotation('arrow',TempX,TempY)
    text(TOS(N_REAC),X_CO(N_REAC)*100-5,['CO conversion = ' num2str(CurrCon) ' % '],'HorizontalAlignment','right')
    plot([0 4*ceil((max(TOS)+1)/4)],[TarCon TarCon],'r--')
    text(4*ceil((max(TOS)+1)/4),TarCon+1,[num2str(TarCon) ' %'],'HorizontalAlignment','right','color','r')
end
```

D.6 Example activity and selectivity excel sheet

Below is an example of the output provided by the MATLAB code in appendix D.5 for the catalyst CoRe80(500ppm).

Catalyst: CoRe80(500ppmK)
SynGas Bottle AGA751
Date: 27.2.2018
Catalyst mass: 1,0026 g
Co content: 20 %
Dispersion: 15 %

Injection no.	Time on stream		T	P	Inlet Composition	
	Total	Step			N2	CO
	[h]	[h]	[C]	[bar]	[mol%]	
1	0	0	0	0	0	0
2	1,07472222	1,07472222	210	20	3	31,3
3	2,12166667	2,12166667	210	20	3	31,3
4	3,16861111	3,16861111	210	20	3	31,3
5	4,21555556	4,21555556	210	20	3	31,3
6	5,2625	5,2625	210	20	3	31,3
7	6,30916667	6,30916667	210	20	3	31,3
8	7,35583333	7,35583333	210	20	3	31,3
9	8,40194444	8,40194444	210	20	3	31,3
10	9,44861111	9,44861111	210	20	3	31,3
11	10,495	10,495	210	20	3	31,3
12	11,5413889	11,5413889	210	20	3	31,3
13	12,5875	12,5875	210	20	3	31,3
14	13,6336111	13,6336111	210	20	3	31,3
15	14,6797222	14,6797222	210	20	3	31,3
16	15,7258333	15,7258333	210	20	3	31,3
17	16,7719444	16,7719444	210	20	3	31,3
18	17,8180556	17,8180556	210	20	3	31,3
19	18,8641667	18,8641667	210	20	3	31,3
20	19,9102778	19,9102778	210	20	3	31,3
21	20,9566667	20,9566667	210	20	3	31,3
22	22,0033333	22,0033333	210	20	3	31,3
23	23,0505556	23,0505556	210	20	3	31,3
24	24,0975	24,0975	210	20	3	31,3
25	25,145	25,145	210	20	3	31,3
26	25,3861111	-0,1138889	210	20	3	31,3
27	26,4333333	0,93333333	210	20	3	31,3
28	27,4811111	1,98111111	210	20	3	31,3
29	28,5283333	3,02833333	210	20	3	31,3
30	29,5755556	4,07555556	210	20	3	31,3
31	30,6236111	5,12361111	210	20	3	31,3
32	31,6711111	-0,0455556	210	20	3	31,3
33	32,7188889	0,00222222	210	20	3	31,3
34	33,7666667	0	210	20	3	31,3
35	34,8147222	1,04805556	210	20	3	31,3

H2	CO2	H2O	GHSV Total [mL SynGas/g_	Conversion CO [%]	 H2	Reaction Rate [mL CO/g_cat'
0	0	0	0	0	0	0
65,7	0	0	17851,5859	2,49628325	10,697038	139,480984
65,7	0	0	17851,5859	5,64932682	9,57549868	315,658756
65,7	0	0	17851,5859	13,5942865	17,1644708	759,587062
65,7	0	0	17851,5859	19,1271021	22,574887	1068,7357
65,7	0	0	17851,5859	20,4689858	23,8518424	1143,71408
65,7	0	0	17851,5859	20,1929429	23,4421728	1128,29005
65,7	0	0	17851,5859	19,9373429	23,095868	1114,00828
65,7	0	0	17851,5859	19,6314848	22,7968563	1096,91832
65,7	0	0	17851,5859	19,4290789	22,5489199	1085,6088
65,7	0	0	17851,5859	19,2364064	22,3897378	1074,84313
65,7	0	0	17851,5859	19,0939795	22,2488062	1066,88496
65,7	0	0	17851,5859	18,925066	22,0330594	1057,44684
65,7	0	0	17851,5859	18,8072809	21,879086	1050,86554
65,7	0	0	17851,5859	18,6882617	21,7628881	1044,21529
65,7	0	0	17851,5859	18,6264242	21,6240364	1040,76009
65,7	0	0	17851,5859	18,4892652	21,4417751	1033,09627
65,7	0	0	17851,5859	18,3443633	21,363826	1024,99981
65,7	0	0	17851,5859	18,1597443	21,1341553	1014,68413
65,7	0	0	17851,5859	18,0847172	21,1089496	1010,49196
65,7	0	0	17851,5859	18,0184909	21,0607504	1006,79153
65,7	0	0	17851,5859	17,9189499	21,0082049	1001,22964
65,7	0	0	17851,5859	17,7564962	20,8725555	992,152463
65,7	0	0	17851,5859	17,7277403	20,7729272	990,545713
65,7	0	0	17851,5859	17,6979899	20,5611514	988,883393
65,7	0	0	5979,6529	17,6782244	20,5314209	330,871191
65,7	0	0	5979,6529	17,8336131	20,4864558	333,779494
65,7	0	0	5979,6529	29,1738315	31,897686	546,026579
65,7	0	0	5979,6529	42,2876588	44,6124278	791,469083
65,7	0	0	5979,6529	48,816688	51,0019613	913,668441
65,7	0	0	5979,6529	51,6615667	53,7910562	966,914082
65,7	0	0	6050,2693	52,4593965	54,7210392	993,441581
65,7	0	0	6190,30521	52,4828949	54,8302359	1016,89048
65,7	0	0	6330,93956	51,8695375	54,3170341	1027,8385
65,7	0	0	6330,93956	50,6729785	53,2562194	1004,12767

Site-time Yield
[s^-1]
0
0,00311104
0,00704059
0,01694215
0,02383753
0,02550988
0,02516586
0,02484731
0,02446613
0,02421388
0,02397375
0,02379625
0,02358574
0,02343895
0,02329062
0,02321355
0,02304262
0,02286203
0,02263194
0,02253844
0,0224559
0,02233185
0,02212939
0,02209355
0,02205647
0,00737989
0,00744476
0,01217881
0,01765326
0,02037885
0,02156646
0,02215814
0,02268115
0,02292534
0,02239649

Catalyst: CoRe80(500ppmK)
SynGas Bottle AGA751
Date: 27.2.2018
Catalyst mass: 1,0026 g
Co content: 20 %
Dispersion: 15 %

Injection no.	Time on stream		Carbon Selectivity [%]			
	Total	Step	CH4	C2		
	[h]	[h]		a-Olefin	n-Paraffin	Total
1	0	0	0	0	0	0
2	1,07472222	1,07472222	6,04711891	0,9606837	0,55446905	1,51515275
3	2,12166667	2,12166667	9,32192653	0,62902741	1,01549661	1,64452402
4	3,16861111	3,16861111	10,8167838	0,26139828	1,06837202	1,32977031
5	4,21555556	4,21555556	11,0104417	0,19975013	1,01087752	1,21062765
6	5,2625	5,2625	11,1421359	0,19253729	0,98998977	1,18252706
7	6,30916667	6,30916667	11,2480138	0,19768018	0,98156822	1,1792484
8	7,35583333	7,35583333	11,2624351	0,19990588	0,97559354	1,17549942
9	8,40194444	8,40194444	11,3623847	0,20364055	0,97952159	1,18316213
10	9,44861111	9,44861111	11,3498405	0,20442421	0,97495531	1,17937952
11	10,495	10,495	11,3984176	0,20535376	0,9759988	1,18135256
12	11,5413889	11,5413889	11,4005734	0,20544594	0,97363995	1,17908589
13	12,5875	12,5875	11,4544962	0,20591583	0,97910515	1,18502098
14	13,6336111	13,6336111	11,5019878	0,2051142	0,98270291	1,18781712
15	14,6797222	14,6797222	11,5456658	0,20467878	0,98538917	1,19006795
16	15,7258333	15,7258333	11,541691	0,2030615	0,98450718	1,18756868
17	16,7719444	16,7719444	11,6969108	0,20241036	0,99543343	1,19784379
18	17,8180556	17,8180556	11,740112	0,20167848	0,99829456	1,19997304
19	18,8641667	18,8641667	11,810556	0,20214852	1,00278749	1,204936
20	19,9102778	19,9102778	11,8170966	0,2012053	1,00543801	1,20664332
21	20,9566667	20,9566667	11,8047809	0,20050622	1,00288188	1,2033881
22	22,0033333	22,0033333	11,8411692	0,20047851	1,00446479	1,2049433
23	23,0505556	23,0505556	11,9106908	0,20151303	1,01039797	1,21191099
24	24,0975	24,0975	11,8869002	0,20066034	1,0101564	1,21081674
25	25,145	25,145	0	0	0	0
26	25,3861111	-0,1138889	11,9411405	0,200784	1,01294804	1,21373204
27	26,4333333	0,93333333	11,8439294	0,19803578	1,0023137	1,20034948
28	27,4811111	1,98111111	10,4925617	0,1153	0,9230049	1,0383049
29	28,5283333	3,02833333	9,81958453	0,07818505	0,93124622	1,00943127
30	29,5755556	4,07555556	9,59004901	0,06825154	0,94514211	1,01339366
31	30,6236111	5,12361111	9,4938797	0,06573751	0,95384861	1,01958612
32	31,6711111	-0,0455556	9,4726242	0,06583478	0,96079963	1,02663441
33	32,7188889	0,00222222	9,46181414	0,066597	0,96564049	1,03223748
34	33,7666667	0	9,47223885	0,06818712	0,96790054	1,03608767
35	34,8147222	1,04805556	9,45485108	0,07021991	0,96491425	1,03513416

C3			C4			C5
a-Olefin	n-Paraffin	Total	a-Olefin	n-Paraffin	Total	a-Olefin
0	0	0	0	0	0	0
3,95302753	1,46474126	5,41776879	2,87593918	1,39171366	4,26765284	1,89352985
4,89821752	1,60462635	6,50284386	3,89153861	1,86859164	5,94800487	2,72053398
4,20373773	1,40439254	5,60813027	3,51596855	1,91454822	5,69979763	2,56949164
3,84872932	1,29453303	5,14326235	3,32614931	1,80002164	5,40277606	2,56433916
3,80750761	1,26214432	5,06965193	3,39198478	1,79152362	5,46296063	2,75331181
3,80720289	1,24922353	5,05642642	3,42956234	1,77026474	5,46962137	2,82822378
3,80378308	1,23443612	5,0382192	3,4417981	1,75296714	5,45694736	2,85105951
3,83764047	1,23111527	5,06875573	3,47706179	1,7525865	5,48964561	2,87879909
3,83718545	1,22109338	5,05827883	3,4768094	1,73933536	5,47351199	2,88955536
3,84008682	1,22039194	5,06047875	3,4817185	1,73509878	5,47310375	2,90098891
3,83928165	1,21713154	5,05641319	3,48367515	1,73348494	5,47289614	2,89836762
3,85015258	1,22120984	5,07136241	3,49739244	1,73824449	5,49251979	2,91191651
3,85589608	1,22469589	5,08059197	3,49792532	1,74080135	5,49527994	2,91312835
3,86119544	1,22591881	5,08711425	3,49843655	1,74596789	5,50173793	2,92198953
3,85358228	1,23115005	5,08473232	3,492885	1,7507747	5,50254148	2,9121042
3,83425884	1,25809685	5,09235568	3,46988345	1,77355872	5,50532667	2,90439314
3,82991555	1,26059082	5,09050637	3,47055417	1,78225351	5,51477745	2,8899896
3,83877236	1,26430748	5,10307984	3,46725708	1,78426231	5,51251013	2,88742086
3,84385184	1,26715392	5,11100576	3,47841049	1,79332672	5,53532208	2,88932218
3,83290467	1,26380652	5,09671119	3,47620795	1,79588557	5,53547626	2,91015225
3,845347	1,26641528	5,11176229	3,47551035	1,79138177	5,53078483	2,8935931
3,86846024	1,27520229	5,14366253	3,50591057	1,81062031	5,58222938	2,93457234
3,85400952	1,26955504	5,12356456	3,49711866	1,80983964	5,5736143	2,94103178
0	0	0	0	0	0	0
3,86279035	1,27537342	5,13816377	3,4978775	1,8101193	5,57387427	2,92313999
3,80949342	1,25816832	5,06766174	3,44071749	1,78258366	5,48495525	2,86212864
2,7358921	1,15423857	3,89013067	1,99300834	1,11715632	3,28018995	1,53107215
2,53464399	1,30551486	3,84015885	1,60238093	1,1702949	2,97908106	0,94402657
2,59709968	1,40535988	4,00245956	1,66049995	1,37487061	3,29335796	0,85703485
2,68925555	1,46174825	4,1510038	1,79759834	1,56392103	3,66292805	0,91821913
2,77522698	1,4970058	4,27223279	1,96853893	1,74505654	4,0553947	1,04523283
2,84320809	1,5139214	4,35712949	2,14980688	1,91918332	4,44927801	1,34403399
2,88802158	1,5160564	4,40407798	2,24235329	1,98402954	4,61707381	1,52402618
2,91816937	1,50388571	4,42205508	0	2,01995965	2,03290074	0

		C5+	C2-4 a-olefins	C2-4 total ole	CO2
n-Paraffin	Total				
0	0	100	0	0	0
0,96431307	2,97030636	82,7523067	7,78965041	7,78965041	0
1,48825677	4,41741639	76,0988269	9,41878354	9,60665816	0,48387378
1,79008269	4,62986971	76,1878127	7,98110457	8,23748654	0,35770525
1,70637757	4,55386208	76,8828002	7,37462877	7,63889142	0,35009202
1,76459013	4,81500798	76,808883	7,39202968	7,6589423	0,33384151
1,73296359	4,84831958	76,71176	7,43444541	7,69142712	0,33493007
1,70824873	4,83781007	76,7384066	7,44548705	7,69531518	0,32849237
1,69819727	4,85319303	76,5757591	7,5183428	7,76586771	0,32029263
1,68751358	4,84960325	76,6140359	7,51841906	7,76371125	0,32495321
1,6851462	4,85838204	76,5836965	7,52715908	7,77134399	0,30295079
1,67567667	4,8437772	76,5769787	7,52840273	7,77183563	0,31405265
1,68214943	4,86459377	76,4811902	7,55346084	7,79782051	0,31541039
1,68120668	4,86487597	76,4138614	7,5589356	7,80332589	0,32046179
1,69195714	4,88615687	76,3537817	7,56431077	7,80927787	0,32163236
1,69276155	4,87624275	76,3748231	7,54952878	7,79637213	0,30864338
1,71510678	4,89553658	76,1839101	7,50655265	7,75596894	0,32365294
1,72401066	4,88798007	76,12672	7,5021482	7,75156091	0,32791117
1,7313169	4,8947895	76,0380381	7,50817795	7,75674891	0,33087988
1,73402049	4,89854296	76,0153752	7,52346764	7,77368788	0,31455706
1,75026992	4,93728947	76,0280973	7,50961885	7,76050748	0,33154632
1,74293485	4,91386966	75,9874603	7,52133587	7,77260017	0,32388011
1,76910872	4,984052	75,8215905	7,57588383	7,82921475	0,32991578
1,77552209	4,99783639	75,884097	7,55178852	7,80561166	0,3210072
0	0	100	0	0	0
1,76591378	7,83837524	75,8049544	7,56145185	7,81486788	0,32813504
1,73398091	4,87112846	76,0845542	7,44824669	7,69731722	0,31854992
0,92551741	2,60414922	80,9287023	4,84420045	5,00590289	0,37011044
0,61138115	1,65681011	81,9628951	4,21520997	4,41304193	0,3888492
0,65698805	1,6308813	81,7100996	4,32585117	4,57428806	0,39064025
0,80961666	1,87689527	81,286927	4,5525914	4,8433489	0,38567534
1,00147804	2,23431219	80,7917382	4,80960069	5,13984135	0,38137571
1,47266317	3,09652869	80,31873	5,05961197	5,42755047	0,38081084
1,74598999	3,6010734	80,0955927	5,19856199	5,57659073	0,37492903
0	0	83,0550589	2,98838928	2,98838928	0

Catalyst: CoRe80(500ppmK)
SynGas Bottle AGA751
Date: 27.2.2018
Catalyst mass: 1,0026 g
Co content: 20 %
Dispersion: 15 %

Injection no.	Time on stream		FT Selectivity [%]			
	Total	Step	CH4	C2		
	[h]	[h]		a-Olefin	n-Paraffin	Total
1	0	0	0	0	0	0
2	1,07472222	1,07472222	6,04711891	0,9606837	0,55446905	1,51515275
3	2,12166667	2,12166667	9,36725221	0,63208591	1,02043423	1,65252014
4	3,16861111	3,16861111	10,8556149	0,26233667	1,07220736	1,33454404
5	4,21555556	4,21555556	11,0491238	0,2004519	1,01442895	1,21488085
6	5,2625	5,2625	11,1794576	0,19318221	0,99330584	1,18648805
7	6,30916667	6,30916667	11,2858134	0,1983445	0,98486683	1,18321133
8	7,35583333	7,35583333	11,2995532	0,20056472	0,97880885	1,17937357
9	8,40194444	8,40194444	11,3988946	0,20429489	0,982669	1,18696389
10	9,44861111	9,44861111	11,3868424	0,20509066	0,97813379	1,18322445
11	10,495	10,495	11,4330541	0,20597777	0,97896458	1,18494235
12	11,5413889	11,5413889	11,43649	0,20609318	0,97670733	1,1828005
13	12,5875	12,5875	11,4907392	0,20656737	0,98220312	1,18877048
14	13,6336111	13,6336111	11,5389658	0,20577363	0,98586222	1,19163586
15	14,6797222	14,6797222	11,5829202	0,20533922	0,98856873	1,19390794
16	15,7258333	15,7258333	11,5774239	0,20369018	0,98755521	1,19124538
17	16,7719444	16,7719444	11,7348911	0,2030676	0,99866564	1,20173324
18	17,8180556	17,8180556	11,7787358	0,20234199	1,00157885	1,20392083
19	18,8641667	18,8641667	11,8497645	0,2028196	1,00611652	1,20893613
20	19,9102778	19,9102778	11,8543854	0,20184021	1,00861067	1,21045088
21	20,9566667	20,9566667	11,8440494	0,2011732	1,00621795	1,20739116
22	22,0033333	22,0033333	11,879645	0,20112993	1,00772862	1,20885856
23	23,0505556	23,0505556	11,9501161	0,20218005	1,01374246	1,21592251
24	24,0975	24,0975	11,9251809	0,20130654	1,01340952	1,21471606
25	25,145	25,145	0	0	0	0
26	25,3861111	-0,1138889	11,9804525	0,20144501	1,01628282	1,21772783
27	26,4333333	0,93333333	11,8817788	0,19866863	1,00551677	1,20418541
28	27,4811111	1,98111111	10,5315401	0,11572833	0,92643372	1,04216205
29	28,5283333	3,02833333	9,85791696	0,07849026	0,9348815	1,01337176
30	29,5755556	4,07555556	9,62765852	0,0685192	0,9488487	1,0173679
31	30,6236111	5,12361111	9,53063702	0,06599203	0,95754161	1,02353364
32	31,6711111	-0,0455556	9,5088888	0,06608682	0,96447791	1,03056473
33	32,7188889	0,00222222	9,49798349	0,06685158	0,96933181	1,03618338
34	33,7666667	0	9,50788668	0,06844374	0,97154314	1,03998688
35	34,8147222	1,04805556	9,45485108	0,07021991	0,96491425	1,03513416

C3			C4			C5
a-Olefin	n-Paraffin	Total	a-Olefin	n-Paraffin	Total	a-Olefin
0	0	0	0	0	0	0
3,95302753	1,46474126	5,41776879	2,87593918	1,39171366	4,26765284	1,89352985
4,92203395	1,61242846	6,53446241	3,91046031	1,87767722	5,97692565	2,73376193
4,2188287	1,40943416	5,62826286	3,52859051	1,92142125	5,7202593	2,57871584
3,86225076	1,29908101	5,16133176	3,3378348	1,80634551	5,4217572	2,57334825
3,82026123	1,26637199	5,08663322	3,40334657	1,79752451	5,48125935	2,7625343
3,81999721	1,25342162	5,07341883	3,44108758	1,77621382	5,48800234	2,83772818
3,8163194	1,23850452	5,05482391	3,45314141	1,75874448	5,4749321	2,86045589
3,84997164	1,23507111	5,08504275	3,48823434	1,75821794	5,50728504	2,8880493
3,84969516	1,2250743	5,07476946	3,48814424	1,74500581	5,49135633	2,89897568
3,85175574	1,22410036	5,0758561	3,49229845	1,74037125	5,48973494	2,90980419
3,851377	1,22096602	5,07234301	3,49465019	1,73894614	5,49013806	2,9074987
3,86233478	1,22507385	5,08740863	3,50845848	1,74374444	5,50989859	2,92113005
3,86829248	1,22863319	5,09692567	3,50917087	1,74639789	5,51294683	2,92249382
3,87365437	1,22987449	5,10352885	3,50972496	1,7516016	5,5194904	2,93141791
3,86551293	1,23496167	5,1004746	3,50369894	1,75619508	5,51957729	2,92112004
3,84670882	1,26218193	5,10889076	3,48115029	1,77931753	5,52320268	2,91382381
3,84251559	1,26473803	5,10725362	3,48197194	1,78811695	5,53292052	2,89949738
3,85151625	1,26850471	5,12002096	3,47876762	1,79018568	5,53081047	2,89700647
3,8559811	1,27115242	5,12713352	3,48938661	1,79898555	5,55278877	2,89843942
3,8456548	1,26801056	5,11366536	3,48777153	1,80185957	5,55388997	2,91983284
3,85784179	1,27053028	5,12837207	3,48680341	1,79720256	5,54875615	2,90299532
3,88126514	1,27942331	5,16068845	3,51751541	1,8166136	5,600707	2,94428601
3,86642101	1,27364353	5,14006454	3,50838082	1,81566807	5,59156362	2,95050311
0	0	0	0	0	0	0
3,87550725	1,27957215	5,1550794	3,50939305	1,81607849	5,59222431	2,93276341
3,82166734	1,26218902	5,08385636	3,45171292	1,78828023	5,50248341	2,87127508
2,74605554	1,1585264	3,90458194	2,00041208	1,12130639	3,29237538	1,53675986
2,54453841	1,31061116	3,85514956	1,6086361	1,17486335	2,99071041	0,94771174
2,60728479	1,41087131	4,0181561	1,66701197	1,38026247	3,3062736	0,8603959
2,6996675	1,46740768	4,16707518	1,80455807	1,56997604	3,67710975	0,92177419
2,78585155	1,50273687	4,28858842	1,9760752	1,75173725	4,0709202	1,04923436
2,85407673	1,51970861	4,37378534	2,15802487	1,92651971	4,46628611	1,34917179
2,89889036	1,52176193	4,42065228	2,25079216	1,99149624	4,63444971	1,5297617
2,91816937	1,50388571	4,42205508	0	2,01995965	2,03290074	0

		C5+	C2-4 a-olefins	C2-4 total olefins
n-Paraffin	Total			
0	0	100	0	0
0,96431307	2,97030636	82,7523067	7,78965041	7,78965041
1,49549307	4,43889504	76,4688396	9,46458016	9,65336828
1,79650889	4,64649046	76,4613189	8,00975588	8,26705824
1,71237245	4,56986079	77,1529064	7,40053746	7,66572852
1,7705008	4,83113632	77,0661618	7,41679001	7,68459667
1,73878731	4,86461263	76,9695541	7,45942928	7,7172746
1,71387869	4,85375429	76,9913172	7,47002552	7,72067701
1,70365395	4,8687874	76,8218138	7,54250087	7,79082113
1,69301508	4,86541356	76,8638073	7,54293005	7,78902193
1,69026688	4,87314527	76,8164125	7,55003196	7,79495888
1,68095576	4,85903714	76,8182284	7,55212036	7,79632018
1,68747189	4,87998575	76,7231831	7,57736063	7,82249347
1,68661163	4,88051616	76,6595259	7,58323698	7,82841296
1,69741658	4,90192304	76,6001526	7,58871855	7,83447609
1,69800232	4,89133954	76,6112788	7,57290204	7,82050961
1,7206758	4,91143258	76,4312822	7,53092671	7,78115287
1,72968248	4,90406103	76,3771693	7,52682952	7,77706277
1,73706449	4,91103914	76,2904679	7,53310347	7,78249963
1,73949219	4,9140003	76,2552415	7,54720791	7,79821772
1,75609218	4,95371332	76,2810041	7,53459953	7,78632275
1,74859821	4,92983642	76,2343683	7,54577513	7,79785587
1,77496461	5,0005496	76,0725659	7,6009606	7,85513007
1,78124	5,01393148	76,1284749	7,57610837	7,83074893
0	0	100	0	0
1,77172744	7,86418037	76,0545159	7,58634531	7,84059562
1,73952216	4,88669503	76,327696	7,4720489	7,72191538
0,92895558	2,61382326	81,2293406	4,86219594	5,02449908
0,61376778	1,66327775	82,2828513	4,23166477	4,430269
0,65956457	1,63727717	82,0305439	4,34281596	4,59222714
0,81275124	1,88416202	81,6016444	4,5702176	4,86210082
1,00531205	2,24286593	81,1010379	4,82801356	5,1595185
1,47829267	3,10836568	80,6257617	5,07895318	5,44829818
1,75256085	3,61462568	80,3970245	5,21812626	5,59757768
0	0	83,0550589	2,98838928	2,98838928

Catalyst: CoRe80(500ppmK)
SynGas Bottle AGA751
Date: 27.2.2018
Catalyst mass: 1,0026 g
Co content: 20 %
Dispersion: 15 %

Injection no.	Time on stream		a-Olefin/n-Paraffin Ratio			
	Total	Step	Carbon no.			
	[h]	[h]	2	3	4	5
1	0	0				
2	1,07472222	1,07472222	1,73261915	2,69878895	2,06647334	1,96360488
3	2,12166667	2,12166667	0,61942837	3,05255957	2,08260518	1,8280004
4	3,16861111	3,16861111	0,24466972	2,99327831	1,83644816	1,43540388
5	4,21555556	4,21555556	0,19760073	2,97306383	1,84783851	1,50279704
6	5,2625	5,2625	0,19448412	3,0166975	1,89335197	1,56031237
7	6,30916667	6,30916667	0,2013922	3,04765544	1,93731607	1,6320157
8	7,35583333	7,35583333	0,20490693	3,0813932	1,96341279	1,66899555
9	8,40194444	8,40194444	0,20789797	3,11720646	1,98396016	1,69520888
10	9,44861111	9,44861111	0,20967547	3,14241769	1,99892987	1,71231533
11	10,495	10,495	0,2104037	3,14660126	2,00663993	1,72150577
12	11,5413889	11,5413889	0,21100812	3,15436871	2,00963681	1,72966997
13	12,5875	12,5875	0,21031023	3,1527363	2,01202561	1,73106887
14	13,6336111	13,6336111	0,20872453	3,14845188	2,0093765	1,73276039
15	14,6797222	14,6797222	0,20771365	3,14963389	2,00372331	1,72698791
16	15,7258333	15,7258333	0,206257	3,13006712	1,99505111	1,72032747
17	16,7719444	16,7719444	0,20333893	3,04766588	1,95645254	1,69341826
18	17,8180556	17,8180556	0,20202302	3,0381909	1,94728423	1,67631771
19	18,8641667	18,8641667	0,2015866	3,03626484	1,94324402	1,66775988
20	19,9102778	19,9102778	0,20011707	3,03345299	1,93964126	1,66625607
21	20,9566667	20,9566667	0,19993005	3,03282554	1,93565114	1,66268769
22	22,0033333	22,0033333	0,1995874	3,03640287	1,94012823	1,66018431
23	23,0505556	23,0505556	0,19943927	3,03360515	1,93630357	1,65878575
24	24,0975	24,0975	0,19864284	3,03571675	1,93228095	1,6564321
25	25,145	25,145				
26	25,3861111	-0,1138889	0,19821747	3,02875243	1,93240164	1,65531297
27	26,4333333	0,93333333	0,19757864	3,02780904	1,9301857	1,65061139
28	27,4811111	1,98111111	0,12491809	2,37030035	1,78400132	1,65428778
29	28,5283333	3,02833333	0,08395744	1,94148996	1,36921124	1,54408845
30	29,5755556	4,07555556	0,07221299	1,84799618	1,20774998	1,30449078
31	30,6236111	5,12361111	0,06891818	1,83975288	1,14941758	1,13414061
32	31,6711111	-0,0455556	0,06852082	1,85385186	1,12806598	1,04369022
33	32,7188889	0,00222222	0,06896666	1,87804208	1,12016755	0,9126554
34	33,7666667	0	0,07044848	1,90495655	1,13020156	0,87287223
35	34,8147222	1,04805556	0,07277321	1,94041964	0	

6	7
1,44968959	0
1,42762085	1,11229847
0,975197	0,76803668
1,01392917	0,66460784
1,06940295	0,69999495
1,14115467	0,73440883
1,18018196	0,77351446
1,20971042	0,80708199
1,23235537	0,82867009
1,24615259	0,8486982
1,25532108	0,86385942
1,26125062	0,87483795
1,2606794	0,880903
1,26072531	0,88256179
1,25756941	0,88421055
1,25169661	0,88945488
1,23045629	0,88169948
1,22129728	0,87793101
1,21820074	0,87205493
1,21286272	0,8672922
1,20906926	0,86342572
1,20441625	0,85730418
1,2037616	0,85386897
1,24167394	1,52226959
1,20241574	0,84352938
1,19967664	0,84823953
1,19958904	0,84613946
1,19272444	0,84860076
1,15773432	0,85325249
1,10866976	0,85201344
0,95496611	0,84756542
0,72173675	0,83595948

Catalyst:	CoRe80(500ppmK)
SynGas Bottle	AGA751
Date:	27.2.2018
Catalyst mass:	1,0026 g
Co content:	20 %
Dispersion:	15 %

Injection no.	GC Areas					
	TCD [uV*s]					FID [pA*s]
	H2	N2	CO	CH4	CO2	Methane
1	0	0	0	0	0	0
2	561,28296	1095,32446	11291	13,1029	0	35,8558
3	654,10944	1260,64001	12574,9	52,6109	4,0445	144,75995
4	652,33264	1372,39539	12536,9	159,9249	7,8326	440,34241
5	649,04877	1460,90601	12490,9	243,8139	11,4815	660,35321
6	649,17175	1485,68591	12492	268,5184	11,9154	737,80914
7	651,32831	1482,6449	12509,7	266,867	11,7689	730,15747
8	653,15027	1480,09717	12528,2	263,3735	11,377	721,80115
9	654,013	1476,31213	12543,9	260,9655	10,8949	712,41638
10	655,22162	1474,30566	12558,4	257,6391	10,9246	705,50781
11	656,8222	1474,87585	12593,3	256,275	10,0878	699,58026
12	657,55548	1473,84607	12606,7	254,248	10,3728	695,40656
13	657,48437	1469,60876	12596,7	252,4628	10,2958	688,24103
14	658,51123	1469,00293	12609,8	251,8279	10,3913	686,52747
15	658,2016	1466,13147	12603,6	250,6935	10,343	688,71368
16	659,41235	1466,2262	12614	249,7941	9,8931	689,67261
17	659,03851	1461,99512	12598,8	250,5642	10,2681	687,22131
18	658,90857	1460,25793	12606,2	249,2222	10,3094	683,37244
19	659,51489	1457,34521	12609,5	247,6993	10,2775	675,17615
20	659,33051	1456,47229	12613,5	246,6647	9,7243	678,28992
21	659,50873	1455,97644	12619,4	245,4217	10,2085	670,72919
22	659,54437	1455,08655	12627	244,6686	9,9113	668,79358
23	658,75055	1450,84375	12615,1	243,1628	9,9753	665,49268
24	658,95221	1449,46289	12607,5	242,0535	9,681	665,32941
25	659,80945	1447,47937	12594,8	0	0	660,48187
26	661,11346	1449,79749	12618	242,5348	9,8706	671,37573
27	660,63232	1447,9231	12577,9	242,3611	9,654	662,61572
28	649,20117	1661,28528	12439,6	402,9967	21,053	1103,45435
29	633,95264	1994,67102	12170,5	656,3875	38,4956	1790,50403
30	622,7464	2214,92651	11985,5	821,733	49,5735	2256,58105
31	616,73114	2325,92993	11886,6	904,0453	54,3915	2491,19507
32	613,95935	2363,03394	11876,9	930,5631	55,487	2579,15088
33	612,55457	2363,32666	11872,5	930,0327	55,4365	2552,823
34	612,3869	2336,13745	11887,4	909,59	53,3218	2485,27637
35	613,60858	2287,67529	11930,2	868,5759	0	2402,21387

Ethane	Ethene	Propane	Propene	i-Butane	n-Butane	trans-2-Buten
0	0	0	0	0	0	0
3,28767	5,69628	8,68504	23,43909	0	8,25203	0
15,76962	9,76815	24,9182	76,06429	0	29,01731	1,2409
43,49255	10,64131	57,17167	171,13072	0,525103	77,93969	3,1834
60,62756	11,98005	77,63985	230,82823	0,740241	107,95662	4,8014
65,55507	12,74942	83,57658	252,12526	0,830347	118,63098	5,3205
63,71786	12,83228	81,09253	247,14209	0,83172	114,91558	4,9665
62,52507	12,81182	79,1141	243,78165	0,791759	112,34637	4,7517
61,41556	12,76817	77,19037	240,61832	0,782015	109,88638	4,5489
60,60337	12,70704	75,90335	238,52003	0,750586	108,11735	4,4596
59,90213	12,60363	74,90181	235,68613	0,742735	106,49205	4,3735
59,38961	12,53169	74,24199	234,18661	0,750462	105,73826	4,3376
58,82933	12,37241	73,37614	231,33562	0,752454	104,44206	4,3053
58,6553	12,2428	73,09931	230,14966	0,725981	103,90447	4,2725
58,77972	12,20935	73,12762	230,32523	0,737671	104,14921	4,2602
58,82913	12,13392	73,56725	230,27043	0,719355	104,61737	4,316
58,48408	11,89209	73,91618	225,27182	0,732537	104,20079	4,3404
58,10907	11,73937	73,3769	222,93303	0,730926	103,74202	4,3136
57,32653	11,55626	72,27689	219,45178	0,710004	102,00124	4,1968
57,71117	11,54899	72,73341	220,63338	0,767117	102,93522	4,2496
56,98218	11,39245	71,80751	217,77965	0,709895	102,03941	4,2374
56,73254	11,3231	71,5276	217,18661	0,713257	101,1779	4,2149
56,45453	11,25925	71,25009	216,14464	0,691021	101,1658	4,2088
56,54012	11,23129	71,05909	215,71527	0,718276	101,29971	4,2443
56,0605	25,45136	156,86076	0	0	0	0
56,95174	11,28883	71,70628	217,18057	0,700629	101,7717	4,2112
56,07504	11,07923	70,38898	213,12439	0,703995	99,72771	4,1368
97,06817	12,12557	121,38595	287,72116	0,875276	117,48618	5,2257
169,80353	14,25627	238,04771	462,16724	1,56325	213,39169	11,9194
222,39613	16,05989	330,68741	611,10907	2,24728	323,51315	19,4936
250,28998	17,24953	383,5629	705,66095	2,79487	410,37305	25,3359
261,60092	17,92511	407,59601	755,62262	3,1471	475,13382	29,6332
260,53241	17,96805	408,46008	767,10522	3,33188	517,80084	32,215
253,95267	17,89058	397,77493	757,74396	3,32225	520,55927	32,0378
245,15779	17,84092	382,0954	741,42542	3,28797	513,21539	0

1-Butene	i-Butene	cis-2-Butene	i-Pentane	n-Pentane	i-Pentene	1-Pentene
0	0	0	0	0	0	0
17,0526	0	0	0	5,7178	0	11,2275
60,4316	0	1,6766	0	23,1111	1,1943	42,2471
143,1322	1,5881	5,6656	1,1714	72,8728	3,583	104,6019
199,4864	2,397	8,6508	1,7577	102,3403	5,1202	153,7967
224,6102	2,7033	9,6506	2,0622	116,8475	5,8442	182,3186
222,6278	2,6433	9,072	2,0264	112,4942	5,4022	183,5923
220,5823	2,586	8,6736	1,9672	109,4804	5,11	182,7223
218,0102	2,5492	8,4216	1,9248	106,4762	4,8974	180,4994
216,119	2,5101	8,2777	1,9013	104,8961	4,7737	179,6152
213,6912	2,469	8,1444	1,8595	103,4262	4,6901	178,0488
212,4955	2,4344	8,0768	1,8576	102,2121	4,638	176,7932
210,1401	2,4048	7,9722	1,8178	101,0716	4,5766	174,9619
208,7832	2,386	7,9286	1,8019	100,3474	4,5423	173,878
208,6862	2,386	7,9664	1,8466	100,9274	4,566	174,3004
208,717	2,4077	8,0264	1,8024	101,1508	4,5836	174,0125
203,8639	2,3374	7,976	1,8003	100,7666	4,6041	170,64
202,0152	2,3209	7,8834	1,8015	100,3518	4,5806	168,2215
198,2133	2,2813	7,732	1,7566	98,9745	4,5161	165,0657
199,6574	2,2665	7,8463	1,7819	99,5311	4,5409	165,8443
197,5127	2,2546	7,7631	1,7483	99,4476	4,5144	165,3503
196,2981	2,2419	7,7347	1,7405	98,4416	4,4943	163,4312
195,8877	2,2356	7,7101	1,7409	98,8464	4,4947	163,965
195,7395	2,2264	7,7362	1,7355	99,3789	4,5328	164,6144
0	0	0	0	0	0	0
196,6638	2,2476	7,7892	1,7412	99,2863	165,8031	164,3499
192,493	2,1883	7,6093	1,6925	97,0086	4,4321	160,1235
209,5955	2,6497	9,1301	1,7203	97,3324	4,4615	161,0158
292,1783	4,5354	19,6179	2,1774	111,4793	5,3685	172,1339
390,723	6,6771	32,2876	3,1615	154,5922	8,294	201,6641
471,69	8,2727	42,6862	4,2878	212,4435	12,2295	240,9408
535,9823	9,4793	50,8035	5,4209	272,6766	16,1961	284,5899
580,0237	10,219	56,8368	7,2723	397,3285	24,5226	362,624
588,3369	10,2655	56,8819	7,8534	458,1037	28,4282	399,866
0	0	0	0	0	0	0

C5-olefin? (ag	n-Hexane	1-Hexene	n-Heptane	1-Heptene
0	0	0	0	0
0,666841	3,2538	4,717	1,2906	0
2,045442	15,825	22,5921	6,4382	7,1612
6,249104	59,6057	58,1273	24,9755	19,1821
10,103793	90,3069	91,5648	51,1619	34,0026
11,767346	113,5773	121,4599	73,3141	51,3195
11,2104	112,6764	128,5812	85,4923	62,7863
10,771777	109,2207	128,9003	88,705	68,6146
10,495206	106,2055	128,4779	88,6107	71,5161
10,265774	103,8078	127,9281	86,9924	72,088
10,159612	102,4974	127,7274	85,5046	72,5676
9,957435	101,1166	126,9338	84,2842	72,8097
9,860209	100,2589	126,4516	82,8438	72,4749
9,803773	100,2093	126,3318	82,9811	73,0983
9,825086	100,1813	126,3011	83,426	73,6286
9,830106	100,2324	126,0492	83,5957	73,9162
9,81341	99,3744	124,3866	82,6477	73,5114
9,56581	99,5755	122,5233	82,7452	72,9564
9,508399	98,1318	119,8481	82,0708	72,0525
9,473431	98,985	120,5836	82,6339	72,0613
9,468467	98,4395	119,3936	82,7344	71,7549
9,429562	99,2121	119,9543	83,8562	72,4036
9,429722	99,2426	119,5294	85,1875	73,0316
9,475547	100,436	120,901	85,8873	73,3365
0	0	0	0	0
9,522372	99,5159	123,5663	96,414	146,7681
9,261498	98,2804	118,1739	84,1928	71,0191
9,336369	98,0941	117,6812	83,6028	70,9152
10,943822	98,062	117,6341	83,4197	70,5847
16,041801	98,5381	117,5288	83,8703	71,1724
22,595923	101,5448	117,5619	83,4883	71,2366
29,461993	109,4794	121,3765	84,1198	71,6712
43,7044	139,4461	133,1663	81,7636	69,3
50,57946	233,6453	168,6304	78,3532	65,5001
0	0	0	0	0

Catalyst: CoRe80(500ppmK)
SynGas Bottle AGA751
Date: 27.2.2018
Catalyst mass: 1,0026 g
Co content: 20 %
Dispersion: 15 %

Injection no.	GC Areas		
	TCD [uV*s]		
	H2	N2	CO
1	669,19263	1102,91394	13338,1
2	682,29498	1208,53589	12739,9
3	675,51343	1212,0238	12852,3
4	674,04175	1211,03479	12854,9
5	674,38586	1212,61047	12876,2
6	674,06592	1210,28162	12859,3
7	673,65448	1205,87305	12819
8	674,8302	1202,93103	12785,4
9	676,10327	1200,39429	12749,6
10	677,21539	1198,34729	12711,4
11	678,07684	1196,29272	12675,3
12	678,94678	1195,55798	12642,4
13	679,89954	1194,05737	12613,4
14	680,44397	1192,74292	12590,3
15	681,11334	1192,15601	12567
16	681,64014	1191,60974	12557,4
17	681,95044	1190,34985	12539,5
18	681,88214	1189,58423	12520,8
19	681,72064	1188,24915	12501,6
20	682,76935	1188,89832	12516,7
21	682,84424	1189,03601	12510,8
22	682,03662	1187,18127	12497,3

E Risk report

ID	23698	**Status**	**Date**
Risk Area	Risikovurdering: Helse, miljø og sikkerhet (HMS)	Created	04.10.2017
Created by	Jonas Steidel Save	Assessment started	04.10.2017
Responsible	Jonas Steidel Save	Actions decided	
		Closed	

Risk Assessment:

CAT, Master student, 2017, Jonas Save

Valid from-to date:

-

Location:

Chemistry hall D, 1st floor

Goal / purpose

Prepare catalysts for Fischer-Tropsch, Co-Re/gamma-alumina (20wt% Co, 0.5wt% Re), using Ethylen Glycol and distilled water for adjusting the size of cobalt particle.

Background

[Ingen registreringer]

Description and limitations

Prerequesites, assumptions and simplifications

[Ingen registreringer]

Attachments

[Ingen registreringer]

References

[Ingen registreringer]

Summary, result and final evaluation

The summary presents an overview of hazards and incidents, in addtition to risk result for each consequence area.

Hazard: **Aluminum oxide**

Incident: **Inhalation**

Consequence area: Helse — Risk before actions: Risiko after actions:

Incident: **Skin contact**

Consequence area: Helse — Risk before actions: Risiko after actions:

Incident: **Eye contact**

Consequence area: Helse — Risk before actions: Risiko after actions:

Hazard: **Ethylene glycol**

Incident: **Eating**

Consequence area: Helse — Risk before actions: Risiko after actions:

Incident: **Inhalation**

Consequence area: Helse — Risk before actions: Risiko after actions:

Hazard: **Cobalt(II) nitrate hexahydrate**

Incident: **Fire**

Consequence area: Helse — Risk before actions: Risiko after actions:
Materielle verdier — Risk before actions: Risiko after actions:

Incident: **Eating**

Consequence area: Helse — Risk before actions: Risiko after actions:

Hazard: **Cobalt(II) nitrate hexahydrate**

Incident: **Skin contact**

Consequence area: Helse — Risk before actions: Risiko after actions:

Incident: **Inhalation**

Consequence area: Helse — Risk before actions: Risiko after actions:

Incident: **Waste disposal**

Consequence area: Ytre miljø — Risk before actions: Risiko after actions:

Hazard: **Perrhenic acid**

Incident: **Fire**

Consequence area: Helse — Risk before actions: Risiko after actions:
Materielle verdier — Risk before actions: Risiko after actions:

Incident: **Inhalation**

Consequence area: Helse — Risk before actions: Risiko after actions:

Incident: **Eye contact**

Consequence area: Helse — Risk before actions: Risiko after actions:

Incident: **Eating**

Consequence area: Helse — Risk before actions: Risiko after actions:

Incident: **Skin contact**

Consequence area: Helse — Risk before actions: Risiko after actions:

Hazard:	**Calcination oven/drying oven**		
Incident:	**Skin contact when hot**		
Consequence area:	Helse	Risk before actions:	Risiko after actions:
Hazard:	**BET characterization**		
Incident:	**Frost damage**		
Consequence area:	Helse	Risk before actions:	Risiko after actions:
Incident:	**N2 leak**		
Consequence area:	Helse	Risk before actions:	Risiko after actions:
Incident:	**CO leak**		
Consequence area:	Helse	Risk before actions:	Risiko after actions:
Hazard:	**Chemisorption**		
Incident:	**H2 leak**		
Consequence area:	Helse	Risk before actions:	Risiko after actions:
	Materielle verdier	Risk before actions:	Risiko after actions:
Incident:	**CO leak**		
Consequence area:	Helse	Risk before actions:	Risiko after actions:
Hazard:	**Acetone**		
Incident:	**Fire hazard**		
Consequence area:	Materielle verdier	Risk before actions:	Risiko after actions:

Hazard:	**Acetone**		
Incident:	**Health hazard**		
Consequence area:	Helse	Risk before actions:	Risiko after actions:

Hazard:	**Potassium nitrate**		
Incident:	**Oxidizing**		
Consequence area:	Materielle verdier	Risk before actions:	Risiko after actions:

Hazard:	**Fischer-Tropsch synthesis**		
Incident:	**Gas leak**		
Consequence area:	Helse	Risk before actions:	Risiko after actions:
	Materielle verdier	Risk before actions:	Risiko after actions:
Incident:	**Explosion due to high pressures and temperatures**		
Consequence area:	Helse	Risk before actions:	Risiko after actions:
	Materielle verdier	Risk before actions:	Risiko after actions:
Incident:	**Hot wax**		
Consequence area:	Helse	Risk before actions:	Risiko after actions:
	Materielle verdier	Risk before actions:	Risiko after actions:

Final evaluation

Organizational units and people involved

A risk assessment may apply to one or more organizational units, and involve several people. These are lsited below.

Organizational units which this risk assessment applies to

- Institutt for kjemisk prosessteknologi

Participants

Edd Anders Blekkan

Ljubisa Gavrilovic

Karin Wiggen Dragsten

Readers

[Ingen registreringer]

Others involved/stakeholders

[Ingen registreringer]

The following accept criteria have been decided for the risk area Risikovurdering: Helse, miljø og sikkerhet (HMS):

Helse

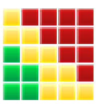

Materielle verdier

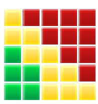

Omdømme

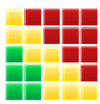

Ytre miljø

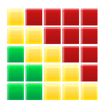

Overview of existing relevant measures which have been taken into account

The table below presents existing measures which have been take into account when assessing the likelihood and consequence of relevant incidents.

Hazard	Incident	Measures taken into account
Aluminum oxide	Inhalation	Ventilation
	Skin contact	Personal protective equipment
	Eye contact	Personal protective equipment
Ethylene glycol	Eating	Personal protective equipment
	Inhalation	Ventilation
Cobalt(II) nitrate hexahydrate	Fire	General guidelines for IKP
	Eating	Personal protective equipment
	Skin contact	Personal protective equipment
	Inhalation	Ventilation
	Waste disposal	General guidelines for IKP
Perrhenic acid	Fire	General guidelines for IKP
	Inhalation	Ventilation
	Eye contact	Personal protective equipment
	Eating	Personal protective equipment
	Skin contact	Personal protective equipment
Calcination oven/drying oven	Skin contact when hot	Personal protective equipment
BET characterization	Frost damage	Personal protective equipment
	Frost damage	General guidelines for IKP
	N2 leak	General guidelines for IKP
	CO leak	General guidelines for IKP
Chemisorption	H2 leak	General guidelines for IKP
	CO leak	General guidelines for IKP
Acetone	Fire hazard	Ventilation
	Fire hazard	General guidelines for IKP
	Health hazard	Personal protective equipment
	Health hazard	Ventilation
Potassium nitrate	Oxidizing	General guidelines for IKP
Fischer-Tropsch synthesis	Gas leak	Personal protective equipment
	Gas leak	General guidelines for IKP
	Gas leak	Mobile gas-detector
	Gas leak	Built-in gas detectors
	Explosion due to high pressures and temperatures	Personal protective equipment

Fischer-Tropsch synthesis	Explosion due to high pressures and temperatures	General guidelines for IKP
	Explosion due to high pressures and temperatures	Emergency button
	Hot wax	Personal protective equipment
	Hot wax	General guidelines for IKP

Existing relevant measures with descriptions:

Personal protective equipment

Gloves, glasses, lab coat and potholder gloves.

Ventilation

Ventilation/Semi-closed cabinets/Avtrekksskap

General guidelines for IKP

[Ingen registreringer]

Mobile gas-detector

Detects flamable gases and should be used around valves and possible places where gas leaks might occurs.

Built-in gas detectors

Local CO-detector with local alarm and shutdown of setup at high alarm. Gas detectors for CH4 in chemistry hall as well.

Emergency button

A red button inside fuse cabinet inside Fischer-Tropsch setup that is to be pushed if there are uncertainties whether the catalyst testing is safe or not. If pushed, also contact operator (Eirik Ø. Pedersen) and room responsible (Karin Wiggen Dragsten).

Risk analysis with evaluation of likelihood and consequence

This part of the report presents detailed documentation of hazards, incidents and causes which have been evaluated. A summary of hazards and associated incidents is listed at the beginning.

The following hazards and incidents has been evaluated in this risk assessment:

- **Aluminum oxide**
  - Inhalation
  - Skin contact
  - Eye contact
- **Ethylene glycol**
  - Eating
  - Inhalation
- **Cobalt(II) nitrate hexahydrate**
  - Fire
  - Eating
  - Skin contact
  - Inhalation
  - Waste disposal
- **Perrhenic acid**
  - Fire
  - Inhalation
  - Eye contact
  - Eating
  - Skin contact
- **Calcination oven/drying oven**
  - Skin contact when hot
- **BET characterization**
  - Frost damage
  - N2 leak
  - CO leak
- **Chemisorption**
  - H2 leak
  - CO leak
- **Acetone**
  - Fire hazard
  - Health hazard
- **Potassium nitrate**
  - Oxidizing
- **Fischer-Tropsch synthesis**
  - Gas leak
  - Explosion due to high pressures and temperatures
  - Hot wax

Detailed view of hazards and incidents:

Hazard: Aluminum oxide

Used for preparation of catalyst.

Incident: Inhalation

If inhaled, take the person outside to fresh air. If the person isn't breathing, give mouth to mouth.

Likelihood of the incident (common to all consequence areas): **Less likely (2)**

Kommentar:

[Ingen registreringer]

Consequence area: Helse

Assessed consequence: **Small (1)**

Comment: [Ingen registreringer]

Risk:

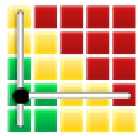

Incident: Skin contact

Wash with soap and lots of water.

Likelihood of the incident (common to all consequence areas): **Likely (3)**

Kommentar:

[Ingen registreringer]

Consequence area: Helse

Assessed consequence: **Small (1)**

Comment: [Ingen registreringer]

Risk:

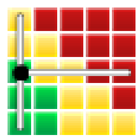

Incident: Eye contact

Rinse with water.

Likelihood of the incident (common to all consequence areas): **Less likely (2)**

Kommentar:

[Ingen registreringer]

Consequence area: Helse

Assessed consequence: **Small (1)**

Comment: [Ingen registreringer]

Risk:

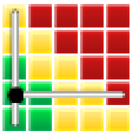

Hazard: Ethylene glycol

Used for preparation of catalyst.

Incident: Eating

Dangerous if swallowed. Can cause organ damage from repeated or long-lasting exposure by swallowing. If swallowed, rinse mouth and contact poison control or doctor.

Likelihood of the incident (common to all consequence areas): **Unlikely (1)**

Kommentar:

[Ingen registreringer]

Consequence area: Helse

Assessed consequence: **Medium (2)**

Comment: [Ingen registreringer]

Risk:

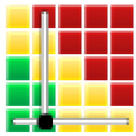

Incident: Inhalation

Should not inhale

Likelihood of the incident (common to all consequence areas): **Less likely (2)**

Kommentar:

[Ingen registreringer]

Consequence area: Helse

Assessed consequence: **Medium (2)**

Comment: [Ingen registreringer]

Risk:

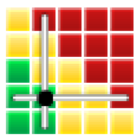

Hazard: Cobalt(II) nitrate hexahydrate

Used for preparation of catalyst.

Incident: Fire

Can cause fire; oxidizing. Should not be in close proximity as flamable materials.

Likelihood of the incident (common to all consequence areas): **Less likely (2)**

Kommentar:

[Ingen registreringer]

Consequence area: Helse

Assessed consequence: **Medium (2)**

Comment: [Ingen registreringer]

Risk:

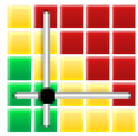

Consequence area: Materielle verdier

Assessed consequence: **Medium (2)**

Comment: [Ingen registreringer]

Risk:

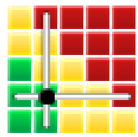

Incident: Eating

Dangerous if swallowed.
Can hurt reproductive abilities if eaten.
Is suspected to give genetic damage.

Likelihood of the incident (common to all consequence areas): **Unlikely (1)**

Kommentar:

[Ingen registreringer]

Consequence area: Helse

Assessed consequence: **Very large (4)**

Comment: [Ingen registreringer]

Risk:

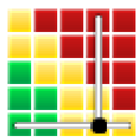

Incident: Skin contact

Can trigger allergic reaction.

Likelihood of the incident (common to all consequence areas): **Less likely (2)**

Kommentar:

[Ingen registreringer]

Consequence area: Helse

Risk:

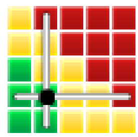

Assessed consequence: **Medium (2)**

Comment: [Ingen registreringer]

Incident: Inhalation

Can give asthma symptoms or breathing difficulties if inhaled.
Is suspected to give genetic damage.
Can cause cancer if inhaled.
Can hurt reproductive abilities if inhaled

Likelihood of the incident (common to all consequence areas): **Less likely (2)**

Kommentar:

[Ingen registreringer]

Consequence area: Helse

Risk:

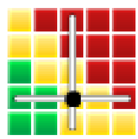

Assessed consequence: **Large (3)**

Comment: [Ingen registreringer]

Incident: Waste disposal

Very toxic to life in water so should be disposed in special disposal, not the drain.

Likelihood of the incident (common to all consequence areas): **Less likely (2)**

Kommentar:

[Ingen registreringer]

Consequence area: Ytre miljø

Risk:

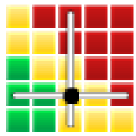

Assessed consequence: **Large (3)**

Comment: [Ingen registreringer]

Hazard: Perrhenic acid

Used for preparation of catalyst.

Incident: Fire

Substance is oxidizing, therefore it should not be in close proximity to flamable material.

Likelihood of the incident (common to all consequence areas): **Less likely (2)**

Kommentar:

[Ingen registreringer]

Consequence area: Helse

Assessed consequence: **Medium (2)**

Comment: [Ingen registreringer]

Risk:

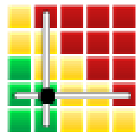

Consequence area: Materielle verdier

Assessed consequence: **Medium (2)**

Comment: [Ingen registreringer]

Risk:

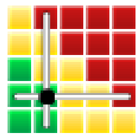

Incident: Inhalation

Can lead to irritation of airways, cough and trouble breathing. Other possible health effects are pneumonia and pulmonary edema.

Likelihood of the incident (common to all consequence areas): **Less likely (2)**

Kommentar:

[Ingen registreringer]

Consequence area: Helse

Assessed consequence: **Large (3)**

Comment: [Ingen registreringer]

Risk:

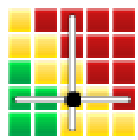

Incident: Eye contact

Can cause permanent sight damage. If it gets in your eye, rinse with a lot of water and contact doctor.

Likelihood of the incident (common to all consequence areas): **Less likely (2)**

Kommentar:

[Ingen registreringer]

Consequence area: Helse

Assessed consequence: **Large (3)**

Comment: [Ingen registreringer]

Risk:

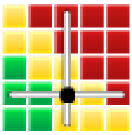

Incident: Eating

Corrosive on mucosal, mouth, throat, stomach and intestine. Risk of perforation.

Likelihood of the incident (common to all consequence areas): **Unlikely (1)**

Kommentar:

[Ingen registreringer]

Consequence area: Helse

Assessed consequence: **Large (3)**

Comment: [Ingen registreringer]

Risk:

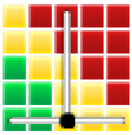

Incident: Skin contact

Corrosive. Can irritate mucosal.

Likelihood of the incident (common to all consequence areas): **Less likely (2)**

Kommentar:

[Ingen registreringer]

Consequence area: Helse

Assessed consequence: **Medium (2)**

Comment: [Ingen registreringer]

Risk:

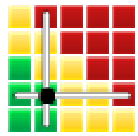

Hazard: Calcination oven/drying oven

Incident: Skin contact when hot

Can give burn damage to skin and tissue, depending on the duration of contact and temperature of contact surface.

Likelihood of the incident (common to all consequence areas): **Less likely (2)**

Kommentar:

[Ingen registreringer]

Consequence area: Helse

Assessed consequence: **Medium (2)**

Comment: [Ingen registreringer]

Risk:

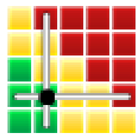

Hazard: BET characterization

Incident: Frost damage

A thermos containing liquid nitrogen can cause serious frost damage if proper handling and equipment is not utilized.

Likelihood of the incident (common to all consequence areas): **Likely (3)**

Kommentar:

[Ingen registreringer]

Consequence area: Helse

Risk:

Assessed consequence: **Medium (2)**

Comment: [Ingen registreringer]

Incident: N2 leak

Can be suffocating if concentration of nitrogen gas gets too high.

Likelihood of the incident (common to all consequence areas): **Less likely (2)**

Kommentar:

[Ingen registreringer]

Consequence area: Helse

Risk:

Assessed consequence: **Medium (2)**

Comment: [Ingen registreringer]

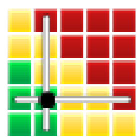

Incident: CO leak

Can at low concentrations provoke nausea, dizziness and/or headache. At low to medium concentrations it can affect the regulation of blood circulation, sourness of the bodily fluids and/or breathing difficulties. At high concentrations it can give breathing difficulties, increased hearth rate and/or change of sourness in bodily fluids. Very high concentrations cause unconsciousness or death.

Likelihood of the incident (common to all consequence areas): **Unlikely (1)**

Kommentar:

[Ingen registreringer]

Consequence area: Helse

Assessed consequence: **Large (3)**

Comment: [Ingen registreringer]

Risk:

Hazard: Chemisorption

Incident: H2 leak

Extremely flamable.

Likelihood of the incident (common to all consequence areas): **Less likely (2)**

Kommentar:

[Ingen registreringer]

Consequence area: Helse

Assessed consequence: **Large (3)**

Comment: [Ingen registreringer]

Risk:

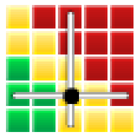

Consequence area: Materielle verdier

Assessed consequence: **Large (3)**

Comment: [Ingen registreringer]

Risk:

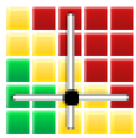

Incident: CO leak

Extremely dangerous

Likelihood of the incident (common to all consequence areas): **Unlikely (1)**

Kommentar:

[Ingen registreringer]

Consequence area: Helse

Assessed consequence: **Very large (4)**

Comment: [Ingen registreringer]

Risk:

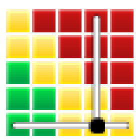

Hazard: Acetone

Used for cleaning equipment.

Incident: Fire hazard

Very flammable liquid and steam.

Likelihood of the incident (common to all consequence areas): **Less likely (2)**

Kommentar:

[Ingen registreringer]

Consequence area: Materielle verdier

Risk:

Assessed consequence: **Large (3)**

Comment: [Ingen registreringer]

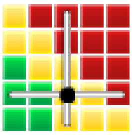

Incident: Health hazard

Serious irritation upon eye contact.
Can cause dizziness or drowsiness.
Repeated contact can cause dry skin.

Likelihood of the incident (common to all consequence areas): **Quite likely (4)**

Kommentar:

[Ingen registreringer]

Consequence area: Helse

Risk:

Assessed consequence: **Small (1)**

Comment: Serious irritation upon eye contact.
Can cause dizziness or drowsiness.
Repeated contact can cause dry skin.

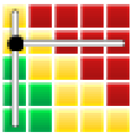

Hazard: Potassium nitrate

Used for preparation of catalyst.

Incident: Oxidizing

Can enhance a fire.

Likelihood of the incident (common to all consequence areas): **Unlikely (1)**

Kommentar:

[Ingen registreringer]

Consequence area: Materielle verdier

Assessed consequence: **Large (3)**

Comment: [Ingen registreringer]

Risk:

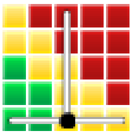

Hazard: Fischer-Tropsch synthesis

Testing the catalysts performance at syngas composition H2:CO = 2.1, temperature at 210 degrees C and pressures at 20 bar.

Incident: Gas leak

Danger of explosion and/or posoining as CO, H2 and CO2 is used. If gas leak is suspected, close valves.

Likelihood of the incident (common to all consequence areas): **Less likely (2)**

Kommentar:

[Ingen registreringer]

Consequence area: Helse

Risk:

Assessed consequence: **Large (3)**

Comment: [Ingen registreringer]

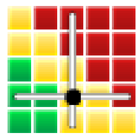

Consequence area: Materielle verdier

Risk:

Assessed consequence: **Medium (2)**

Comment: [Ingen registreringer]

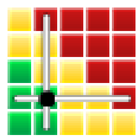

Incident: Explosion due to high pressures and temperatures

Follow instructions for correct use of setup and watch carefully pressures and temperatures.

Likelihood of the incident (common to all consequence areas): **Less likely (2)**

Kommentar:

[Ingen registreringer]

Consequence area: Helse

Risk:

Assessed consequence: **Large (3)**

Comment: [Ingen registreringer]

Consequence area: Materielle verdier

Assessed consequence: **Large (3)**

Comment: [Ingen registreringer]

Risk:

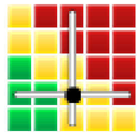

Incident: Hot wax

Hydrocarbon wax (C8-C50) is flamable. Use proper protective equipment upon handling.

Likelihood of the incident (common to all consequence areas): **Less likely (2)**

Kommentar:

[Ingen registreringer]

Consequence area: Helse

Assessed consequence: **Medium (2)**

Comment: [Ingen registreringer]

Risk:

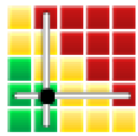

Consequence area: Materielle verdier

Assessed consequence: **Medium (2)**

Comment: [Ingen registreringer]

Risk:

Overview of risk mitiating actions which have been decided:

Below is an overview of risk mitigating actions, which are intended to contribute towards minimizing the likelihood and/or consequence of incidents:

Overview of risk mitigating actions which have been decided, with description:

Detailed view of assessed risk for each hazard/incident before and after mitigating actions